JAAVSO

Volume 41
Number 1
2013

The Journal of the American Association of Variable Star Observers

V1820 Ori: an RR Lyrae Star With Strong, Irregular Blazhko Effect

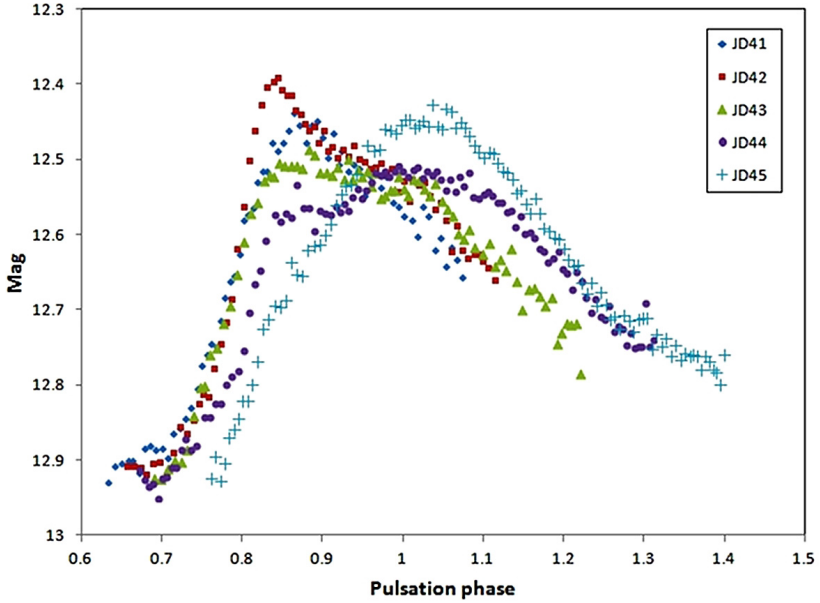

V1820 Ori hump evolution for nights JD 2455941 to 2455945

Also in this issue...

THE AMERICAN ASSOCIATION OF VARIABLE STAR OBSERVERS
FOUNDED 1911

49 Bay State Road
Cambridge, MA 02138
U. S. A.

The Journal of the American Association of Variable Star Observers

ISSN 0271-9053

JAAVSO

The Journal of
The American Association
of Variable Star Observers

Volume 41
Number 1
2013

ISSN 0271-9053

49 Bay State Road
Cambridge, MA 02138
U. S. A.

The *Journal of the American Association of Variable Star Observers* is a refereed scientific journal published by the American Association of Variable Star Observers, 49 Bay State Road, Cambridge, Massachusetts 02138, USA. The *Journal* is made available to all AAVSO members and subscribers.

In order to speed the dissemination of scientific results, selected papers that have been refereed and accepted for publication in the *Journal* will be posted on the internet at the *eJAAVSO* website as soon as they have been typeset and edited. These electronic representations of the *JAAVSO* articles are automatically indexed and included in the NASA Astrophysics Data System (ADS). *eJAAVSO* papers may be referenced as *J. Amer. Assoc. Var. Star Obs., in press,* until they appear in the concatonated electronic issue of *JAAVSO*. The *Journal* cannot supply reprints of papers.

Page Charges

Unsolicited papers by non-Members will be assessed a charge of $15 per published page.

Instructions for Submissions

The *Journal* welcomes papers from all persons concerned with the study of variable stars and topics specifically related to variability. All manuscripts should be written in a style designed to provide clear expositions of the topic. Contributors are strongly encouraged to submit digitized text in MS WORD, LATEX+POSTSCRIPT, or plain-text format. Manuscripts may be mailed electronically to journal@aavso.org or submitted by postal mail to *JAAVSO*, 49 Bay State Road, Cambridge, MA 02138, USA.

Manuscripts must be submitted according to the following guidelines, or they will be returned to the author for correction:

Manuscripts must be:
1) original, unpublished material;
2) written in English;
3) accompanied by an abstract of no more than 100 words.
4) not more than 2,500–3,000 words in length (10–12 pages double-spaced).

Figures for publication must:
1) be camera-ready or in a high-contrast, high-resolution, standard digitized image format;
2) have all coordinates labeled with division marks on all four sides;
3) be accompanied by a caption that clearly explains all symbols and significance, so that the reader can understand the figure without reference to the text.

Maximum published figure space is 4.5" by 7". When submitting original figures, be sure to allow for reduction in size by making all symbols and letters sufficiently large.

Photographs and halftone images will be considered for publication if they directly illustrate the text.

Tables should be:
1) provided separate from the main body of the text;
2) numbered sequentially and referred to by Arabic number in the text, e.g., Table 1.

References:
1) References should relate directly to the text.
2) References should be keyed into the text with the author's last name and the year of publication, e.g., (Smith 1974; Jones 1974) or Smith (1974) and Jones (1974).
3) In the case of three or more joint authors, the text reference should be written as follows: (Smith *et al.* 1976).
4) All references must be listed at the end of the text in alphabetical order by the author's last name and the year of publication, according to the following format:
   Brown, J., and Green, E. B. 1974, *Astrophys. J.*, **200**, 765.
   Thomas, K. 1982, *Phys. Report*, **33**, 96.
5) Abbreviations used in references should be based on recent issues of the Journal or the listing provided at the beginning of *Astronomy and Astrophysics Abstracts* (Springer-Verlag).

Miscellaneous:
1) Equations should be written on a separate line and given a sequential Arabic number in parentheses near the right-hand margin. Equations should be referred to in the text as, e.g., equation (1).
2) Magnitude will be assumed to be visual unless otherwise specified.
3) Manuscripts may be submitted to referees for review without obligation of publication.

Journal of the American Association of Variable Star Observers
Volume 41, Number 1, 2013

Table of Contents continued on following pages

Abstracts of Papers and Posters Presented at the 101st Annual Meeting of the American Association of Variable Star Observers, Held in Woburn, Massachusetts, November 1–3, 2012

Period Analysis of AAVSO Visual Observations of 55 Semiregular (SR/SRa/SRb) Variable Stars

John R. Percy
Paul Jx Tan
Department of Astronomy and Astrophysics, University of Toronto. Toronto, ON M5S 3H4, Canada; john.percy@utoronto.ca

Received April 26, 2012; revised June 21, 2012; accepted July 18, 2012

Abstract We have used AAVSO visual data, and Fourier analysis and self-correlation analysis, to study the periodicity of 55 semiregular (SR) variables—21 SRa and 34 SRb. According to the standard system of variable star classification, these are pulsating red giants, with visual amplitudes less than 2.5 magnitudes, which show noticeable periodicity (SRa) or less-obvious periodicity (SRb). We find that their behavior ranges from highly periodic to irregular; some are not significantly variable. We have used a simple index, based on self-correlation analysis, to show that, on average, the SRa variables have a larger component of periodicity than the SRb variables, as expected. The distributions of this index for the two groups, however, overlap considerably. Of our 55 stars, 11 definitely or possibly show two radial periods, and at least 16 definitely or possibly show a long secondary period. We also analyzed three non-SR stars: T Cet is a double-mode SRc star; T Cen is an RVa star which should be reclassified as RVb; V930 Cyg is an irregular (Lb) star with a strong 250-day period.

1. Introduction

Pulsating red giants are classified in the *General Catalogue of Variable Stars* (GCVS; Kholopov *et al.* 1985) as Mira (M) stars if their visual amplitude is greater than 2.5 magnitudes, and semiregular (SR) or irregular (L) variables if their visual amplitude is less than that value. See Kiss and Percy (2012) for a brief review of SR variables. SR variables are subdivided into SRa and SRb (both giants), where SRb have less obvious periodicity than SRa, and SRc (supergiants). There are also SRs variables which are SR variables with "short" periods (generally 30 days or less); about 100 stars are placed in this (arbitrary) class.

These types are defined thus: SR: "...giants or supergiants of intermediate and late spectral types showing noticeable periodicity in their light changes, accompanied or sometimes interrupted by various irregularities...." L: "Slow irregular variables. The light variations of these stars show no evidence of periodicity, or any periodicity present is very poorly defined, and appears only occasionally...." Clearly these definitions are qualitative at best, but they were

reasonable in the early days of variable star astronomy, especially if they were based on dense, long-term visual or photographic light curves.

Kiss *et al.* (1999) carried out an important study of a large sample of SR variables, also using AAVSO visual observations. They found that many of these stars had two or more periods, some identified with low-order radial pulsation modes, and some being "long secondary periods" whose nature and cause is unknown (Nicholls *et al.* 2009). And at least one star, R Dor, is known to switch between two periods (Bedding *et al.* 1998).

SR variables obey a series of period-luminosity relationships, corresponding to different radial modes. These P-L relationships were first observed in the MACHO and OGLE large-scale surveys of the Magellanic Clouds (Wood 2000), and later in a large sample of nearby variables with Hipparcos parallaxes (Tabur *et al.* 2009).

In a series of earlier papers (Percy and Terziev 2011 and references therein), we analyzed AAVSO visual observations of a large number of "irregular" (L-type) pulsating red giants. We found some to be slightly periodic, some to be irregular, and many to be not significantly variable (or microvariable at best).

In the present study, we analyzed 55 SRa and SRb variables which were not studied by Kiss *et al.* (1999), for the purpose of examining the periodicity of the stars in these two groups, and determining whether there are any differences in the periodicity. We used both Fourier analysis and self-correlation analysis to look for periods, including long secondary periods. An important subsidiary purpose was to provide feedback to AAVSO observers on how their thousands of measurements are used in astronomical research. Another purpose was to demonstrate how undergraduate students (such as co-author Tan) can carry out meaningful astronomical research using archival variable star data.

2. Data and analysis

We have used visual observations of 55 SR variables in the AAVSO International Database (AID), as listed in Tables 1 and 2. We chose stars which had a sufficient number of measurements, but which had not been studied by Kiss *et al.* (1999). AI Cyg, GY Cyg, RS Gem, RX UMa, and V930 Cyg (see below) were classified as "uncertain" by Kiss *et al.* (1999), so we re-analyzed them here. There were more SRb stars that obeyed these criteria than SRa stars. Our methodology was very similar to that used in our studies of L-type variables (Percy and Terziev 2011): we use Fourier analysis and self-correlation analysis. The latter shows the cycle-to-cycle behavior of the star, averaged over the dataset (Percy and Sen 1991; Percy and Mohammed 2004). We initially called this method *autocorrelation*, because it is a simple version of that well-established technique. Laurent Eyer then pointed out that it was actually a form of *variogram* analysis (Eyer and Genton 1999). We have since used the name *self-correlation* to avoid any confusion. Fourier analysis is much

better for analyzing multiperiodic variables, unless the periods are an order of magnitude different, as in the case of the "long secondary periods." In that case, self-correlation is certainly valid and useful.

The self-correlation diagram (Figures 1–4) allows us to define a simple measure of the fraction of the stars' variability which is periodic. Let A be the intercept on the vertical axis; it is a measure of the average observational error in the data (because, if two measurements are independently made, a short time apart, they will on average differ by the average observational error). Let B be the level of the first maximum in the diagram, and let C be the level of the first deep minimum. Then define k = (B–C)/(B–A). If k = 1, the star is periodic; if k = 0, the star is irregular. The values of k are given in the Tables. For RW Sgr (Figure 2), for instance: A = 0.30, B = 0.76, C = 0.36, and k = 0.87.

3. Results

The results are summarized in Tables 1 and 2 for the SRa and SRb stars, respectively. The tables list the stars, their range and period from the *Variable Star Index* (VSX; Watson *et al.* 2012), the intercept on the vertical axis of the self-correlation diagram (which, as mentioned, is a measure of the average observational error in the data), the period and amplitude determined from Fourier analysis, the period and amplitude determined from self-correlation analysis, the index k, and the presence or absence of a long secondary period. VSX is located on the AAVSO website. Many of the SRb variables had VSX periods that were uncertain or unknown. The VSX periods come from various sources, including the GCVS "living" version maintained by the Sternberg Astronomical Institute.

As mentioned: self-correlation analysis is not useful for determining multiple periods, unless they are of different orders of magnitude. The self-correlation periods marked with an asterisk (*) were not independently determined by self-correlation but, for these stars, the forms of the self-correlation diagrams are consistent with the Fourier periods. The periods that we would prefer are in bold face.

For the ten stars which clearly have two radial periods, the period ratios are tightly clustered between 0.499 (AY Dra) and 0.598 (RV Mon); in fact, 9 stars have ratios between 0.499 and 0.544. This is consistent with the result of Kiss *et al.* (1999). The identification of these two radial periods is important, because it indicates which radial modes the periods correspond to, and which P-L relationship these stars would obey.

The long secondary periods in Tables 1 and 2 are typically an order of magnitude longer than the radial periods, as has been found in other pulsating red giants. The median ratio is 9.3, with a tendency for a higher ratio in stars with longer periods. There may be other LSPs which eluded us; Houk (1963), for a few stars, gives LSPs which we did not find (see sections 3.1 and 3.2).

The mean k values were 0.67 for the SRa variables, and 0.52 for the SRb variables. This indicates that the SRa variables have a slightly greater component of periodicity than the SRb variables, as might be expected. But there is considerable overlap between the two distributions of k values; each group contains some stars that are highly periodic, and some that are irregular.

We analyzed three stars which were on our original list of SR variables, but which are actually of other types. T Cet is an SRc star; it has periods of 160.8 and 287.7 days. T Cen is an RVa star with a period of 90.5 days (Fourier) or 91 days (self-correlation) and an amplitude of 0.59 magnitude. It also has an LSP of 900 days, so it should be reclassified as an RVb star. V930 Cyg (classified by Kiss *et al.* (1999) as "uncertain") is an Lb star with a period of 252.3 days (Fourier) or 248 days (self-correlation) and an amplitude of 0.41 magnitude, so it should probably be re-classified as SR.

As in our studies of L-type variables using visual observations, a few stars show low-level signals at periods of a year (TV And, TX Tau, V380 Sco, BR Eri, RR Eri, RT Ori, RV Mon, TT Per, and TU Gem), or a month (V380 Sco), which we ascribe to the Ceraski effect, which is an artifact of the visual observation process.

3.1. Notes on individual SRa stars

AK Peg: our results support the VSX period of 193.6 days.

AO Dra: we find a period of 143.5 days, which is not consistent with the VSX period of 103 days.

AY Dra: in addition to the VSX period of 262.5 days, we find a period of 130.8 days.

AY Her: we find a period of 127.3 days, which is close to the VSX period of 129.75 days.

BD Peg: we do not find the VSX period of 78 days in our data, with an amplitude greater than 0.02 mag.

DX Peg: the VSX period of 80.66 days is not present in our data.

EP Vel: we find a period of 259 days, which is close to the VSX period of 240 days; we find an additional period of 515 days. Both periods are strong and coherent.

RS Dra: we find a period of 278.2 days, which is close to the VSX period of 282.72 days; we find an additional period of 143 days. The 278.2-day period is strongest in the first half of the data, the 143.4-day period in the second half.

RT Cas: our results support the VSX period of 399.8 days.

RW Eri: our results support the VSX period of 91.4 days; we also find a long secondary period of 950 days.

RW Sgr: we find a period of 188.4 days, which is close to the VSX period of 186.82 days.

SZ Lyr: we find a period of 143.7 days, which is close to the VSX period of 133.1 days; we also find a weak period of 74 days.

TV And: we find a period of 111.7 days; the VSX period is 110 days.

TV Tau: we find no evidence for the VSX period of 120 days.

TX Tau: we find no evidence for the VSX period of 40.1 days, with an amplitude greater than 0.02 magnitude.

TY Cep: we find a period of 344.1 days, which is close to the VSX period of 330 days.

V380 Sco: we find no evidence for the VSX period of 187.17 days; the star appears irregular.

V577 Cyg: our results support the VSX period of 479 days.

V927 Cyg: we find no evidence for the VSX period of 229 days.

VY Aps: we find a period of 164.7 days, which is close to the VSX period of 152 days.

X Oct: we find a period of 200.8 days, which is consistent with the VSX period of 200 days.

3.2. Notes on individual SRb stars

AI Cyg: we find periods of 142 and 273 days, which are not consistent with the VSX period of 197.3 days.

BG Mon: we find no evidence for the VSX period of 30: days, with an amplitude greater than 0.02 mag; the star appears irregular.

BR Eri: the VSX period of 73.3 days is weakly present in our data, but is uncertain; otherwise, the star appears irregular.

DP Ori: we find periods of 246.1 and 127: days; the VSX period of 90: days is not present in our data.

FX Ori: we find a period of 692.2 days, which is close to the VSX period of 720 days.

GY Cyg: we find a period of 250 days which is not inconsistent with the VSX period of 300: days.

R Dor: we find periods of 176.3 and 329.8 days, the former being close to the VSX period of 172 days. This star has been extensively studied by Bedding *et al.* (1998), who found mode-switching between the 176- and 330-day periods.

RR Eri: we find a period of 93: or 90 days, which supports the VSX period of 94.6 days.

RS Gem: we find periods of 270.3 and 147: days, the latter being consistent with the VSX period of 140: days.

RT Ori: we do not find strong evidence for the VSX period of 321 days, or for any other period. Houk (1963) gives an LSP of 3200 days.

RT Psc: we find a period of 515.7 days, but no evidence for the VSX period of 70 days.

RU Per: we find periods of 93 and 602: days, but no evidence for the VSX period of 170: days.

RV Mon: we find periods of 585 and 979 days, but no evidence for the VSX period of 121.3 days. The long-term light curve is complex; there may be a 2700-day LSP. Houk (1963) gives a period of 132 days.

RX UMa: we find a period of 200.2 days, which is close to the VSX period of 195 days.

RY Cam: we find a period of 135.1 days, which is consistent with the VSX period of 135.75 days.

S Lep: we find a period of 855.5 days, and possibly 90 days with an amplitude of 0.02 or less; the VSX period is 97.3 days.

SW Mon: we find periods of 103.5 and 193.5 days; the VSX period is 112 days.

SY Eri: we find a possible period of 330: days with very low amplitude, but no evidence for the VSX period of 96: days.

SY For: we find a period of 151.3 days, but no evidence for the VSX period of 55: days.

TT Per: we find a long period of 2360 days, but no evidence for the VSX period of 82 days.

TT Tau: we find no evidence for the VSX period of 166.5 days, or for any other period.

TU Gem: we find periods of 215 and 2406 days; the former is close to the VSX period of 230 days.

TW Aur: we find periods of 1350 and possibly 285 days, but no evidence for the VSX period of 150: days.

UX And: we find a period of 218.7 days, which is close to the VSX period of 200 days.

V Hor: we find a period of 63 days; there is no period given in VSX.

V Lyn: we find a period of 87.2 days; there is no period given in VSX.

V Pav: we find a possible period of 324: days, but no evidence for the VSX period of 225.4 days; the star is essentially irregular. Houk (1963) gives an LSP of 3735 days.

V431 Ori: we find possible periods of 273: and 2400 days, but no evidence for the VSX period of 122: days; the variability is weak.

V465 Cas: we find periods of 97 and 898.4 days, but no evidence for the VSX period of 60 days.

VZ Tel: we find a period of 81.2 days, but no evidence for the VSX period of 117.8 days.

W Nor: we find a period of 147 days; the VSX period is 134.7 days. Houk (1963) gives an LSP of 1300 days.

XZ Aur: we find a possible period of 120: days, but no evidence for the VSX period of 250 days; the star is essentially irregular.

Z Eri: we find periods of 78 and 729.0 days; the former is close to the VSX period of 74.0 days.

Z Psc: we find a period of 155.9 days, which is consistent with the VSX period of 155.8 days.

4. Discussion

We found one or more periods in almost all of the 55 stars. Most were new periods, or ones which differed from those in VSX. In the Tables, we have marked our preferred periods in bold face. Generally we have preferred our own periods, since we know how they were derived, and we have confidence in them. In most cases, it is not obvious how the VSX periods were derived. Where our periods are uncertain, and the VSX period appears to be well-determined, we have preferred it.

We have not attempted to form P-L relationships for our sample. A few of the brightest stars have Hipparcos parallaxes good to 25%, but most are fainter stars without accurate parallaxes.

Using our k index, we have estimated the proportion of the stars' variability that is periodic. Within each sub-class (SRa and SRb), there is a wide range of k. It is not clear how the stars were initially classified—presumably from inspection of the light curve. One could possibly define stars with k greater than 0.5 as SRa and those with k less than 0.5 as SRb.

One of the purposes of this paper was to provide feedback to AAVSO observers. It is often felt that visual observations are obsolete. The study of red giants (and other variables) has certainly been revolutionized by the ultra-precise photometric monitoring by space missions such as MOST, CoRoT, and Kepler (for example, Hekker *et al.* 2011), as well as by CCD photometry from the ground (Tabur *et al.* 2009), but these have not yet amassed the long (decades) datasets such as those in the AID. It is definitely desirable to extract as much scientific information as possible from the AAVSO data, which were so diligently collected over so many years. In this paper, we have done so. These data have provided information on the stars' basic periodicity, and on their long-term behavior.

This paper also has an educational dimension. Co-author Paul Tan was in the third year of the Astronomy and Physics Program at the University of Toronto. This project enabled him to integrate and apply a wide range of science, math, and computing skills. Based in part on his success in this project, he was awarded a 2012 summer research assistantship in the prestigious Dunlap Institute of Astronomy and Astrophysics.

We did not analyze all of the SRb stars in the AID, nor did we analyze the stars which were classified as SR or SR:. Furthermore: there may be SRa and SRb stars which we did not analyze because of small numbers of observations, which could still yield useful results from our methods of analysis. This can be a project for yet another undergraduate student.

5. Conclusions

We have used Fourier and self-correlation analysis to study the periodicity

of 55 semiregular (SRa/SRb) pulsating red giants. For most of them, we have determined new or improved periods. Of the 55 stars, 11 show evidence for two radial periods, and at least 16 show evidence for long secondary periods. We have used a simple index, based on self-correlation analysis, to measure the fraction of the stars' variability which is periodic. The SRa variables show a higher index of periodicity than the SRb stars, as would be expected from their classification. But the distributions of the index overlap and, in each group, there are some stars with strong periodicity, and others with little or no periodicity.

6. Acknowledgements

We thank the hundreds of AAVSO observers who made the observations which were used in this project, and we thank the AAVSO staff for processing and archiving them in the AAVSO International Database. This research has made use of the International Variable Star Index (VSX) database, operated at AAVSO, Cambridge, Massachusetts, USA.This project was supported by the Ontario Work-Study Program. It made use of the SIMBAD database, which is operated by CDS, Strasbourg, France.

References

Bedding, T. R., Zijlstra, A. A., Jones, A., and Foster, G. 1998, *Mon. Not. Roy. Astron. Soc.*, **301**, 1073.

Eyer, L., and Genton, M. G. 1999, *Astron. Astrophys., Suppl. Ser.*, **136**, 421.

Hekker, S. *et al.* 2011, *Mon. Not. Roy. Astron. Soc.*, **414**, 2594.

Houk, N. 1963, *Astron. J.*, **68**, 253.

Kholopov, P. N. *et al.* 1985, *General Catalogue of Variable Stars*, 4th ed., Moscow.

Kiss, L. L., and Percy, J. R. 2012, *J. Amer. Assoc. Var. Star Obs.*, **40**, 528.

Kiss, L. L., Szatmary, K., Cadmus, R.R. Jr., and Mattei, J.A. 1999, *Astron. Astrophys.*, **346**, 542.

Nicholls, C. P., Wood, P. R., Cioni, M. -R. L., and Soszyński, I. 2009, *Mon. Not. Royal Astron. Soc.*, **399**, 2063.

Percy, J. R., and Mohammed, F. 2004, *J. Amer. Assoc. Var. Star Obs.*, **32**, 9.

Percy, J. R., and Sen, L. V. 1991, *Inf. Bull. Var. Stars*, No. 3670, 1.

Percy, J. R., and Terziev, E. 2011, *J. Amer. Assoc. Var. Star Obs.*, **39**, 1.

Tabur, V., Bedding, T. R., Kiss, L. L., Moon, T. T., Szeidl, B., and Kjeldsen, H. 2009, *Mon. Not. Roy. Astron. Soc.*, **400**, 1945.

Watson, C. L., *et al.* 2012, Variable Star Index (VSX; http://www.aavso.org/vsx/).

Wood, P. R. 2000, *Publ. Astron. Soc. Australia*, **17**, 18.

Table 1. Periodicity analysis of AAVSO visual observations of SRa variables.

Star	*Range*	*P(d)*[1]	δ*v*	*P(Δv)[F]*'[1]	*P(Δv)[SC]*[1]	*k*	*LSP*
AK Peg	8.6–10.24V	**193.6**	0.32	193.1/0.36	193/0.20; 2500:	0.70	Y:
AO Dra	11.0–12.5p	103	0.20	**143.5**/0.40	142.5/0.35	0.83	N
AY Dra	10.6–12.6p	262.5	0.2:	**130.8**/1.63; **262.2**/1.6	130*; 260*	0.96	N
AY Her	10.5–12.8V	129.75	0.15	**127.3**/1.14	127/1.0	0.67	N
BD Peg	9.4–10.3p	78	0.20	**3300**/0.18	3300/0.1	0.83:	Y
DX Peg	8.7–9.6V	80.66	0.24	**499.2**/0.11	500/0.02	0.60:	?
EP Vel	9.8–11.2p	240	0.33	**259**/0.5; **515**/0.58	260*; 517/0.5:	0.76	N
RS Dra	9–12V	282.72	0.26	**143**/0.5; **278.2**/0.94	140*; 280*	0.81	Y:
RT Cas	11.0–14.0p	**399.8**	0.42	393:	400/0.90	0.95	N
RW Eri	10.2–11.7p	91.4	0.09	**91.4**/0.16; **950**/0.15	88:/0.1; 950:	0.32	Y:
RW Sgr	9–11.7V	**186.82**	0.30	188.4/0.34	188/0.45	0.87	N
SZ Lyr	10.3–12.5V	133.1	0.42	74:/0.08; **143.7**/0.14	144/0.14	0.60	N
TV And	8.3–11.5V	110	0.33	**111.7**/0.21	113.1/0.20	0.71	N
TV Tau	9.3–12.2V	120	0.37	—	—	0.65	N
TX Tau	10.5–12.3V	40.1	0.37	—	—	0.72	N
TY Cep	9.7–13.3V	330	0.23	**344.1**/0.29	335/0.27	0.71	N
V380 Sco	9.16–10.6V	187.17	0.38	—	—	0.00	N
V577 Cyg	10.3–11V	479	0.30	**480**/0.26	450/0.1	0.67	Y:
V927 Cyg	10.5–12.0p	229	0.35	**2900**/0.25	3000/0.12	0.29:	Y
VY Aps	11–14.52B	152	0.29	**164.7**/0.27	164/0.15; 2000:/0.1	0.52	Y:
X Oct	6.8–10.9V	200	0.57	**200.8**/1.38	201/1.4	1.00	N

[1] *The self-correlation periods marked with an asterisk (*) in column 6 were not independently determined by self-correlation but, for these stars, the forms of the self-correlation diagrams are consistent with the Fourier periods. The periods that we would prefer are shown in bold face in columns 3 and 5.*

Table 2. Periodicity analysis of AAVSO visual observations of SRb variables.

Star	*Range*	*P(d)*[1]	δ*v*	*P(d)/Δv[F]*[1]	*P(d)/Δv[SC]*[1]	*k*	*LSP*
AI Cyg	9.2–11.8p	197.3	0.15	**142**/0.13; **273**/0.13	142*; 273*	0.50	Y
BG Mon	9.2–10.4V	30:	0.25	—	—	0.33:	N
BR Eri	6.5–8.16V	73.3:	0.32	—	—	0.38	N:
DP Ori	10.5–12.5p	90:	0.21	**127:**/0.1; **246.1**/0.23	125*; 242/0.1	0.59	N
FX Ori	7.7–10.4V	720	0.26	**692.2**/0.34	680/0.22	0.81	N
GY Cyg	10.6–12.5p	300:	0.14	**250**/0.08	250/0.03	0.36	N
R Dor	4.78–6.32V	172	0.28	**176.3**/0.1; **329.8**/0.15	175*; 335*	0.68	N
RR Eri	6.80–7.62V	94.6	0.22	93:	90/0.02	0.33	N
RS Gem	9.1–12V	140:	0.27	**147:**; **270.3**/0.22	150*; 270/0.15	0.64	N
RT Ori	9.7–11.8p	321	0.34	351:	—	0.57	N:
RT Psc	8.2–10.4p	70	0.27	**515.7**/0.20	525/0.08	0.69	N
RU Per	10–12V	170:	0.22	**93**/0.05; **602:**	90/0.02; 600	0.33	N
RV Mon	6.88–7.7V	121.3	0.31	**585**/0.1:; **979**/0.15	500; 1000	0.50:	Y:
RX UMa	9.8–12.2V	195	0.25	**200.2**/0.35	200/0.35	0.63	N
RY Cam	7.7–8.7V	**135.75**	0.23	135.1/0.20	135/0.18	0.81	N
S Lep	6–7.58V	**97.3**	0.19	855.5/0.24	90:/0.02; 854/0.13	0.60	Y:
SW Mon	9.05–10.9V	112	0.37	**103.5**/0.13; **193.5**/0.14	100*; 190*	0.65	N
SY Eri	10.4–11.4p	96:	0.24	330:/0.02	—	0.75:	Y:
SY For	11–12.57B	55:	0.25	**151.3**/0.30	147/0.25	0.82	N
TT Per	9.2–10.6p	82	0.28	**2360**/0.08	2400:/0.03	0.43	Y
TT Tau	10.2–12.2p	166.5	0.22	—	—	0.00	N
TU Gem	9.4–12.5p	230	0.25	**215**/0.1:; **2406**/0.1	215/0.03; 2400/0.02	0.50	Y:

Table continued on next page

Table 2. Periodicity analysis of AAVSO visual observations of SRb variables, cont.

Star	*Range*	*P(d)*[1]	δ*v*	*P(d)/Δv[F]*[1]	*P(d)/Δv[SC]*[1]	*k*	*LSP*
TW Aur	9.1–10.6p	150:	0.20	**1350**/0.22	1333/0.08; 285;/0.03	0.40	Y:
UX And	8.2–9.9V	200	0.24	**218.7**/0.23	218/0.13	0.67	N
V Hor	8.7–9.8p	—	0.29	**63**/0.08	65/0.06	0.43:	N
V Lyn	9.5–12.0p	—	0.30	**87.2**/0.24	90/0.1	0.54	N
V Pav	9.3–11.2p	225.4	0.35	—	324:/0.05	0.40	N
V431 Ori	9.3–11.1V	122:	0.49	**273:**; **2400**/0.18	275:; 2400/0.03	0.33	Y
V465 Cas	6.1–7.2V	60	0.23	**97**/0.16; **898.4**/0.16	95/0.01; 900/0.04	0.40	Y
VZ Tel	12.7–14.0V	117.8	0.25	**81.2**/0.21	80/0.2	0.50	N
W Nor	10.3–11.6p	**134.7**	0.25	147/0.2	140:	0.75	N
XZ Aur	11.3–12.5V	250	0.36	—	120:	0.33	N
Z Eri	6.17–7.18V	**74.0**	0.26	78/0.06; **729.0**/0.15	75/0.02; 727/0.04	0.40	Y
Z Psc	6.37–7.49V	155.8	0.27	**155.9**/0.13	157/0.04; 260–300::	0.70	N

[1] *The self–correlation periods marked with an asterisk (*) in column 6 were not independently determined by self–correlation but, for these stars, the forms of the self–correlation diagrams are consistent with the Fourier periods. The periods that we would prefer are shown in bold face in columns 3 and 5.*

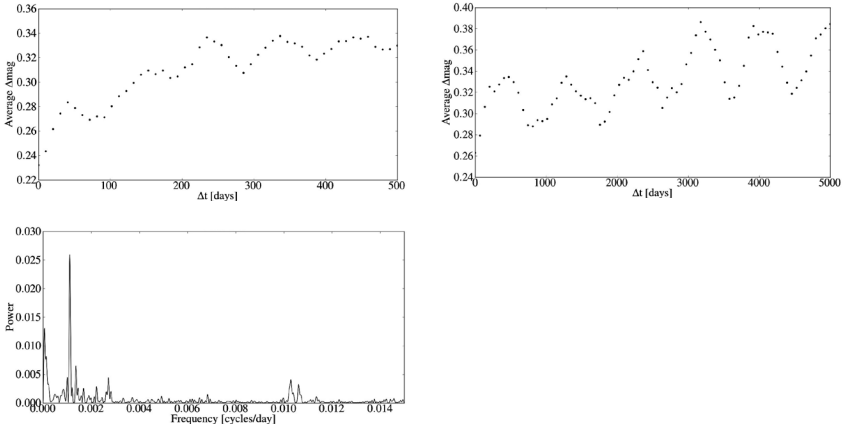

Figure 1. The self-correlation diagrams (top) and Fourier spectrum (bottom) for V465 Cas. The 90-day and 900-day periods show up as repeating minima in the self-correlation diagrams, and as peaks in the Fourier spectrum. The 900-day period is a "long secondary period" whose nature and cause are unknown.

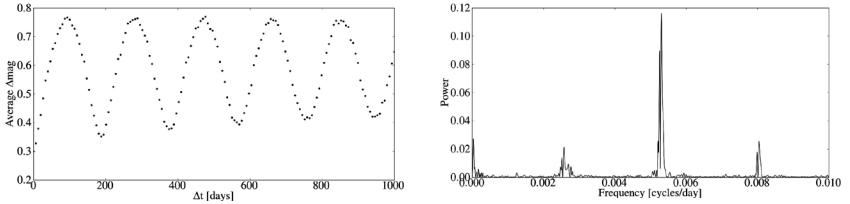

Figure 2. The self-correlation diagram (left) and Fourier spectrum (right) of RW Sgr. There is a single, strong period (and its one-cycle-per-year aliases in the Fourier spectrum).

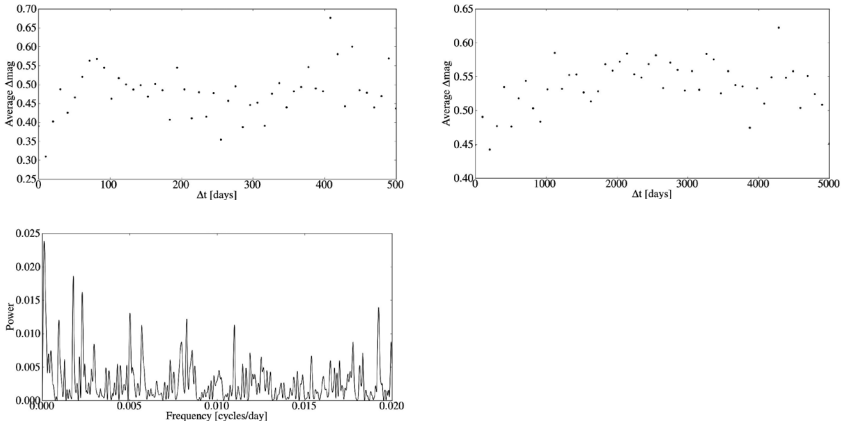

Figure 3. The self-correlation diagrams (top) and Fourier spectrum (bottom) for V Pav. There is no pattern of repeating minima in the self-correlation diagram, or conspicuous peaks in the Fourier spectrum. This star can be classified as irregular.

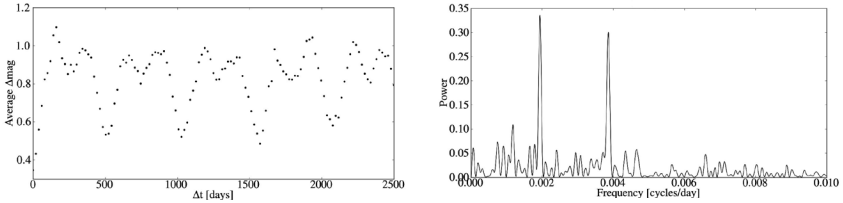

Figure 4. The self-correlation diagram (left) and Fourier spectrum (right) for EP Vel. They are consistent with the presence of two periods of 259 and 515 days, with approximately equal amplitudes.

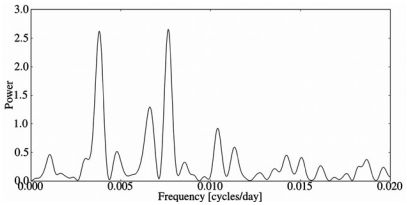

Figure 5. The Fourier spectrum for AY Dra, showing peaks corresponding to periods of 130.8 and 262.8 days, and aliases which are offset in frequency by 0.00274 cycle/day (a period of one year). There is no evidence of an LSP.

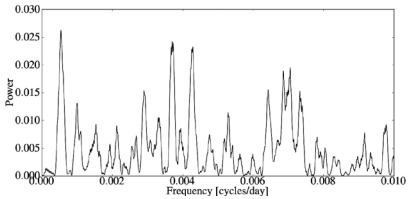

Figure 6. The Fourier spectrum for AI Cyg, showing peaks corresponding to periods of 142 and 273 days, and possibly an LSP. The input visual data are rather sparse.

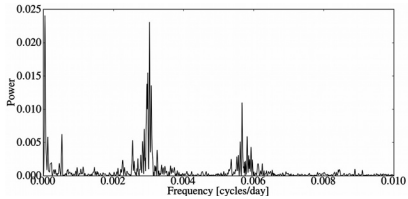

Figure 7. The Fourier spectrum for R Dor, showing peaks corresponding to periods of 176.3 and 329.8 days. The very low frequency signal presumably reflects the very slow, apparently-irregular variations in the mean magnitude of this star.

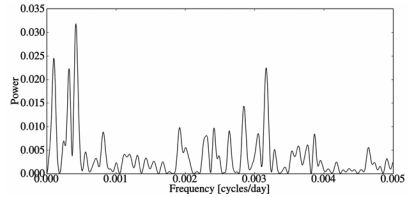

Figure 8. The Fourier spectrum for V431 Ori, showing peaks corresponding to low-amplitude periods of 273 and 2400 days, both visible in the self-correlation diagrams (not shown). The data are very noisy; the average error is 0.49 magnitude.

Period Analysis of AAVSO Visual Observations of Semiregular (SR) Variable Stars. II

John R. Percy
Tomas Kojar
Department of Astronomy and Astrophysics, University of Toronto, Toronto, ON M5S 3H4, Canada; john.percy@utoronto.ca

Received October 26, 2012; revised January 8, 2013; accepted January 8, 2013

Abstract We have used visual measurements from the AAVSO International Database, and Fourier and self-correlation analysis to study the periodicity of 44 pulsating red giants, classified as semiregular: 16 SR, 15 SR:, 12 SRb, and one misclassified RV:. Within each of the three groups, the average degree of periodicity (or regularity) is about the same and there is a wide variety of behavior, from irregular to highly periodic. About a dozen stars show definite or possible double-mode pulsation, and half a dozen show evidence of a long secondary period.

1. Introduction

Pulsating red giants are classified in the *General Catalogue of Variable Stars* (GCVS; Kholopov *et al.* 1985) as Mira (M) variables if their visual amplitude is greater than 2.5 magnitudes, and semiregular (SR) or irregular (L) variables if their visual amplitude is less than that value. SR variables are subdivided into SRa and SRb (both giants), where SRb have less obvious periodicity than SRa, and SRc (supergiants). Percy and Terziev (2011, and references therein) described time-series analysis of AAVSO visual measurements of L-type pulsating red giants. Percy and Tan (2013) carried out a study of 55 SR variables—21 SRa and 34 SRb—using visual measurements from the AAVSO International Database (AID). They found that their behavior ranged from highly periodic to irregular. They used self-correlation analysis to define a simple index k of periodicity. Based on this index, the SRa variables were slightly more periodic than the SRb variables, but the distributions of k overlapped considerably. Of the 55 stars, 11 showed or possibly showed two radial periods, and at least 16 showed or possibly showed a long secondary period, an order of magnitude longer than the primary period.

This paper extends that study to a dozen more SRb variables, and to 31 which are classified as SR or SR:. We chose stars from a version of the old AAVSO Validation List, dating from a few years ago. We used the AAVSO Light Curve Generator to assess whether there was a sufficient number, distribution, and length of measurements for time-series analysis to be meaningful.

2. Data and analysis

We used visual observations of 44 SR variables in the AID, as listed in Table 1. We chose stars which had sufficient measurements but which had not been studied by Kiss *et al.* (1999) or Percy and Tan (2013). In fact, our star list inadvertantly included three stars which had been analyzed by Kiss *et al.* (1999), but this was useful because it provided a random check on the results. Note also that our datasets are over a decade longer than those of Kiss *et al.* (1999). Our list also included four stars which had been observed and analyzed by Tabur *et al.* (2009), a 5.5-year high-precision CCD photometric study of 261 nearby pulsating red giants. See section 3.1 for notes on these stars in common.

We used Fourier analysis and self-correlation analysis; see Percy and Tan (2013) and Percy and Mohammed (2004) for further information about the latter technique. For Fourier analysis, we used the AAVSO's TS software rather than PERIOD04, which we used in our previous papers. A few stars show low-amplitude variability with a period of one year or one month, which we ascribe to the Ceraski effect (Percy and Terziev 2011), a spurious physiological effect of visual observing.

3. Results

Table 1 gives the name of each star, the GCVS type, the *Variable Star Index* (VSX; Watson *et al.* 2012) period, the average observational error as determined from the intercept on the vertical axis of the self-correlation diagram, the *k* index of regularity as defined by Percy and Tan (2013), the presence or absence of a long secondary period (LSP), and information about the period(s) and amplitude(s) which we have determined. Notes about individual stars are contained in section 3.1. As did Percy and Tan (2013), we have indicated our "recommended" periods in bold face. Figures 1 and 2 show self-correlation diagrams and Fourier spectra for two representative stars, FK Pup and RS Cam. Diagrams for several other representative SR stars are given in Percy and Tan (2013).

The average values of *k* for each of the three types of variable are: 0.45 for SR, 0.43 for SR:, and 0.41 for SRb, that is, not significantly different. Percy and Tan (2013) obtained an average *k* value of 0.53 for their SRb stars. In each group, the *k* value ranges from 0.00 (irregular) to 0.8 or higher—distinctly periodic. Each group thus contains stars of a wide variety of regularity types.

3.1 Notes on individual SR stars

BI And There are periods of 165 and 288 days; the former is consistent with the VSX period of 159.5 days.

T Cae There are no obvious periods; the VSX period of 156 days is not apparent.

RS Cam There are periods of 90 and 160–170 days; the first is consistent with the VSX period of 88.6 days. There is also a very weak period of about 1,000 days which may be an LSP. Kiss *et al.* (1999) obtained periods of 966 (0.17), 160 (0.15), and 90 (0.12) days; the numbers in parentheses are the visual amplitudes, in good agreement with our results.

UV Cam There is a one-year period, with an amplitude of only 0.01, which is almost certainly spurious, and due to the Ceraski effect. There is also a possible LSP.

UW Cam There is a 530 ± 10-day period, which is consistent with the VSX period of 544 days.

VZ Cam The VSX period of 23.7 days may be present but, if so, the amplitude is less than 0.01 magnitude. Tabur *et al.* (2009) found several periods, none equal to 23.7 days.

AI Cam There is a period of 186 days, in good agreement with the VSX period of 187.5 days.

X Cnc There are periods of 193 and 371 days; the former is consistent with the VSX period of 180 days.

RT Cnc There is a weak period of about 90 days, which is consistent with the VSX period of 90.04 days. Kiss *et al.* (1999) found periods of 1,870 (0.08), 350 (0.08), and 193 (0.09) days; the numbers in parentheses are the visual amplitudes.

BC CMi There is a period of about 363 days; the amplitude (0.07) is a bit large for it to be a spurious (Ceraski effect) period. There is a probable 4,500-day LSP. The VSX period of 35 days, if present, has an amplitude less than 0.01. Tabur *et al.* (2009) found periods of 27.7, 143.3, and 208.3 days. This suggests that our 363-day period may be spurious.

AC Car The data are scattered, and the results uncertain, but there do not appear to be any significant periods; in particular, the VSX period of 99: days does not appear to be present.

V393 Cas There is a possible one-year period (probably spurious), but the amplitude is only 0.01 magnitude.

RS Cet There is a possible 250-day period but the amplitude is only 0.035 magnitude.

V1805 Cyg There is a period of 104 days, and possibly one of 55 days, and very possibly an LSP of 750 days.

LV Del This star is classified as RV: but the colors are indicative of a pulsating red giant. It has no visual measurements, but we analyzed about 60 V measurements. There are suggestions of periods of 9 and 100 days.

BG Dra There is a coherent period of 180.5 days.

BF Eri The data are sparse, and the results uncertain. The VSX period of 198 days does not appear to be present. The most likely period is 29 days.

Y Gem There are periods of 148 and 290 days; the VXS period is 160: days.

BQ Gem There are possible periods of 950 days, and half this value, but the amplitude is only 0.03 magnitude.

V566 Her The star is essentially non-variable.

RT Hya The 254-day period is not inconsistent with the VSX period of 245.5 days, but our results definitely favor the longer period. Kiss *et al.* (1999) obtained a single period of 255 days, with a visual amplitude of 0.20, in good agreement with our result.

AK Hya There is a period of 389 days; the VSX period of 75 days is not present in our data. Tabur *et al.* (2009) obtained periods of 78.6, 88.7, and 133.7 days.

HM Lib There is a period of 363.4 days, which is close to one year, but the amplitude seems too large for this to be a spurious (Ceraski) effect.

SV Lyn There is a period of 64.4 days, which is consistent with the VSX period of 70: days.

SX Mon There is a period of 400 days in the self-correlation diagram, but that period is not obvious in the Fourier spectrum. The VSX period of 77.67 days does not appear to be present.

EG Mus The results are uncertain; there are possible periods of 25 and 400 days.

CK Ori The star is essentially non-variable.

GP Ori There are periods of 183 and 351 days. The VSX period of 370: days may refer to the latter.

AZ Per There appears to be a period of 200–300 days. The VSX period is 305: days.

V466 Per The data are sparse, and the results uncertain, but there appears to be a 60-day period; there is no VSX period.

R Pic There is a period of 167 days, which is consistent with the VSX period of 170.9 days.

TV Psc There is a weak signal at a period of 50 days (consistent with the VSX period of 49.1 days) but the amplitude is only 0.015 magnitude. Tabur *et al.* (2009) obtained periods of 55.1, 216.5, and 266.7 days.

RT Pup There is a strong one-year period in the Fourier spectrum, but not in the self-correlation diagram; there is a 1,990-day LSP. The VSX period of 100: days does not appear to be present.

FK Pup Data are sparse; periods of 250 and/or 500 days may be present.

T Ret There are periods of 57 and (possibly) 101 days; the former is consistent with the VSX period of 59.7 days.

V4152 Sgr There appears to be a period of 363 days, and the amplitude is a bit too large to be spurious. The VSX period of 20.0 days does not appear to be present.

FG Ser The results are complicated. There seems to be a 370-day period with an amplitude (0.15 magnitude) which is too large to be spurious, and a possible 120-day period.

W Sex A 201-day period is present. There is no evidence for the VSX period of 134 days.

X Sex A period of 205 days is present.

TU Tau A period of 207 days is present, in good agreement with the VSX period of 200.2 days; a period of 416 days may also be present.

RZ UMa There are periods of 147 and 247 days, but no evidence for an LSP. The VSX period of 115 days does not appear to be present.

RR UMi No periods stand out. In particular: the VSX period of 43.3 days, if present, has an amplitude less than 0.01.

X Vel There appears to be a period of about 300 days, but it does not stand out in the Fourier spectrum. There is no evidence for the VSX period of 140 days.

NSV 3043 There are periods of 373 and (possibly) 182 days. The VSX period of 28.4 days does not appear to be present.

4. Discussion

The mean values of k for the three classification types are about the same. This amplifies the conclusion of Percy and Tan (2013) that there is much overlap between SRa and SRb types. In other words, the types are only marginally meaningful.

For about 70 percent of the stars in Table 1, our results provide new or improved periods for the stars, and/or information about their amplitudes and possible long secondary periods. Therefore, there is useful science within these archival visual observations!

As Percy and Tan (2013) found in their study, the ratio of the radial periods in double-mode SR stars lies in the range 0.48 to 0.58, being slightly greater for shorter-period stars.

Very few of the stars in Table 1 show long secondary periods (LSPs). This may be partly because the stars in this study are, on average, less studied and less variable than those studied by Percy and Tan (2013); most of these are classified only as SR or SR:. The number and extent of the measurements are also smaller, on average. This makes it more difficult to detect long-term variations which could truly be described as "periodic." The cause of these long secondary periods is presently unknown (Nicholls *et al.* 2009).

As in our previous studies of SR and L variables, using visual observations, we occasionally find low-amplitude periods of about one year, which may be due to the Ceraski effect, a physiological effect which is a result of the visual observing procedure. When the period that we find is of low amplitude and equal to one year, within the errors of determination, it is not possible to be sure whether the period is real or spurious. PEP or CCD observations would help.

There are still some SR variables in the AID with sufficient measurements for analysis—but very few. We have "harvested" most of the variables which are ripe for analysis. Any with fewer observations would be even more challenging to analyze and interpret.

This project, like our previous projects, has three goals: to do useful science with AAVSO data—especially visual data; to provide students such as co-author Kojar with projects which develop and integrate science and math skills; and to show AAVSO observers how their measurements contribute to science and education. We believe that we have succeeded in those goals.

5. Conclusions

We have studied the periodicity of 44 pulsating red giants of types SR, SR:, or SRb, using visual measurements from the AAVSO International Database, and Fourier and self-correlation analysis. We find new or improved periods for most of these stars. For each of the three types, the degree of periodicity ranges from high to nearly none, but is about the same on average for each group. A dozen of the stars show definite or possible double-mode pulsation, and about half a dozen show long secondary periods of unknown cause. The results of this and our previous papers show that there is still significant science to be found in the AAVSO's database of visual measurements.

6. Acknowledgements

We thank the hundreds of AAVSO observers who made the observations which were used in this project, and we thank the AAVSO staff for processing and archiving the measurements. We also thank the referee for useful suggestions. This project was supported by the University of Toronto Work-Study Program. It made use of the SIMBAD database, which is operated by CDS, Strasbourg, France.

References

Kholopov, P. N., *et al.* 1985, *General Catalogue of Variable Stars*, 4th ed., Moscow.

Kiss, L. L., Szatmáry, K., Cadmus, R. R., Jr., and Mattei, J. A. 1999, *Astron. Astrophys.*, **346**, 542.

Nicholls, C. P., Wood, P. R., Cioni, M.-R. L., and Soszyński, I. 2009, *Mon. Not. Roy. Astron. Soc.*, **399**, 2063.

Percy, J. R., and Mohammed, F. 2004, *J. Amer. Assoc. Var. Star Obs.*, **32**, 9.

Percy, J. R., and Tan, P. J. 2013, *J. Amer. Assoc. Var. Star Obs.*, **41**, 1.

Percy, J. R., and Terziev, E. 2011, *J. Amer. Assoc. Var. Star Obs.*, **39**, 1.

Tabur, V., Bedding, T. R., Kiss, L. L., Moon, T. T., Szeidl, B., and Kjeldsen, H., 2009, *Mon. Not. Roy. Astron. Soc.*, **400**, 1945.

Watson, C. L., *et al.* 2012, *Variable Star Index* (VSX; http://www.aavso.org/vsx/).

Table 1. Periodicity analysis of AAVSO visual observations of SR variables.

Star	*Type*	*VSXP(d)*	δ*v*	*k*	*LSP?*	*Period(s)/Amplitude(s) (days)*
BI And	SR	**159.5**	0.20	0.22	N	165/0.10, 288/0.10
T Cae	SR	156	0.28	0.00	N	none
RS Cam	SRb	**88.6**	0.27	0.69	Y	90/0.15, 160–170/0.05, 1000/0.03
UV Cam	SR:	294:	0.34	0.00	Y?	year/0.02, 7000:/0.05
UW Cam	SR	**544**	0.15	0.62	N	530 ± 10/0.25
VZ Cam	SR	23.7	0.15	0.17	N	none:
AI Cam	SR:	**187.5**	0.10	0.71	N	186:
X Cnc	SRb	180	0.27	0.6:	N	**193**/0.06, **371**/0.08
RT Cnc	SRb	**90.04**	0.32	0.33:	N	90 ± 10/0.02
BC CMi	SRb	35	0.13	0.55	Y?	363(year?)/0.07, 4500:/0.07
AC Car	SRb	99:	0.15	0.00	N	none:
V393 Cas	SR	393	0.19	0.00	N?	year/0.01
RS Cet	SR:	—	0.18	0.00	N?	250:/0.035
V1805 Cyg	SR:	—	0.05	0.59	Y?	**104**/0.1, 55:/0.05, 750/0.03
LV Del	RV:	—	0.05V	—	N?	9:, 100: (V data)
BG Dra	SR:	—	0.14	0.79	N	**180.5**/0.50
BF Eri	SR	198	0.25	0.3:	N	29:/0.1,
Y Gem	SRb	160:	0.28	0.53	N	**148**/0.05, **290**/0.05
BQ Gem	SRb	50:	0.17	0.7:	N	475:/0.03, 950:/0.02
V566 Her	SR:	137	0.20	0.00	N	non-var?
RT Hya	SRb	245.5	0.27	0.79	N	**254**/0.20
AK Hya	SRb	75	0.12	0.43	Y?	**389**/0.05
HM Lib	SR:	—	0.09	0.88	N	**363.4**/0.15
SV Lyn	SRb	70:	0.25	0.00	N	**64.4**/0.04, year/0.03
SX Mon	SR	77.67	0.25	1.00	?	400:/0.1:
EG Mus	SR:	140:	0.30	0.47	N	25:, 120:/0.02, 400/0.10
CK Ori	SR:	—	0.21	0.00	N	non-var?
GP Ori	SR:	370:	0.40	0.83	N?	**183**/0.31, **351**/0.23
AZ Per	SR	**305:**	0.15	0.90	N	200–300/0.1
V466 Per	SR	—	0.25	0.65	N	60:/0.10
R Pic	SR	**168**	0.30	0.67	N	167/0.60
TV Psc	SR	**49.1**	0.17	0.3:	N	50:/0.015
RT Pup	SRb	100:	0.45	0.00	Y	year?, 1990/0.07
FK Pup	SR	502	0.25	0.56	N?	250:/0.15, 500:/0.15
T Ret	SR	**59.7**	0.15	0.33	N	57/0.05, 101/0.05

Table continued on next page

Table 1. Periodicity analysis of AAVSO visual observations of SR variables, cont.

Star	*Type*	*VSXP(d)*	δ*v*	*k*	*LSP?*	*Period(s)/Amplitude(s) (days)*
V4152 Sgr	SR:	20.0	0.31	0.36	N?	363(year?)/0.06
FG Ser	SR:	—	0.30	0.43	N	370:/0.15, 120:
W Sex	SR	134	0.35	0.62	N	**201**/0.07
X Sex	SR:	—	0.20	0.68	N	**205**/0.20
TU Tau	SR:	**200.2**	0.50	0.7:	N	207/0.07, 416:/0.06
RZ UMa	SRb	115	0.28	0.29	N	**147**/0.03, **247**/0.05
RR UMi	SR:	43.3	0.18	0.00	N?	none
X Vel	SR	140:	0.35	0.47	N?	year:/0.05
NSV3043	SR	28.4	0.18	0.53	N	182:/0.05, 373/0.05

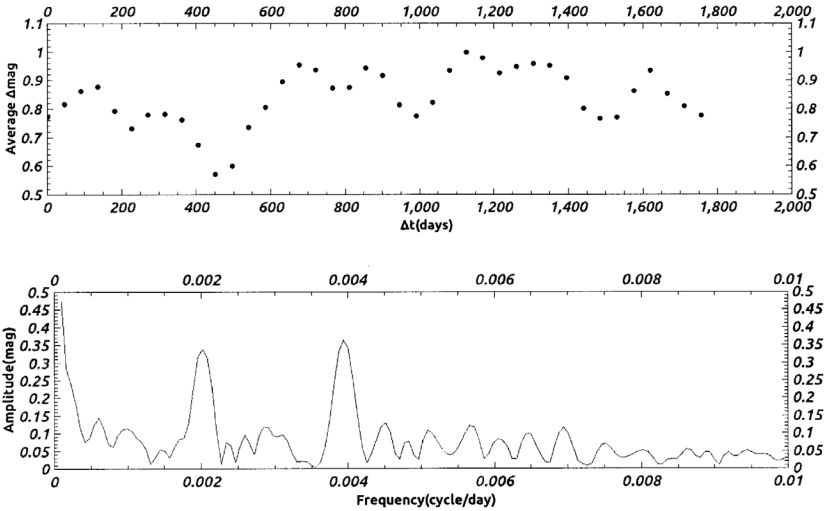

Figure 1. Self-correlation diagram (top) and Fourier spectrum (bottom) for FK Pup. Periods of approximately 250 and 500 days are present, producing the alternating deep and shallow minima in the self-correlation diagram, and the two peaks in the Fourier spectrum. The Fourier spectrum rises at very low frequencies, indicating some very slow variations. The VSX period is 502 days.

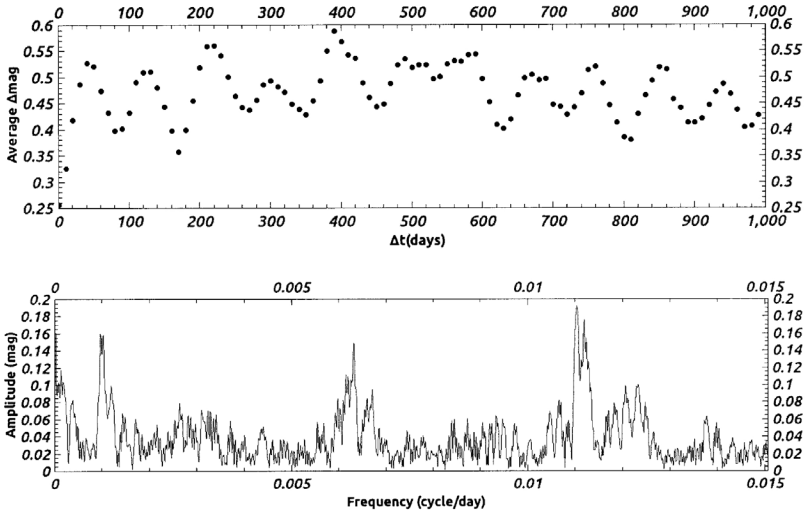

Figure 2. Self-correlation diagram (top) and Fourier spectrum (bottom) for RS Cam. Periods of 90 and 160–170 days are present, producing the alternating deep and shallow minima in the self-correlation diagram, and the two peaks in the Fourier spectrum. There is also a peak at a period of about 1,000 days, which we assume to be a long secondary period. The VSX period is 88.6 days.

Intermediate Report on January 2013 Campaign: Photometry and Spectroscopy of P Cygni

Ernst Pollmann
Emil-Nolde-Str. 12, 51375 Leverkusen, Germany; ernst-pollmann@t-online.de

Wolfgang Vollmann
Dammäckergasse 28/D1/20, 1210 Wien, Austria; vollmann@gmx.at

Received January 21, 2013; revised February 23, 2013; accepted February 25, 2013

Abstract In this campaign on the Luminous Blue Variable star P Cygni, we are trying for the first time, by way of contemporaneous measurements of photometric V brightness and Hα equivalent width (EW), to realize a long-term monitoring of the intrinsic Hα line flux. Photometric and spectroscopic observers started this campaign in November 2008 in order to continue former investigations whose results are based on multi-daily averaging of V and EW. The campaign results enable us to represent the quantitative behavior of the Hα line flux for the time span August 2005 to December 2011, which reflects variabilities in mass-loss rate, stellar wind density, and the ionization structure.

1. Introduction

The international observing campaign, Photometry and Spectroscopy of P Cygni, begun in 2008, is a cooperative project of the American Association of Variable Star Observers (AAVSO), Active-Spectroscopy-in-Astronomy (ASPA), and the Bundesdeutsche Arbeitsgemeinschaft für Veränderliche Sterne (BAV). One goal of the campaign is the monitoring of the behavior of the Hα-line equivalent width (EW) and the contemporaneous changes of the V-band magnitude of P Cyg. Another goal is to gather further information about the intrinsic flux of this spectral line.

P Cyg stars are characterized by very high luminosity, and belong to the spectral classes Ope to Fpe. Their irregular brightness variations, with time scales from weeks to months to years, cover amplitudes up to several V-magnitudes, connected with density inhomogeneity in their mostly spherical shell. P Cyg (Nova Cyg No. 1) was discovered on August 18, 1600, as its brightness suddenly had risen up to 3rd V-magnitude. Also, in the following century, the star showed remarkable changes of brightness from weeks to years, with occasional fadings to the limit of visual visibility. Since 1786 no strong changes of brightness have occurred. A slow brightness increase from 5.2 to 4.9 V took place in 1786 to 1879. Since then the variable has been a B1 supergiant of the "luminous blue variable" (LBV) class.

Typical for these stars are the profiles of individual lines. They consist in the simplest case as an emission line with a blueward-shifted absorption component. Such profiles point to mass-loss of the star in the form of a stellar wind. P Cygni stars are now believed to be in a development phase which lies temporally before the Wolf-Rayet stage of massive stars. De Groot and Lamers (1992) show that the theory of this phase of development is applicable, and in further spectroscopic investigations by Lamers *et al.* (1983), Markova and Puls (2008), Markova *et al.* (2001a, 2001b, 2005), and Richardson *et al.* (2011), the physical properties of P Cyg have been determined: Spectral type—B1 Ia; T_{eff} = 19300 ± 2000 K; R_{star}/R_{sun} = 76 ± 14; L_{star}/L_{sun} = 5.86 ± 0.3.

2. Details

Our campaign assumed that the variability of the EW is caused by variations of the continuum flux and not by variations of the line flux (Markova *et al.* 2001b), which would indicate variations in the stellar wind density. Therefore, the variability of the continuum flux was our primary concern when the properties of the stellar winds and rate of mass loss were studied. To find correlations of photometric to spectroscopic data, an AAVSO call for observations was made at the beginning of the campaign for photoelectric photometry (PEP), and DSLR measurements, based on the Johnson-V system. To date, sixteen photometric observers are involved worldwide.

3. Photometric measurements

Figure 1 shows the comparison of PEP measurements (123) and DSLR measurements (141) through November 4, 2012. Except for occasional outliers (which occur in both) the observations on the 0.01-magnitude accuracy level are rather similar in both forms of measurement.

Photometric and spectroscopic changes in P Cyg seem to be weakly anti-correlated on short- and long-term scales. We observed a total change of 35Å in the equivalent width (EW) of the Hα line, and of ~0.25 magnitude in the V-band brightness. Our observations extend from JD 2454671 (July 23, 2008) through JD 2456244 (November 12, 2012).

4. Results

Figure 2 compares the time behavior of the V-brightness (upper) and the Hα EW (lower) in our campaign. In addition, the data from Richardson *et al.* (2011) have been plotted. As can be seen, the 20-day average V magnitude used does not recognize the quick variations, which were found very clearly in our monitoring.

As can be seen in Figure 2, when EW decreases, the contemporaneous

stellar brightness increases, and vice versa. Strict anti-correlation is expected if the variation of the continuum flux is independent from variations of the EW. If the Hα line flux is constant over time, an increase of the continuum brightness will yield a smaller line flux from the measured EW and vice versa.

To find out if and how the flux obtained from the spectral line profiles varies, the EW measurements were corrected for continuum variations (Pollmann and Bauer 2012). It is important to consider the absolute flux of the line because its variations are caused by the effects of mass loss, stellar wind density, and changes of the ionization state of chemical elements in it. In the current campaign we have already obtained 170 nearly simultaneous measurements of the EW and the flux in the V band.

Figure 3 attempts to display if and to what extent the intrinsic line flux (as continuum-corrected EW) depends on V magnitude. From a statistical point of view one can say that the low (0.25) correlation coefficient (which should be zero after the continuum correction), with consideration of the measurement uncertainties, suggests the conclusion that the Hα line flux is independent of V magnitude.

Comparable investigations of this kind have been published by Richardson *et al.* (2011). The essential difference between these investigations (Figure 3 of Markova *et al.* 2001b) and our work is that they used non-contemporaneous EW and Vphot for their consideration of correlations. Their selected 20-daily average shows a weakly suggested positive correlation, whereas our correlation result in Figure 3 (this paper) delivers an extremely small correlation coefficient of only 0.25 from 170 spectra.

Thus, we have some doubts regarding the persuasive power of the positive correlation (which they found) of the relative flux with the interpolated magnitude. We would be very interested, together with the author of Markova *et al.* (2001a), to perform a new, comprehensive analysis with the data from both investigations to clarify these circumstances.

With consideration of the standard deviation and possibly other kinds of errors, the temporal variation of the line flux of Hα in the plot of Figure 4 will represent the result of variations in the mass loss rate, stellar wind density, and changes of the ionization from August 2005 through November 2012.

Although our data set of 170 spectra is of rather modest extent, we tried nevertheless to find a certain periodicity in the time behavior of the observed Hα line flux.

The usage of the period search program, AVE, did detect three dominant periods in the power spectrum, 242 days, 363 days, and 600 days (Figure 5). Although the 600-day period finds a certain confirmation in investigations about variability of the Hα EW in Markova (1993), our data set is, so far, still too limited to give these three periods a greater degree of confidence.

Variations of the mass-loss rate manifest themselves in P Cyg generally also in a varying absorption depth and proportionally to it in a varying emission

strength of the HeI line at 6678Å, which is developed in the helium-forming zones closer to the star due to its higher excitation potential. While Markova preferentially investigated the correlations of velocity variations to variations of emission and absorption intensity in only 58 spectra at HeI λ3926, λ3867, λ4471, as well as NII λ4630 and SI IV λ4116 (Markova 1986a), our more extensive spectrum collection (> 160 spectra from 2003 to 2012 at HeI λ6678) clearly shows the variability of the emission and absorption intensity and their correlation to each other. Figure 6 shows "extreme" HeI 6678 spectra, taken between April 2003 and November 2012, for illustration of the variability of the absorption depth and the emission strength as a consequence of a variable mass-loss rate of the star (in units of the normalized continuum).

In Figure 7 it can be clearly seen that a portion of the profile at 6674.5 Å varies 2.8/1.5 times stronger than the variation of the emission intensity at 6678.138 Å.

The grey-scale diagram of the 100 spectra in Figure 8 clarifies that the absorption maximum around 6675Å is shifting with time towards shorter wavelengths, which could be due to increasing optical depth as a result of increasing mass-loss.

The plot of absorption depth versus emission strength in Figure 9 shows that both measured variables are related only with a correlation quality of ~0.44. Even if the emission comes by recombination, one would expect that a higher density (= higher mass loss) would produce both more absorption and more emission. The small coefficient of correlation could therefore be an expression for not implausible temperature variations in the stellar wind, whereby the absorption could increase also without change of mass loss, thereby without the emission increasing.

5. Acknowledgements

We are grateful to Dr. John R. Percy and to an anonymous referee for their critical comments which have lead to essential improvements in this work. We also offer many thanks to all the participants of the campaign for their worthwhile contributions and measurements which has made this campaign possible.

The following observers took part in the project: AAVSO (Vmagnitude): A. Ormsby, R. E. Crumrine, J. Fox, K. Hutton, N. Stoikidis, D. Williams, E. G. Williams, C. L. Calia, T. L. Peairs, J. G. Horne, M. Durkin, D. Loughney, W. Vollmann, G. Galli, E. Høeg, and D. R. Garcia. Spectroscopy (Hα-EW): M. Fuji, B. Mauclaire, J. Guarro, B. Hanisch, E. Pollmann, T. Garrel, V. Desnoux, O. Thizy, J. N. Terry, C. Buil, S. Charbonnel, P. Dubreul, A. Lopez, T. Lemoult, F. Teyssier, and from the literature, Balan *et al.* (2010) and Markova (1986a).

The EW, V(phot), and line flux data are available at the following website: http://astrospectroscopy.de/Data_PCyg_Campaign/Campaign_data_2013.txt

References

Balan, A., Tycner, C., Zavala, R. T., Benson, J. A., Hutter, D. J., and Templeton, M. 2010, *Astron. J.*, **139**, 2269.

De Groot, M. J. H., and Lamers, H. 1992, *Nature*, **355**, 422.

Lamers, H. J. G. L. M., de Groot, M., and Cassatella, A. 1983, *Astron. Astrophys.*, **123**, L8.

Markova, N. 1986a, *Astron. Astrophys.*, **162**, L3.

Markova, N. 1986b, *Astrophys. Space Sci.*, **123**, 5.

Markova, N. 1993, *Astron. Astrophys.*, **273**, 555.

Markova, N. 2000, *Astron. Astrophys., Suppl. Ser.*, **144**, 391.

Markova, N., Morrison, N., Kolka, I., and Markov, H. 2001a, *Astron. Astrophys.*, **376**, 898.

Markova, N., and Puls, J. 2008, *Astron. Astrophys.*, **478**, 823.

Markova, N., Puls, J., Scuderi, S., and Markov, H. 2005, *Astron. Astrophys.*, **440**, 1133.

Markova, N., Scuderi, S., de Groot, M., Markov, H., and Panagia, N. 2001b, *Astron. Astrophys.*, **366**, 935.

Pollmann, E., and Bauer, T. 2012, *J. Amer. Assoc. Var. Star Obs.*, **40**, 894.

Richardson, N. D., Morrison, N. D., Gies, D. R., Markova, N., Hesselbach, E. N., and Percy, J. R. 2011, *Astron. J.*, **141**, 120.

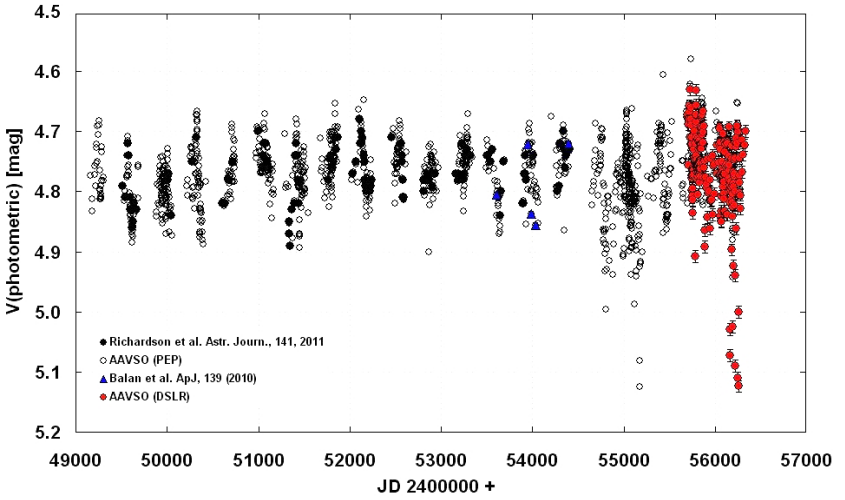

Figure 1. Comparison of AAVSO PEP observations with AAVSO DSLR observations of P Cyg.

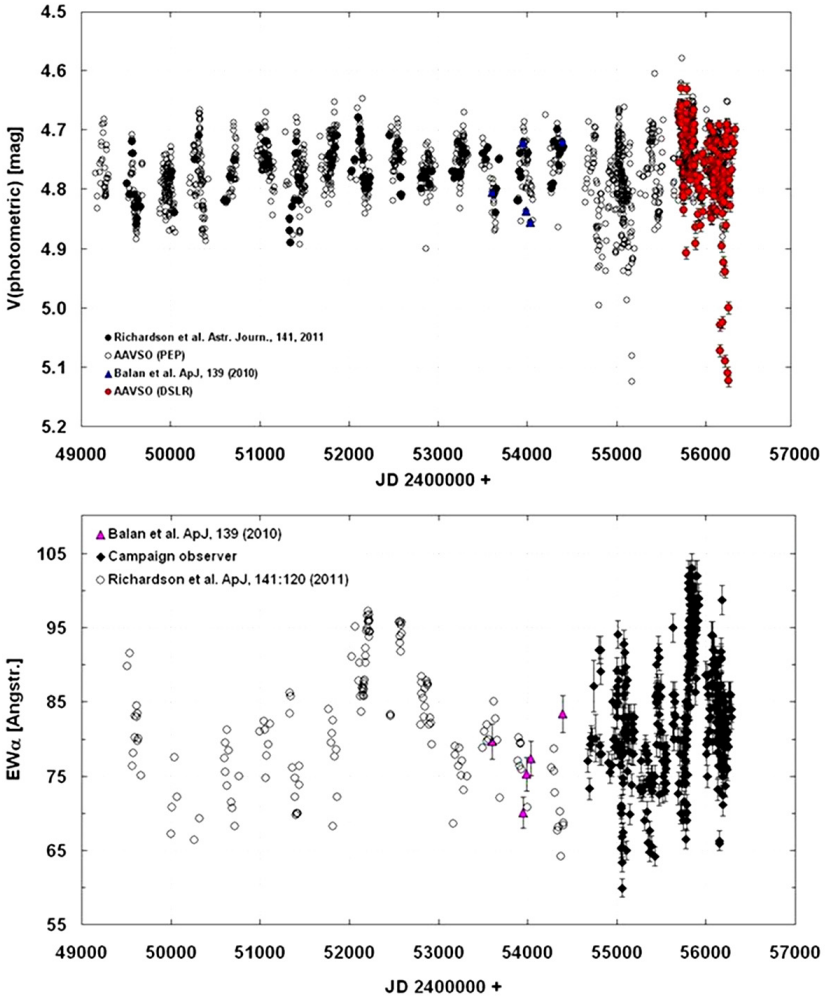

Figure 2. Our V magnitude photometric and spectroscopic observations (upper) and Hα-EW (lower) during the P Cyg campaign (including data of Balan *et al.* 2010 and Richardson *et al.* 2011).

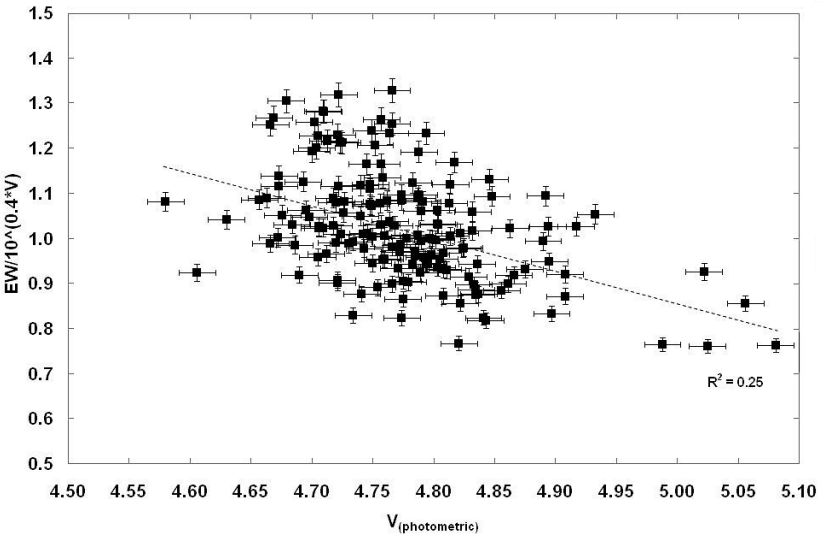

Figure 3. Hα-line flux versus photometric V brightness for P Cyg (170 contemporaneous measurements).

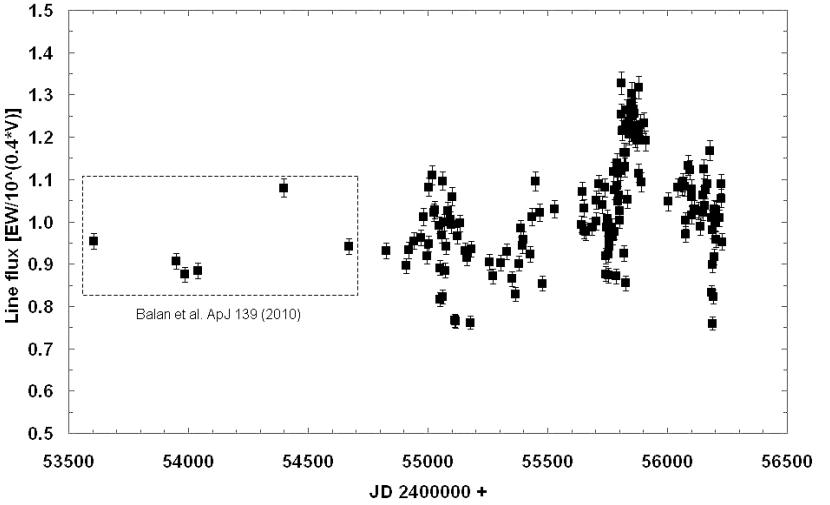

Figure 4. The intrinsic Hα-line flux for P Cyg from JD 2453605 (August 22, 2005) to JD 2455911 (November 12, 2012).

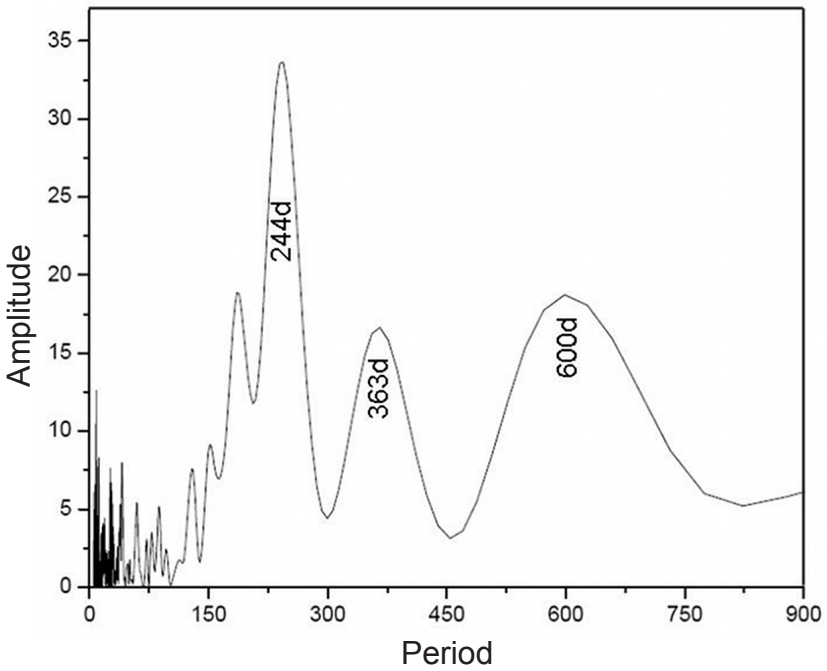

Figure 5. Scargle periodogram with data from Figure 4.

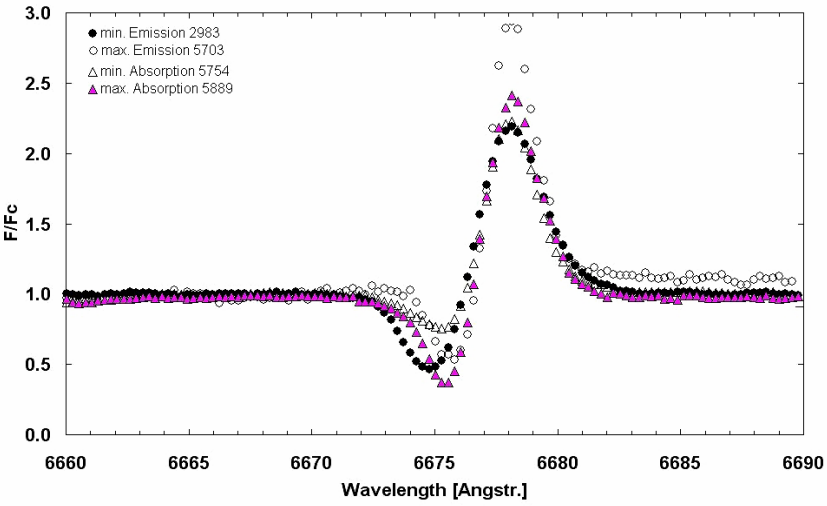

Figure 6. Variability of the absorption depth and emission strength in extreme-profile-spectra of P Cyg (JD 2452983, 2455703, 2455754, 2455889).

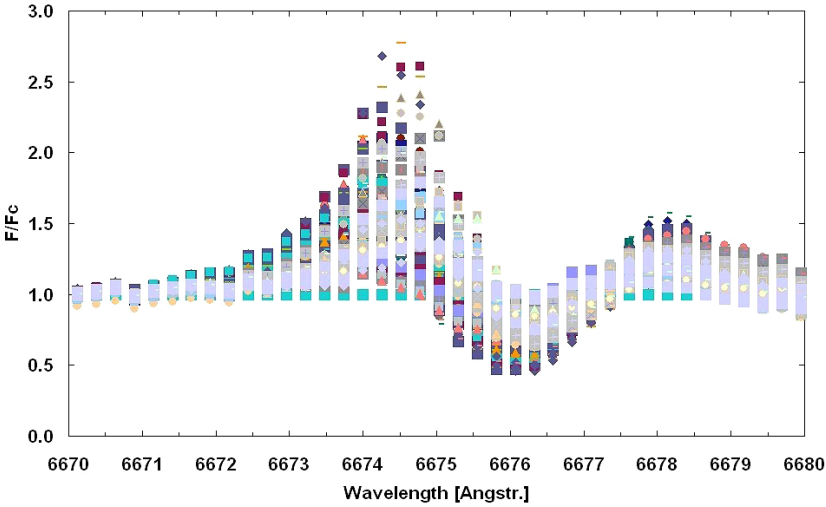

Figure 7. Division spectra with absorption maximum at 6674.5Å related to a maximum-intensity spectrum at JD 2455703 for P Cyg.

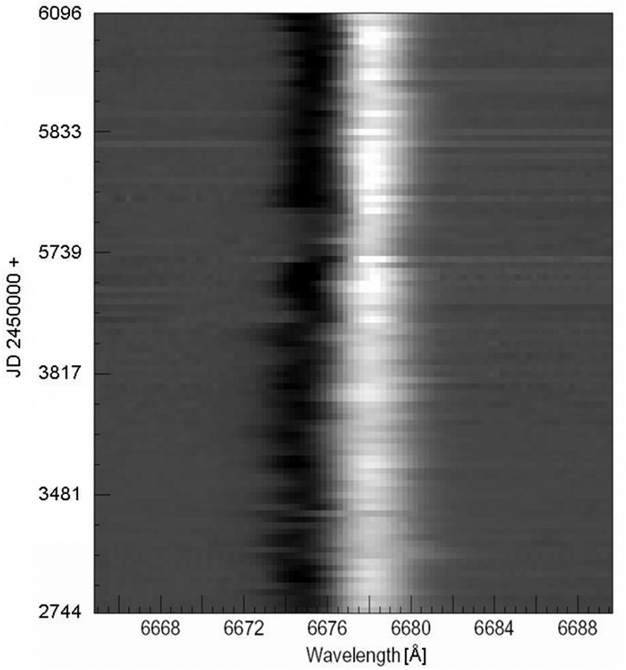

Figure 8. The moving absorption maximum (around 6675Å) of the He6678 line profile with time for P Cyg. 100 Spectra sorted by Julian Date.

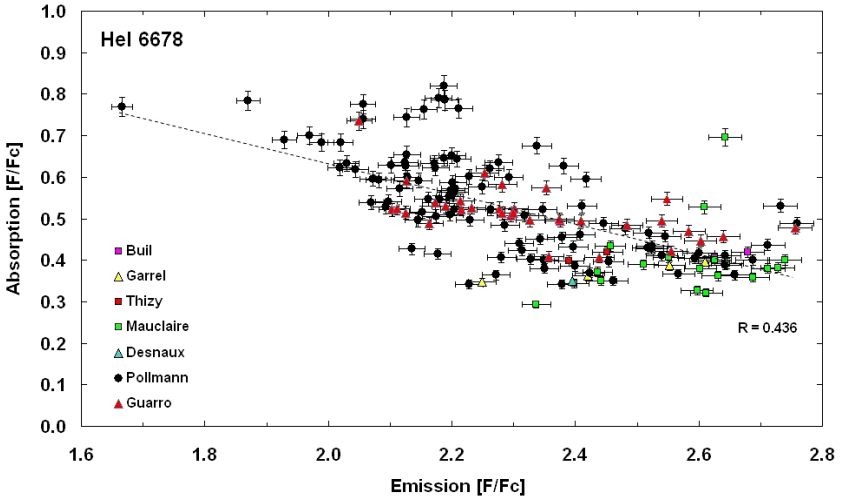

Figure 9. Variability of the absorption depth versus emission strength of the HeI 6678 line (April 2003 until November 2012) for P Cyg.

The Interesting Light Curve and Pulsation Frequencies of KIC 9204718

Garrison Turner
R.A.S.G. Hebrew Academy, Department of Science, Miami Beach, FL 33138; gturner@rasg.org

John Holaday
Purdue University, School of Material Engineering, Lafayette, IN; jholaday@purdue.edu

Received October 22, 2012; revised December 3, 2012; accepted December 4, 2012

Abstract In previous work by Uytterhoeven *et al.* (2011) the Kepler object KIC 9204718 (HD 176843) was identified as a binary system with a δ Scuti-type component. Both long- and short-cadence data were obtained from the MAST archive and analyzed. In this paper we show the results of period analysis on one quarter of short-cadence data in which were obtained two pulsation periods, the dominant of which has a period of 0.026479 day and the secondary of 0.029068 day, respectively. We also present the interesting light curve of the object over several quarters of long-cadence data sets.

1. Introduction

The Kepler satellite has been continually monitoring about 150,000 stars in and near the constellation Cygnus since 2009 with a primary objective of detecting exoplanets, specifically planets close to Earth in size and composition. A secondary objective of the mission deals with asteroseismology. One particularly special type of system in which asteroseismology is useful occurs in binary systems where one component is an intrinsic variable. Kepler is well suited for observing these types of systems as the long-cadence (l.c.) data sequence is well suited for determining the orbital periods of binary systems if they happen to be eclipsing. On the other hand, the short-cadence (s.c.) data sequence is particularly well suited to finding low-amplitude, short-period pulsations in variables such as δ Sct stars. δ Sct stars typically have A–F spectral types and have periods between about 0.02 and 0.3 day (Breger 2000) with low amplitudes.

During a study of stars with spectral types A–F in the Kepler field, Uytterhoeven *et al.* (2011) labeled KIC 9204718 (HD 176843) as a binary system with a δ Sct component. As their goal was to perform analysis on single δ Sct stars, the authors did not attempt to determine any pulsation periods for δ Sct stars in binary systems.

2. Observations

The l.c. data are obtained by making observations every thirty minutes for a three-month span, whereas the s.c. data are taken every minute for about one month (Uytterhoeven *et al.* 2011). Typically, the number of usable data points in an l.c. data set is around 4,000. In contrast, there are about 40,000 usable points in an s.c. data set. An overview of the mission characteristics and instrumentation can be found in Borucki *et al.* (2008).

For the present study, the l.c. data were obtained from 2009 May 2 UT through 2010 September 22 (quarters 1–6 of six quarters in the study). The s.c. observations were obtained from 2009 November 21 UT through 2009 December 17 (third quarter). Table 1 shows the observation information taken from the MAST website (http://archive.stsci.edu/). KIC 9204718 has a magnitude of 8.767 and has coordinates of R.A. 19^{h} 00^{m} 03.362^{s}, Dec. +45° 36' 27.54" (J2000).

3. Analysis

The s.c. data contained a total of almost 40,000 data points. The raw fluxes for this object were in the range of 10^{5} for the s.c. data (photometric errors, while existent, are orders of magnitude smaller than the fluxes, and thus are neglected). Each data point was then divided by the average of the set for normalization. This allows the various pixel variations on the CCD chips on the satellite to be averaged out and the data sets strung together. The resulting data were then fit with second-degree polynomials to eliminate any effects in the light curve not due to pulsation (such as brightening or dimming apparent in the l.c. light curve, see Figure 5). Figure 1 shows a representative sample of the s.c. data after the polynomial fitting. Note the light curve shows evidence of beating. Period analysis was then performed on the resulting data set using PERANSO (Vanmunster 2007) with the Lomb-Scargle technique (Lomb 1976; Scargle 1982). The period analysis found two significant periods of 0.026479 ± 0.000003 and 0.029068 ± 0.000004 day, respectively, both of which are in the δ Sct regime and which confirms the presence of the beats. These peaks correspond to the highest thetas found in the period analysis (theta is the Lomb-Scargle statistic). The resulting period analysis was then prewhitened to remove the 0.026479-day peak. The resulting peak found was at a period of 0.029068 day, thus bolstering the likelihood that both peaks correspond to physical pulsations rather than any spurious periods. Figure 2 shows the resulting power spectrum of the initial period analysis, while Figure 3 shows the power spectrum after prewhitening. Figure 4 shows the data phased onto the 0.026479-day period. The un-normalized fluxes were then converted to a magnitude scale with all of the preceding analysis done to find the amplitude in variability. The amplitudes

were measured using the half-amplitude method. The primary amplitude was found to be about 0.33 mmag while the secondary amplitude was found to be about 0.22 mmag.

The l.c. data were analyzed similarly with a total of close to 24,000 data points. An average for each data set was found and then each flux was divided by this average for normalization. Once this procedure was done, the data sets for all the quarters were strung together and plotted as shown in Figure 5. As can be seen, the light curve is very irregular with various upward and downward trends throughout. It is thought that the two significant downward trends are instrumental effects. There is also a periodicity running through the data that should be on the order of days. Uytterhoeven *et al.* (2011) labeled this object as a binary and not as an eclipsing binary; it is fairly conclusive that the periodic variability is not due to eclipsing phenomena as the amplitude of the variation (see description above) is ~ 0.2 mmag. Period analysis was performed on the data with the intervals of about 150–450 and 550–650 days with a total of almost 18,000 data points. The determined period was found to be 8.6946 ± 0.0.0141 days, which would also exclude γ Doradus-type pulsations. Therefore, at the current moment it is unknown what might be causing the variability. The power spectrum is shown in Figure 6 and the phase diagram (normalized flux) is in Figure 7. Closer inspection of the l.c. power spectrum shows some peaks at about 0.9, 1.8, 4.3, and 5.4, and 6.0 days. To investigate whether these peaks may be real or not, the power spectrum was pre-whitened, removing the ~8.7-day peak. Figure 8 shows the pre-whitened power spectrum which indicates the 4.3-day peak may be spurious while the others remain. Since γ Dor stars pulsate between about 8 hours and 3 days (Uytterhoeven *et al.* 2011), this object may be a hybrid δ Sct/γ Dor object. The periods in the γ Dor regime are found at 0.9133 ± 0.0004 and 1.8259 ± 0.0013 day. The amplitude of the 1.8259-day period was found to be about 0.01 mmag. It is assumed that the 0.9133-day peak has a similar amplitude. There is also a peak at about 5.43 days, although this is out of the γ Dor regime.

In general, the amplitudes of these periods are much smaller than periods detected from ground-based observations (which are generally on the order of a few mmag.) This is due to the precision characteristic of the Kepler satellite. On the other hand, objects are classified as hybrid stars as long as detected frequencies are in each respective regime, the amplitudes are similar, and at least two periods are found in each regime (Uytterhoeven *et al.* 2011). Thus it is concluded that this object may a hybrid pulsator.

4. Conclusion

We have presented evidence for pulsation in KIC 9204718. Uytterhoeven *et al.* (2011) indicated the system is a binary with a pulsating component but did not attempt to find any pulsation periods. Analysis of over 40,000 data

points using the short-cadence method found two dominant pulsation periods, 0.026479 day and 0.029068 day, respectively.

We also wanted to investigate the behavior of the light curve over longer intervals; therefore we plotted the normalized flux of several quarters of the Kepler mission. The resulting light curve shows curious downward trends which are thought to be instrumental. A period of 8.6946 days and low amplitude also runs through the data. At the present time, the cause of the variability is unknown. Evidence for γ Dor-type variability is also given, with periods of 0.9311 and 1.8259 day shown in the pre-whitened power spectrum. Clearly this object deserves further study to uncover some of its curiosities.

5. Acknowledgement

The authors would like to thank an anonymous referee for helpful comments which aided in the writing and refinement of this paper.

References

Borucki, W., *et al.* 2008, in *Exoplanets: Detection, Formation and Dynamics*, eds. Yi-S. Sun, S. F. Mello, and J.-L. Zhou, IAU Symp. 249, Cambridge Univ. Press, Cambridge, 17.

Breger, M. 2000, in *Delta Scuti and Related Stars, Reference Handbook and Proceedings of the 6th Vienna Workshop in Astrophysics*, eds. M. Breger and M. H. Montgomery, ASP Conf. Ser. 210, Astron. Soc. Pacific, San Francisco, 3.

Lomb, N. R. 1976, *Astrophys. Space Sci.*, **39**, 447.

Scargle, J. D. 1982, *Astrophys. J.*, **263**, 835

Uytterhoeven, K., *et al.* 2011, *Astron. Astrophys.*, **534**, A125.

Vanmunster, T., 2007, PERANSO period analysis software (http://www.peranso.com).

Table 1. Summary of the observations by Kepler for KIC 9204718. The data set designation is indicated, along with the quarter, and start and end times for each set. The data type is indicated as either long-cadence (l.c.) or short-cadence (s.c.), and the number of usable data points from each set N is given.

Data Set	*Quarter*	*Start Time*	*End Time*	*Data Type*	*N*
2009131105131	0	2009-05-02 00:54:56	2009-05-11 17:51:31	l.c.	476
2009166943257	1	2009-05-13 00:15:49	2009-06-15 11:32:57	l.c.	1639
2009259160929	2	2009-06-20 00:25:09	2009-09-16 23:09:29	l.c.	4070
2009350155506	3	2009-09-18 17:19:58	2009-12-16 23:55:06	l.c.	4133
2010078095331	4	2009-12-19 21:03:56	2010-03-19 16:53:31	l.c.	4109
2010174085026	5	2010-03:20 23:47:15	2010-06-23 15:50:26	l.c.	4499
2010265121752	6	2010-06-24 22:44:09	2010-09-22 19:03:09	l.c.	4275
2009350160919	3	2009-11-21 00:22:29	2009-12-17 00:09:19	s.c.	37992

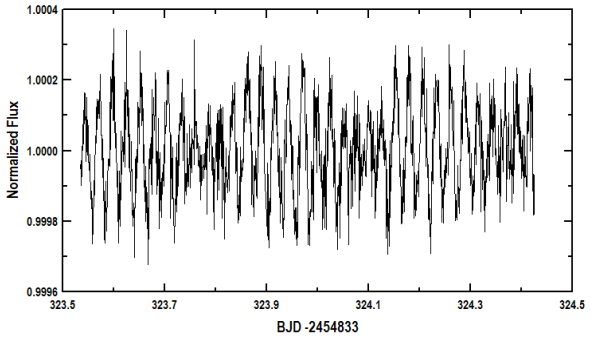

Figure 1. Sample normalized light curve of KIC 9204718 from the Q1 data set. From an initial inspection it appears there is a beat frequency.

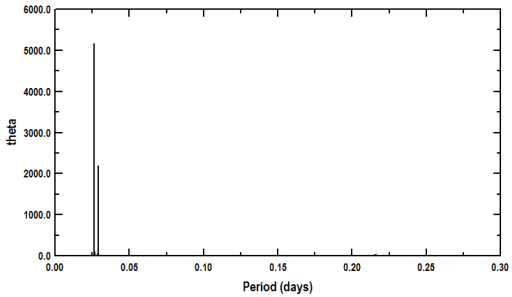

Figure 2. The power spectrum of the short-cadence data showing the 0.026479-day peak. Note the two periods found indicate beats should be observable in the light curve.

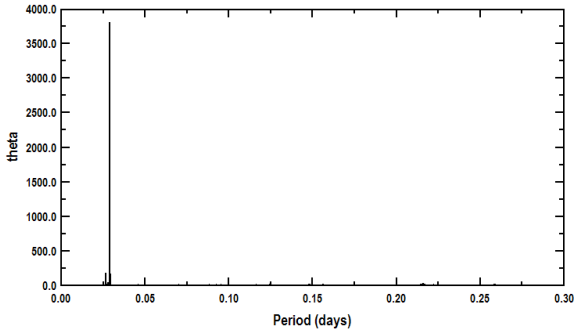

Figure 3. The power spectrum of the short-cadence data set after removing the 0.026479-day peak. The resulting peak is at 0.029068 day.

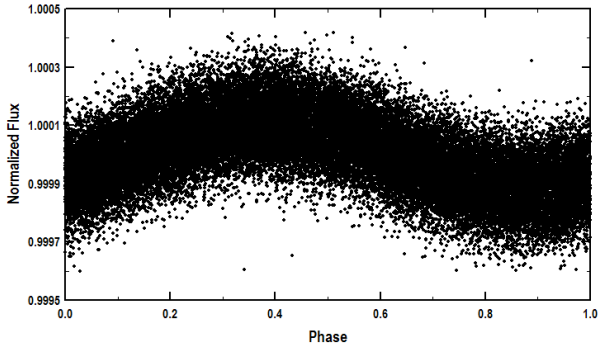

Figure 4. The result of phasing the s.c. data onto the 0.026479-day period.

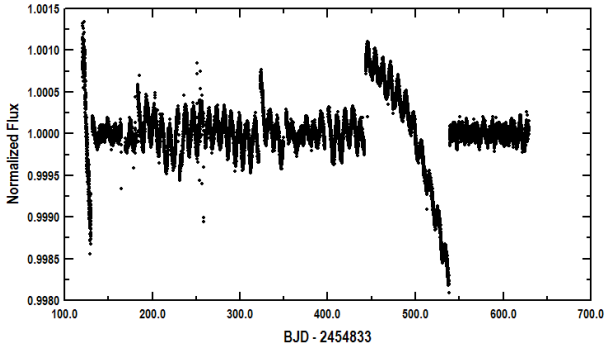

Figure 5. The l.c. light curve of KIC 9204718 over quarters 1–5 after normalization.

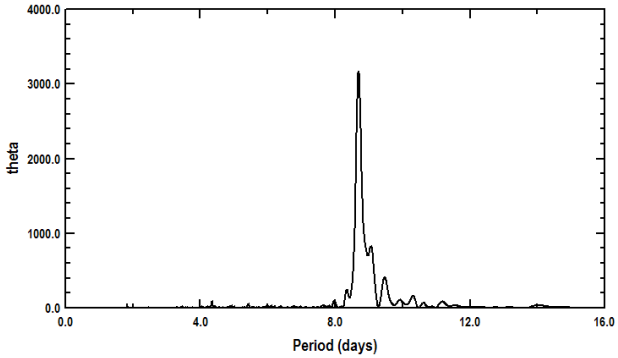

Figure 6. The power spectrum of the l.c. data. The peak is at 8.6946 days.

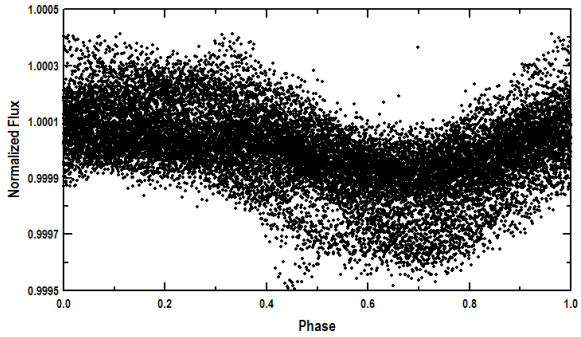

Figure 7. The l.c. data phased onto the 8.6946-day period.

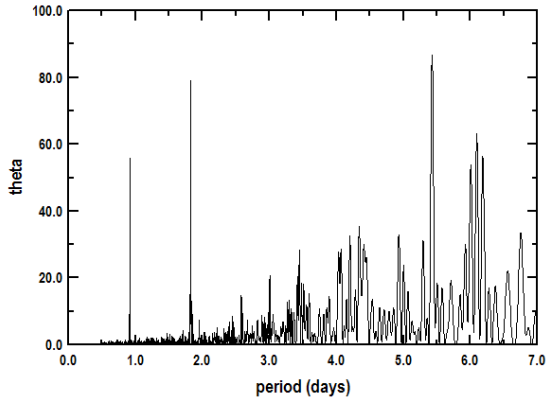

Figure 8. The pre-whitened power spectrum of the l.c. data indicating possible γ-Dor periods at 0.9133 and 1.8259 days.

Nine New Variable Stars in Cygnus and Variability Type Determination of [Wm2007] 1176

Riccardo Furgoni
Keyhole Observatory, Via Fossamana 86, S. Giorgio di Mantova (MN), Italy

and

AAMN Gorgo Astronomical Observatory MPC 434, S. Benedetto Po (MN), Italy; riccardo.furgoni@alice.it

Received October 3, 2012; revised November 28, 2012; accepted December 3, 2012

Abstract I report the discovery of nine new variable stars in Cygnus: five pulsating (VSX J192319.8+280832, VSX J192405.8+280352, VSX J192220.7+275518, VSX J192304.4+280231, VSX J192255.1+274744) and four eclipsing (VSX J192252.4+280217, VSX J192251.4+280456, VSX J192226.0+281019, VSX J192524.9+275342). The variability type of the variable star [WM2007] 1176, that was considered in literature a possible RRC, was found to be a W UMa variable with an obvious O'Connell effect.

1. Introduction

A photometric campaign aimed at the study of the variable star [WM2007] 1176 discovered in the CCD/Transit Instrument Survey (CTI-I; Wetterer and McGraw 2007) database was carried out in order to accurately determine its type. This variable was in fact considered in the literature RRC but the assignment was uncertain. Moreover, all the light curves of the stars present in the imaging field between magnitude 9 V and 16 V have been inspected visually: nine of these were found to present a periodic variability. This study highlights how the simple visual inspection of the light curves is a good way to search for new variables, especially for those who have light variations of the order of a few hundredths of a magnitude and low SNR. In the latter case, the creation of the classic diagram "mean magnitude versus RMS-scatter" does not often immediately reveal variable stars.

2. Instrumentation used

The data were obtained with a Celestron C8 Starbright, a Schmidt-Cassegrain optical configuration with aperture of 203 mm and central obstruction of 34%. The telescope was positioned at coordinates 45° 12' 33" N, 10° 50' 20" E (WGS84) at the Keyhole Observatory, a new roll-off roof structure managed by the author and shown in Figure 1.

The telescope is equipped with a focal reducer Baader Planetarium Alan

Gee II able to bring the focal length from 2030 mm to 1396 mm, and the focal ratio to *f* 6.38 from the original *f* 10.

The pointing is maintained with a Syntha NEQ6 mount with software SYNSCAN 3.27, guided using a Baader Vario Finder telescope equipped with a Barlow lens capable of bringing the focal length of the system to 636 mm and focal ratio of *f* 10.5.

The guide camera is a Magzero MZ-5 with Micron MT9M001 monochrome sensor equipped with an array of 1280X1024 pixel. The size of the pixels is 5.2 μm × 5.2 μm for a resulting sampling of 1.68 arcsec/pixel.

The CCD camera is an SBIG ST8300m with monochrome sensor Kodak KAF8300 equipped with an array of 3352 × 2532 pixels. The pixels are provided with microlenses for improving the quantum efficiency, and the size of the pixels is 5.4 μm × 5.4 μm for a resulting sampling of 0.80 arcsec/pixel. The camera has a resolution of 16 bits with a gain of 0.37e-/ADU and a full-well capacity of 25,500 electrons. The dark current is 0.02e-/pixel/sec at a temperature of –15° C. The typical read noise is 9.3e-RMS.

This camera has some unusual features compared to a CCD normally used in photometry: a high gain and a characteristic peak sensitivity in the V passband. Most of the CCDs normally used in photometry are much more sensitive in the R passband.

The camera is equipped with a 1,000× antiblooming: after exhaustive testing it has been verified that the zone of linear response is between 1,000 and 20,000 ADU, although up to 60,000 ADU the loss of linearity is less than 5%. The CCD is equipped with a single-stage Peltier cell T = 35 ± 0.1° C which allows cooling at a stationary temperature.

3. Data collection

The observed field is centered at coordinates R.A. (J2000) 19^h 23^m 52^s, Dec. +27° 57' 56" and its dimensions are 44.6' × 33.7' with a position angle of 358°.

The observations were performed with the CCD at a temperature of –5° C in binning 1 × 1. The exposure time was 55 seconds with a delay of 1 second between the images and an average download time of 11 seconds per frame. The observations were carried out without the use of photometric filters to maximize the signal-to-noise ratio. The spectral sensitivity of the CCD, as shown in Figure 2, is maximized at a wavelength of 540 nm, making the data more compatible with a magnitude CV (Clear Filter – Zero Point V).

The observations were conducted over seven nights as presented in Table 1.

The CCD control program was Software Bisque's CCDSOFT V5. Once the images were obtained, the calibration frames were taken for a total of 100 dark of 55 seconds at –5° C, 200 darkflat of 2 seconds at –5° C, 100 flat of 2 seconds at –5° C. The darkflats and darks were taken only at the first observation session

and were used for all other sessions. The flats were taken for each session as the position of the CCD camera as well as the focus point could be varied slightly.

The calibration frames were combined with the method of the median and the masterframe obtained was then used for the correction of the images taken. All images were then aligned and an astrometric reduction made to implement the astrometrical coordinate system WCS in the FITS header. These operations were conducted entirely through the use of software MAXIMDL V5.18 made by Diffraction Limited.

4. Deriving a magnitude in unfiltered photometry

Unfortunately it is not always possible to have AAVSO comparison star sequences in all fields of view. Furthermore, by performing unfiltered differential photometry it is crucial to use stars of color as close as possible to the star to be measured in order to avoid a different atmospheric extinction degrading the data obtained, especially when the photometric sessions are long and involve different air masses.

I used this approach to provide a CV magnitude (unfiltered photometry with V-zero point) as accurate and as close to the likely real values for the V magnitude as possible. From an estimate made in this photometric campaign and in others made for the same purpose, it has been observed that in the presence of comparison stars of color similar to the star to be measured, the results obtained with an unfiltered CCD with a peak sensitivity in the V band allow you to get closer to the real values V with deviations of only a few hundredths of magnitude than those obtained using a photometric filter.

Proof of this is evident by analyzing the difference between the average magnitude of the δ Scuti stars discovered in this research campaign with respect to V magnitudes obtained from the magnitude r' in the Carlsberg Meridian Catalog 14 (Copenhagen Univ. Obs. 2006), as described later in this work. Only δ Scuti stars were used for comparison because of the minimal amplitude of their variation. For the other stars the comparison does not make sense since we do not know at what time of their phase CMC14 made a measurement. The results are presented in Table 2.

In detail, the method used was as follows: when by a first rough inspection of the light curve a star was detected as a possible new variable, its color was determined by using the value of J–H on the magnitudes provided by 2MASS All-Sky Catalog of Point Sources (Cutrie *et al.* 2003). The VizieR catalog, operated by CDS in Strasbourg, was searched for stars with a J–H index as close as possible to the candidate variable, a shorter angular distance, and adequate SNR. A comparison star and a check star were identified for each variable in order to provide a V magnitude as correct as possible for the comparison star. Existing photometric data were used when possibile or V magnitudes were derived. The sources used in order of preference were:

APASS (Henden *et al.* 2012): this survey is certainly one of the best available for star magnitude determination in different passbands. Unfortunately, in the observed field there are not APASS data available.

ASAS3 (Pojmański 2002): this survey usually provides precise photometric results for the V passband. The short focal length of the telescopes used, however, produces significant blending problems and sometimes even if a star is listed in a specific position, the data provided regard different stars mixed together. When this phenomenon was evident or suspected (often in the case of a crowded field such as this one), it was decided to not use the ASAS3 data for reference.

TASS MARK IV (Droege *et al.* 2006): this survey provides good photometric results for the V passband. The short focal length of the telescopes used produces problems similar to those found in ASAS3. The data were used in this case with the same criterion as those relating to ASAS3.

UCAC3 (Zacharias *et al.* 2010) and *CMC14* (Copenhagen Univ. Obs. 2006): these surveys provide photometry in different bands with respect to V passband. Transformation equations were used, however, to derive a magnitude in the V passband with reasonable accuracy. The problems of blending are much more rare. The equations used are:

$$V_{\text{Johnson-Cousins}} = 0.6278\ (J_{\text{2MASS}} - K_{\text{2MASS}}) + 0.9947\ \text{r'CMC14}\ (9 < \text{r'} < 16) \quad (1)$$

$$V_{\text{Johnson-Cousins}} = 0.531\ (J_{\text{2MASS}} - K_{\text{2MASS}}) + 0.9060\ \text{fmagUCAC3} + 0.95 \quad (2)$$

Equation (1) for CMC14 is described in Dymock and Myles (2009). Equation (2) for UCAC3 is described in Pavlov (2009).

5. Magnitude determination and period calculation

The star's brightness was measured with MAXIMDL V5.18 software, using the aperture ring method. With a FWHM of the observing sessions at times arrived at values of 4" it was decided to choose values providing an adequate signal-to-noise ratio and the certainty of being able to properly contain the whole flux sent from the star. I have used the following apertures: Aperture radius, 12 pixels; Gap width, 2 to 28 pixels; Annulus thickness, 8 pixels.

Before proceeding further in the analysis, the time of the light curves obtained was heliocentrically corrected (HJD) in order to ensure a perfect compatibility of the data with observations carried out even at a considerable distance in time. The determination of the period was calculated using the software PERIOD04 (Lenz and Breger 2005), using a Discrete Fourier Transform (DFT). The average zero-point (average magnitude of the object) was subtracted from the dataset to prevent the appearance of artifacts centered at frequency 0.0 of the periodogram. The calculation of the uncertainties was carried out with PERIOD04 using the method described in Breger *et al.* (1999).

6. VSX J192319.8+280832

Position (UCAC4): R.A. (J2000) = 19^h 23^m 19.895^s, Dec. (J2000) = +28° 08' 32.27"

Cross Identification: 2MASS J19231989+2808322; GSC 02136-00868; UCAC3 237-177327; UCAC4 591-080941

Variability Type: δ Sct

Magnitude: 13.23 CV (0.03 magnitude amplitude)

Main Period: 0.14296(2) d

Secondary Period: 0.064818(4) d

Epoch Main Period: 2456105.298(2) HJD

Epoch Secondary Period: 2456105.4085(7) HJD

Comparison Star: 2MASS J19233744+2808289

Comp. Star Magnitude: 12.685 V (UCAC3 derived V magnitude)

Check Star: 2MASS J19225994+2809312

Finding chart, phase plots, and Fourier spectrum are shown in Figures 3, 4, 5, and 6.

About this star and all other pulsating stars discovered in this work I want to clarify that they are to the limit of the detection capability of the instrumentation and the only information obtainable from these data is that there exists a periodic pulsation. Considering the color index of these stars, the amplitude of the pulsation, and the duration of the period, there is no possibility that they are anything other than δ Scuti type variables.

7. VSX J192405.8+280352

Position (UCAC4): R.A. (J2000) = 19^h 24^m 05.820^s, Dec. (J2000) = +28° 03' 52.06"

Cross Identification: 2MASS J19240582+2803520; GSC 02133-00013; TYC 2133-13-1; UCAC3 237-178258; UCAC4 591-081338

Variability Type: δ Sct

Magnitude: 11.47 CV (0.01 magnitude amplitude)

Period: 0.0365621(12) d

Epoch: 2456105.4662(4) HJD

Comparison Star: 2MASS J19243630+2808488

Comp. Star Magnitude: 12.289 V (UCAC3 derived V magnitude)

Check Star: 2MASS J19233463+2810322

Finding chart, phase plot, and Fourier spectrum are shown in Figures 7, 8, and 9.

8. VSX J192252.4+280217

Position (UCAC4): R.A. (J2000) = 19^h 22^m 52.436^s, Dec. (J2000) = +28° 02' 17.32"

Cross Identification: 2MASS 19225244+2802175; CMC14 J192252.4+280217; UCAC3 237-176692; UCAC4 591-080622; USNO-B1.0 1180-0416101

Variability Type: eclipsing binary β Per type

Magnitude: maximum 15.37 CV; minimum 17.7: CV

Period: 2.2957(8) d

Epoch: 2456135.468(6) HJD

Comparison Star: 2MASS J19231832+2808483

Comp. Star Magnitude: 12.895 V (UCAC3 derived V magnitude)

Check Star: 2MASS J19222259+2756428

The minimum in CV magnitude was calculated using a binning method due to the very low SNR of the star. Finding chart and phase plot are shown in Figures 10 and 11.

9. VSX J192251.4+280456

Position (UCAC4): R.A. (J2000) = 19^h 22^m 51.419^s, Dec. (J2000) = +28° 04' 56.51"

Cross Identification: 2MASS J19225142+2804564; CMC14 J192251.4+280456; UCAC3 237-176666; UCAC4 591-080609; USNO-B1.0 1180-0416062

Variability Type: eclipsing binary β Lyr type

Magnitude: maximum 13.53 CV; minimum 13.83 CV (secondary minimum 13.75 CV)

Period: 0.3562496(92) d

Epoch: 2456126.4155(6) HJD

Comparison Star: 2MASS J19230552+2802117

Comp. Star Magnitude: 13.492 V (Mean value of UCAC3 derived V magnitude and CMC14 derived V magnitude)

Check Star: 2MASS J19225414+2759330

Finding chart, phase plot, and Fourier spectrum are shown in Figures 12, 13, and 14.

10. VSX J192226.0+281019

Position (UCAC4): R.A. (J2000) = 19^h 22^m 26.026^s, Dec. (J2000) = +28° 10' 19.32"

Cross Identification: 2MASS J19222602+2810193; CMC14 J192226.0+281019; UCAC3 237-176164; UCAC4 591-080337; USNO-B1.0 1181-0395081

Variability Type: eclipsing binary W UMa type

Magnitude: Max 13.04 CV – Min 13.20 CV (possible presence of O'Connell effect)

Period: 0.2852148(26) d

Epoch: 2456135.3331(2) HJD

Comparison Star: 2MASS J19221496+2803136

Comp. Star Magnitude: 12.126 V (Mean value of ASAS3 Vmag, TASS Mark IV Vmag, UCAC3 derived Vmag and CMC14 derived Vmag)

Check Star: 2MASS J19223002+2805008

Finding chart, phase plot, and Fourier spectrum are shown in Figures 15, 16, and 17.

11. VSX J192524.9+275342

Position (UCAC4): R.A. (J2000) = 19^h 25^m 24.927^s, Dec. (J2000) = +27° 53' 42.95"

Cross Identification: 2MASS J19252492+2753429;
CMC14 J192524.9+275342; UCAC3 236-180684; UCAC4 590-083884; USNO-B1.0 1178-0464728

Variability Type: eclipsing binary W UMa type

Magnitude: maximum 14.23 CV; minimum 14.40 CV

Period: 0.518611(13) d

Epoch: 2456126.425(1) HJD

Comparison Star: 2MASS J19250662+2744573

Comp. Star Magnitude: 12.477 V (Mean value of ASAS3 V magnitude, TASS Mark IV V magnitude, UCAC3 derived V magnitude and CMC14 derived V magnitude)

Check Star: 2MASS J19251846+2752372

Finding chart, phase plot, and Fourier spectrum are shown in Figures 18, 19, and 20.

12. VSX J192220.7+275518

Position (UCAC4): R.A. (J2000) = $19^h\ 22^m\ 20.781^s$, Dec. (J2000) = +27° 55' 17.97"

Cross Identification: 2MASS J19222078+2755179; CMC14 J192220.7+275517; UCAC3 236-176830; UCAC4 590-082049; USNO-B1.0 1179-0436072

Variability Type: δ Sct

Magnitude: 12.24 CV (0.02 magnitude amplitude)

Period: 0.075664(5) d

Epoch: 2456135.4681(7) HJD

Comparison Star: 2MASS J19232689+2759395

Comp. Star Magnitude: 11.427 V (Mean value of ASAS3 V magnitude, TASS Mark IV V magnitude, UCAC3 derived V magnitude and CMC14 derived V magnitude)

Check Star: 2MASS J19222757+2754528

Finding chart, phase plot, and Fourier spectrum are shown in Figures 21, 22, and 23.

13. VSX J192304.4+280231

Position (UCAC4): R.A. (J2000) = $19^h\ 23^m\ 04.402^s$, Dec. (J2000) = +28° 02' 31.85"

Cross Identification: 2MASS J19230439+2802318; CMC14 J192304.4+280231; UCAC4 591-080752; USNO-B1.0 1180-0416528

Variability Type: δ Sct

Magnitude: 13.28 CV (0.02 magnitude amplitude)

Period: 0.113080(12) d

Epoch: 2456126.4211(12) HJD

Comparison Star: 2MASS J19232689+2759395

Comp. Star Magnitude: 11.462 V (ASAS3 V magnitude)

Check Star: 2MASS J19222757+2754528

Finding chart, phase plot, and Fourier spectrum are shown in Figures 24, 25, and 26.

14. VSX J192255.1+274744

Position (UCAC4): R.A. (J2000) = 19^h 22^m 55.127^s, Dec. (J2000) = +27° 47' 44.62"

Cross Identification: 2MASS J19225512+2747445; CMC14 J192255.1+274744; UCAC3 236-177521; UCAC4 589-080251; USNO-B1.0 1177-0462865

Variability Type: δ Sct

Magnitude: 12.02 CV (0.02 magnitude amplitude)

Period: 0.069443(5) d

Epoch: 2456125.3931(8) HJD

Comparison Star: 2MASS J19232689+2759395

Comp. Star Magnitude: 11.462 V (ASAS3 V magnitude)

Check Star: 2MASS J19222757+2754528

Finding chart, phase plot, and Fourier spectrum are shown in Figures 27, 28, and 29.

15. [WM2007] 1176

Position (UCAC4): R.A. (J2000) = 19^h 24^m 03.116^s, Dec. (J2000) = +28° 02' 27.64"

Cross Identification: 2MASS J19240312+2802276; CMC14 J192403.1+280227; UCAC3 237-178198; UCAC4 591-081311

Variability Type: eclipsing binary W UMa type

Magnitude: maximum 13.47 V; minimum 13.83 V (secondary maximum 13.50 V), presence of O'Connell effect

Period: 0.613472(1) d

Epoch: 2456126.4101(7) HJD

Comparison Star: 2MASS J19232689+2759395

Comp. Star Magnitude: 11.462 V (ASAS3 V magnitude)

Check Star: 2MASS J19243203+2804542

The magnitude range in the V passband was determined using CTI-I V magnitude data. The period is based on the best fit for both FRIC dataset and CTI-I dataset. The best period for only CTI-I dataset is 0.613470 day: therefore a possibile variation of the period occurred over time. Finding chart, phase plot, and Fourier spectrum are shown in Figures 30, 31, and 32.

16. Acknowledgements

I wish to thank Dr. Patrizia Caviezel for her contribution in discovering the EA-type variable VSX J192252.4+280217. This work has made use of the VizieR catalogue access tool, CDS, Strasbourg, France, and the International Variable Star Index (VSX) operated by the AAVSO. This work has made use of NASA's Astrophysics Data System and data products from the Two Micron All Sky Survey, which is a joint project of the University of Massachusetts and the Infrared Processing and Analysis Center/California Institute of Technology, funded by the National Aeronautics and Space Administration and the National Science Foundation. This work has made use of *ASAS3 Public Catalog*, *Carlsberg Meridian Catalog 14*, the *Third U.S. Naval Observatory CCD Astrograph Catalog* (UCAC3), and the *Fourth U.S. Naval Observatory CCD Astrograph Catalog* (UCAC4).

References

Breger, M., *et al.* 1999, *Astron. Astrophys.*, **349**, 225.

Copenhagen University Observatory, Institute of Astronomy. 2006, *Carlsberg Meridian Catalog 14* (CMC14), Copenhagen Univ. Obs. Inst. Astron., Cambridge.

Cutri, R. M., *et al.* 2003, *The IRSA 2MASS All-Sky Point Source Catalog*, NASA/IPAC Infrared Science Archive (http://irsa.ipac.caltech.edu/applications/Gator/).

Droege, T. F., Richmond, M. W., Sallman, M. P., and Creager, R. P. 2006, *Publ. Astron. Soc. Pacific*, **118**, 1666.

Dymock, R., and Miles, R. 2009, *J. British Astron. Assoc.*, **119**, 149.

Henden, A. A. *et al.* 2012, AAVSO Photometric All-Sky Survey, Data Release 6 (http://www.aavso.org/apass).

Lenz, P., and Breger, M. 2005, *Commun. Asteroseismology*, **146**, 53.

Pavlov, H. 2009, "Deriving a V magnitude from UCAC3" (http://www.hristopavlov.net/Articles/index.html).

Pojmański, G. 2002, *Acta Astron.*, **52**, 397.

Wetterer, C. J., and McGraw, J. T. 2007, *Astron. J.*, **133**, 2883.

Zacharias, N., *et al.* 2010, *Astron. J.*, **139**, 2184.

Table 1. Dates and times of observations.

Date dd-mm-yyyy	*UTC Start hh:mm:ss*	*UTC End[1] hh-mm-ss*	*Useful Exposures*
26-06-2012	21:26:38	00:40:17	170
03-07-2012	20:30:24	00:45:47	221
16-07-2012	20:22:05	00:30:31	217
17-07-2012	20:23:23	00:49:15	232
18-07-2012	20:20:24	23:00:25	140
26-07-2012	20:12:51	01:04:41	255
02-08-2012	19:59:13	22:14:59	118

[1] *When the UTC end exceeds 23:59 it refers to the day after the start of exposures.*

Table 2. Average CV magnitude (CV=Clear passband with V zero-point) of the Delta Scuti stars discovered in this research campaign compared to the V magnitude derived from the magnitude r' in the *Carlsberg Meridian Catalog 14*.

Star	*CMC14 r' mag.*	*2MASS Jmag.*	*2MASS Kmag.*	*CMC 14 Vmag.*	*CV mag Furgoni*	*Abs. Mag. Difference*
VSX J192319.8+280832	13.13	12.08	11.74	13.28	13.23	0.05
VSX J192405.8+280352	11.50	10.76	10.62	11.53	11.47	0.06
VSX J192220.7+275518	12.15	11.30	11.09	12.21	12.24	0.03
VSX J192304.4+280231	13.13	12.15	11.87	13.23	13.28	0.05
VSX J192255.1+274744	11.87	10.99	10.77	11.95	12.02	0.07

Figure 1. The Keyhole Observatory.

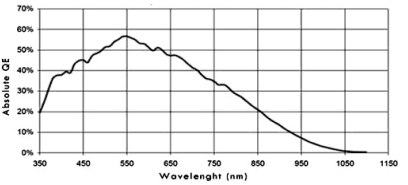

Figure 2. Quantum efficiency of the sensor KAF8300 Monochrome with microlens.

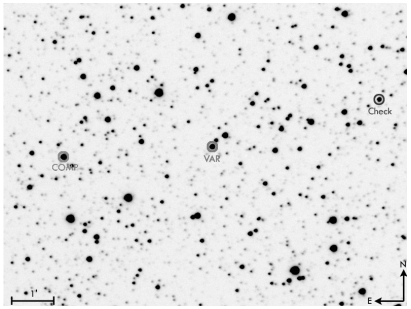

Figure 3. Finding chart of VSX J192319.8+280832. Scale marker indicates one arc minute.

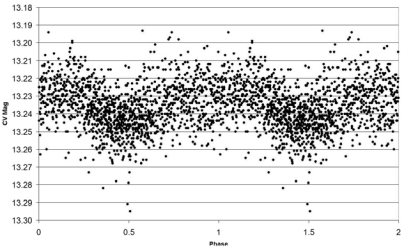

Figure 4. Main period phase plot of VSX J192319.8+280832.

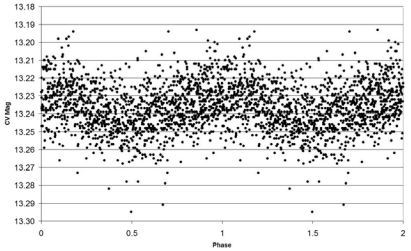

Figure 5. Secondary period phase plot of VSX J192319.8+280832.

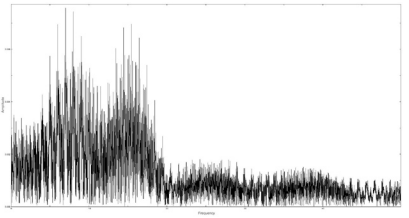

Figure 6. Fourier spectrum of VSX J192319.8+280832.

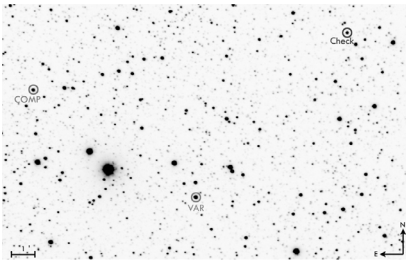

Figure 7. Finding chart of VSX J192405.8+280352.

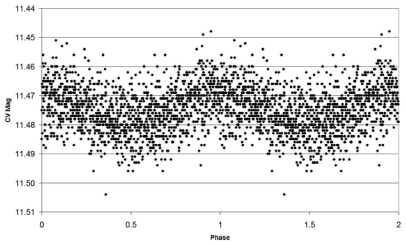

Figure 8. Phase plot of VSX J192405.8+280352.

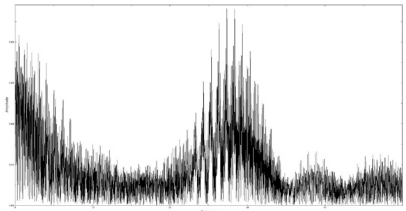

Figure 9. Fourier spectrum of VSX J192405.8+280352.

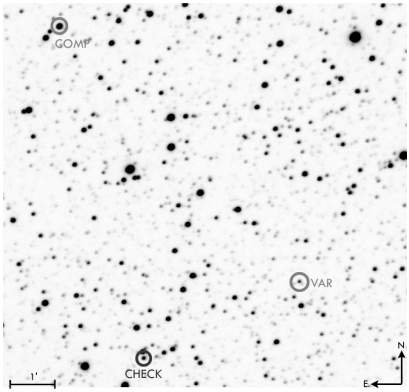

Figure 10. Finding chart of VSX J192252.4+280217.

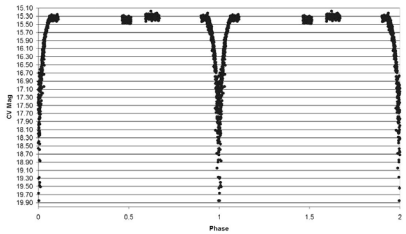

Figure 11a. Phase plot of VSX J192252.4+280217.

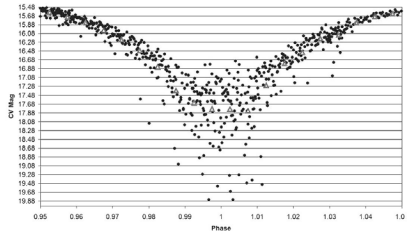

Figure 11b. Phase plot of VSX J192252.4+280217, zoom between phase 0.95 and 1.05. White triangles are binning points.

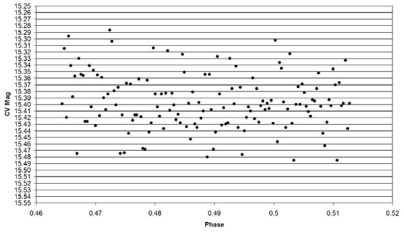

Figure 11c. Phase plot of VSX J192252.4+280217, zoom between phase 0.46 and 0.52. White triangles are binning points. The zoom on Phase between 0.46. 0.52 regards the presence of the secondary minimum, not detected for this variable.

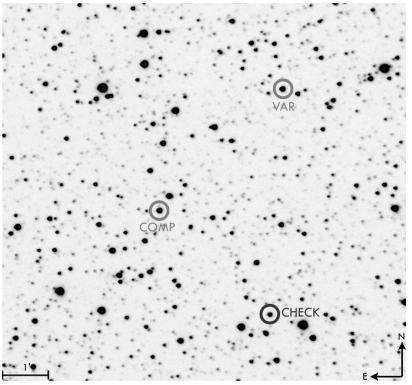

Figure 12. Finding chart of VSX J192251.4+280456.

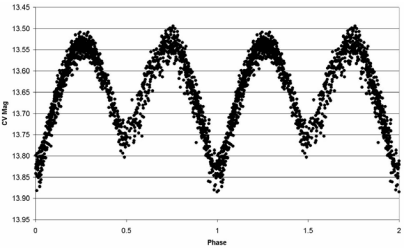

Figure 13. Phase plot of VSX J192251.4+280456.

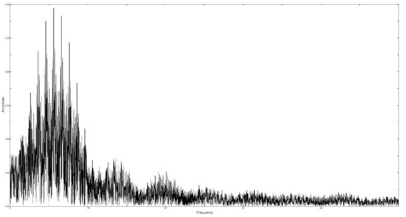

Figure 14. Fourier spectrum of VSX J192251.4+280456.

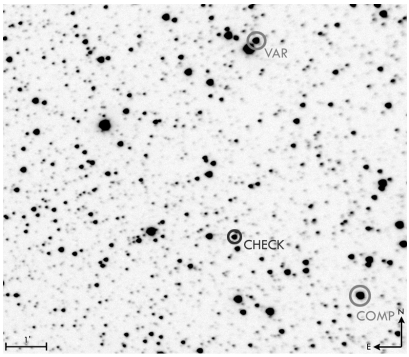

Figure 15. Finding chart of VSX J192226.0+281019.

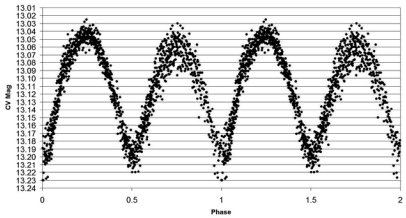

Figure 16. Phase plot of VSX J192226.0+281019.

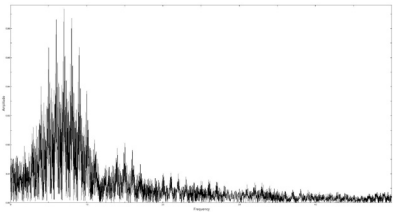

Figure 17. Fourier spectrum of VSX J192226.0+281019.

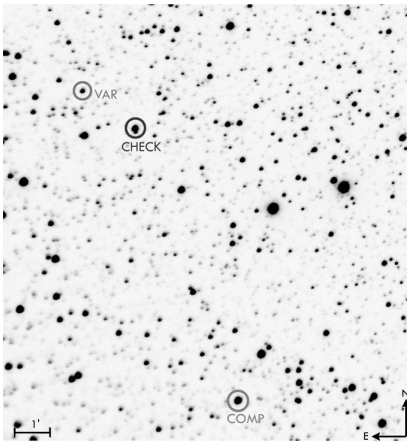

Figure 18. Finding chart of VSX J192524.9+275342.

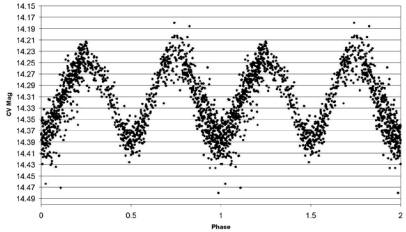

Figure 19. Phase plot of VSX J192524.9+275342.

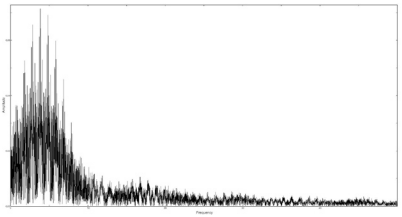

Figure 20. Fourier spectrum of VSX J192524.9+275342.

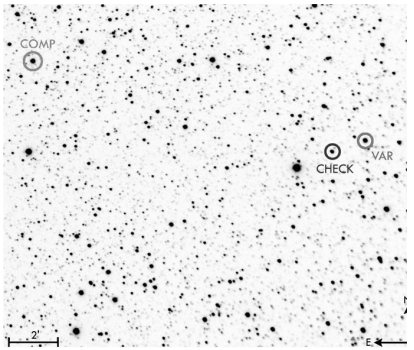

Figure 21. Finding chart of VSX J192220.7+275518.

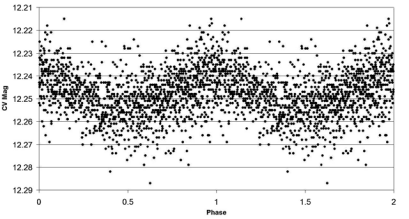

Figure 22. Phase plot of VSX J192220.7+275518.

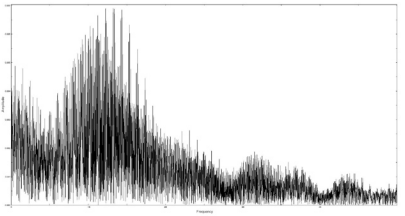

Figure 23. Fourier spectrum of VSX J192220.7+275518.

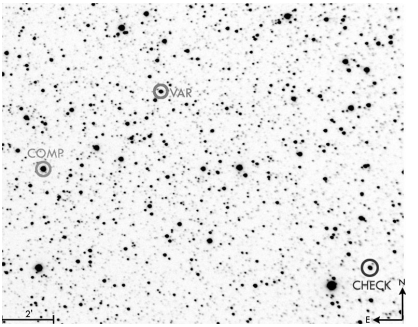

Figure 24. Finding chart of VSX J192304.4+280231.

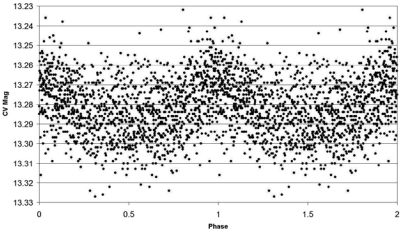

Figure 25. Phase plot of VSX J192304.4+280231.

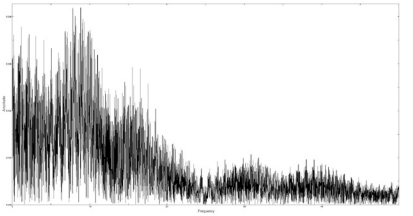

Figure 26. Fourier spectrum of VSX J192304.4+280231.

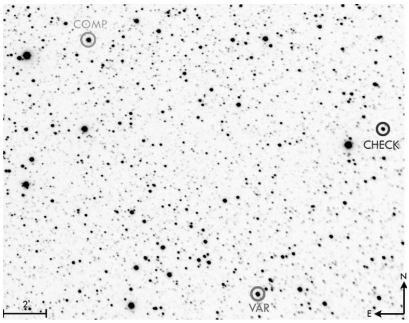

Figure 27. Finder chart of VSX J192255.1+274744.

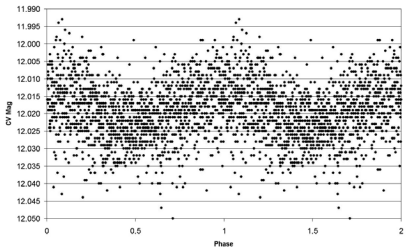

Figure 28. Phase plot of VSX J192255.1+274744.

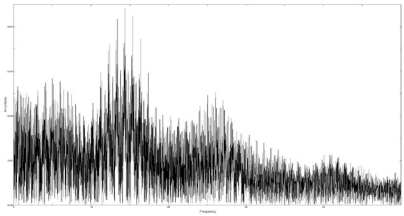

Figure 29. Fourier spectrum of VSX J192255.1+274744.

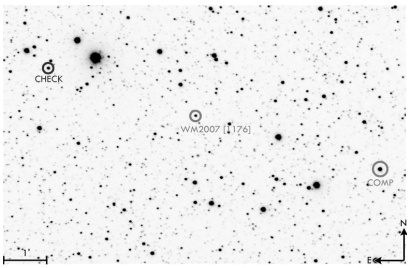

Figure 30. Finding chart of [WM2007] 1176.

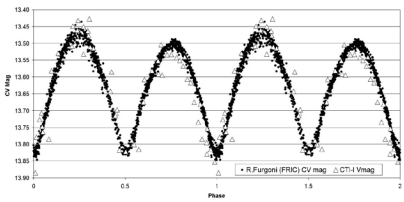

Figure 31. Phase plot of [WM2007] 1176.

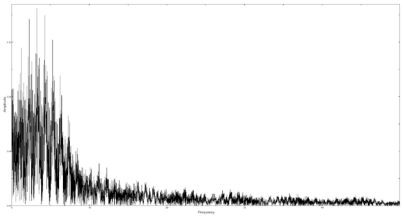

Figure 32. Fourier spectrum of [WM2007] 1176.

V1820 Orionis: an RR Lyrae Star With Strong and Irregular Blazhko Effect

Pierre de Ponthière
15 Rue Pré Mathy, Lesve, Profondeville 5170, Belgium; pierredeponthiere@gmail.com

Franz-Josef (Josch) Hambsch
12 Oude Bleken, Mol, 2400, Belgium; hambsch@telenet.be

Tom Krajci
P.O. Box 1351, Cloudcroft, NM 88317; tom_krajci@tularosa.net

Kenneth Menzies
318A Potter Road, Framingham, MA, 01701

Patrick Wils
Aarschotsebaan 31, Hever B-3191, Belgium; patrickwils@yahoo.com

Received October 12, 2012; revised November 27, 2012; accepted November 29, 2012

Abstract The Blazhko effect in V1820 Orionis and its period were reported for the first time by Wils *et al.* (*MNRAS*, **368**, 1757; 2006) from a data analysis of the Northern Sky Variability Survey. The results of additional V1820 Orionis observations over a time span of four years are presented herein. From the observed light curves, 73 pulsation maxima have been measured. The times of light maxima have been compared to ephemerides to obtain the (O–C) values. The Blazhko period (27.917 ± 0.002 d) has been derived from light curve Fourier analysis and from ANOVA analyses of the (O–C) values and of magnitudes at maximum light (M_{max}). During one Blazhko cycle, a hump in the ascending branch of the light curve was clearly identified and has also created a double maximum in the light curve. The frequency spectrum of the light curve, from a Fourier analysis with PERIOD04, has revealed triplet, quintuplet structures, and a second Blazhko weak modulation (period = 34.72 ±0.01 d). V1820 Orionis can be ranked as a strongly modulated star based on its observed amplitude and phase variations. The amplitude ratio of the largest triplet component to main pulsation component is quite large: 0.34.

1. Introduction

The star V1820 Orionis is classified in the *General Catalogue of Variable Stars* (Samus *et al.* 2011) as an RR Lyr (RRab) variable star with a period of 0.479067 day and with maximum and minimum V-band magnitudes of 12.5 and 13.4, respectively. This star was identified as an RRab with a Blazhko period of 28 days by Wils *et al.* (2006). At this time the star was classified as NSV 02724

in the *New Catalogue of Suspected Variable Stars* (Kukarkin *et al.* 2011).

The current data were gathered during 157 nights between December 2006 and March 2012. During this period of 1,918 days, a total of 22,592 magnitude measurements covering 70 Blazhko cycles were collected. The 7,300 observations from December 2006 to February 2010 were made by Hambsch using 30-cm and 50-cm telescopes located in Cloudcroft (New Mexico). From September 2011 to March 2012 the observations were made by Hambsch using the telescope in Cloudcroft and a 40-cm telescope in San Pedro de Atacama (Chile). de Ponthière contributed additional measurements with a 20-cm telescope located at Lesve (Belgium).

The comparison stars used by the authors are given in Table 1. The star coordinates and magnitudes in B and V bands were obtained from the NOMAD catalogue (Zacharias *et al.* 2011). C1 was used as a magnitude reference and C2 as a check star. The Johnson V magnitudes from different instruments have not been transformed to the standard system since measurements were performed with only a V filter. However, two simultaneous measurements from the instruments in Cloudcroft and San Pedro de Atacama were observed to differ by only 0.025 mag. Dark and flat field corrections were performed with the MAXIMDL software (Diffraction Limited 2004), aperture photometry was performed using LESVEPHOTOMETRY (de Ponthière 2010) custom software which also evaluates the SNR and estimates magnitude errors.

2. Light curve maxima analysis

The times of maxima of the light curves have been evaluated with custom software (de Ponthiere 2010) fitting the light curve with a smoothing spline function (Reinsch 1967). Table 2 provides the list of observed maxima and Figure 1 shows the (O–C) values.

A linear regression of all available (O–C) values has provided a pulsation period of 0.4790486 d (2.087471 d^{-1}). The (O–C) values have been re-evaluated with this new pulsation period. The new pulsation elements derived from a linear least-square fitting are:

$$HJD_{Pulsation} = (2\ 454\ 075.8935 \pm 0.0060) + (0.4790486 \pm 0.0000018)\ E \quad (1)$$

The folded light curve on this pulsation period is shown in Figure 2.

The Blazhko period was determined by a period analysis of the (O–C) values and the M_{max} (Magnitude at Maximum) values with the ANOVA algorithm of PERANSO (Vanmunster 2007). Both periodograms, presented in Figure 3a and 3b, show a primary peak and a series of aliases equally spaced around the main modulation frequency. The lists of prominent peaks are indicated below.

From (O–C) analysis, the main frequencies and periods are tabulated below:

	Frequency (cycles / day)	Period (days)	Peak value
f_0	0.03637 ± 0.00004	27.50 ± 0.03d	31.8
f_1	0.03583	27.91	27.3
f_2	0.03471	28.81	28.0
f_3	0.03691	27.09	18.2
f_4	0.03747	26.69	20.0

From M_{max} analysis, the main frequencies and periods are tabulated below:

	Frequency (cycles / day)	Period (days)	Peak value
f_0	0.03581 ± 0.00004	27.92± 0.03d	154.1
f_1	0.03527	28.35	69.6
f_2	0.03471	28.81	61.7
f_3	0.03637	27.50	63.2
f_4	0.03693	27.08	36.3

These aliases are apparently due to the presence of two groups of measurements separated by four years. The first group of 13 maxima is centered on January 2007 and the second group of 52 maxima is centered on December 2011. The alias spacing of 0.00054 d^{-1} (1,851 d) is approximately the reciprocal of the time span between the two measurement groups (that is, 59 months or 1,770 days). A Spectral Window analysis on (O–C) and M_{max} data points provided peaks separated by 0.00057 d^{-1} (1754d), which supports the origin of the aliases.

From the (O–C) period analysis it is not possible to deduce which peak corresponds to the Blazhko period since none of them is emerging significantly. However, the prominent peak of the M_{max} analysis is also found as an important peak in the (O–C) analysis. Therefore, the Blazhko period is estimated as 27.92 ± 0.03 days. Wils *et al.* (2006) have reported a value of 28 days.

The highest recorded maximum was observed at HJD 2455955.6847, and the Blazhko ephemeris origin has been selected as 69 Blazhko cycles before this highest recorded maximum. On the basis of this origin, the first observations have a positive value for $E_{Blazhko}$.

$$HJD_{Blazhko} = 2454029.2047 + (27.92 \pm 0.03)\, E_{Blazhko} \quad (2)$$

The folded (O–C) and M_{max} versus the Blazhko phase curves are presented in Figures 4 and 5. The magnitudes at maximum values differ by about 0.85 magnitude, that is, 52% of the light curve peak to peak variations. If the humps are not taken into account, the (O–C) values differ in a range of 0.075 day, that is, 15% of the pulsation period.

RR Lyrae stars of type RRab are known to frequently show a hump in their light curves that appears before light maximum (Smith 1995). The evolution of a strong hump during five consecutive nights (JD 2455941 to 2455945) was observed. The folded light curves for those nights (JD41–45) are given in Figure 6. During the first night (JD 2455941), the shape of the maximum appears normal, but on the second night (JD 2455942) the light curve shows a shoulder in the decreasing branch. On JD 2455943 two maxima are separated by 0.0685 day (that is, 14% of the pulsation period) and on the fourth night, the maximum is preceded by a classical hump in the increasing branch. The (O–C) values for the maxima occurring on nights JD 2455941, JD 2455942, and for the first maximum on night JD 2455943 appear to be outliers in the (O–C) diagram (Figure 1), but the (O–C) value of the shoulder on the second night JD 2455942 is close to what is expected. The evolution of a shockwave phenomenon generating the hump has probably distorted the light curve on JD 2455942 to the point that the magnitude of the hump is larger than at normal maximum magnitude. The same phenomenon is not repeated at each Blazhko cycle, but it probably occurred on nights of JD 2454126 and JD 2454770 as the corresponding (O–C) values appear to be outliers in the (O–C) diagram (Figure 1). These irregularities in the (O–C) values occur around the Blazhko phase equal to 0.5 (Figure 4). The observed shoulder in the decreasing branch on JD 2455942 is similar to the "bump" detected by Jurcsik *et al.* (2012) in the RZ Lyrae light curve. This phenomenon of light curve distortion for both stars occurs when the Blazhko amplitude modulation is weakest. The bump appearing in the descending branch of RZ Lyrae occurs around pulsation phase 0.25–0.30 but the shoulder in the decreasing branch of V1820 Orionis happens around pulsation phase 0.0. Based on the different pulsation phases at which the light curve distortions occur and the night-to-night evolution for V1820 Orionis, it can be supposed that the phenomena are probably different for the two stars.

The relationship between M_{max} and (O–C) can be plotted on a diagram. These two quantities vary with the Blazhko phase and if they are repetitive from cycle to cycle, the data will lie on a loop and if they are sinusoidal the loop will be elliptical. The loop will run in a clockwise progression if the M_{max} has positive phase delay versus (O–C) phase and vice-versa. However M_{max} and (O–C) values for V1820 Orionis, represented by small diamonds in Figure 7, are poorly repetitive from cycle to cycle and are largely scattered. The mean values of (O–C) and M_{max} have been evaluated for 10 bins of the Blazhko phase and are represented as large squares in the Figure 7. An inspection of the successive points indicates that the loop is progressing in counter-clockwise direction. The point in the lower left of the diagram with (O–C = –0.1 day) corresponds to the strong hump described above. Le Borgne *et al.* (2012) have shown that for most of the analyzed Blazhko stars the M_{max} versus (O–C) diagrams exhibit a similar counterclockwise rotation.

3. Frequency spectrum analysis

A Blazhko effect on the light curve can be modeled as an amplitude and/or phase modulation of the periodic pulsation, with the reciprocal of the modulation frequency being the Blazhko period. Szeidl and Jurcsik (2009) have shown that the Fourier spectrum of an amplitude and phase modulation model is given by an infinite series including the fundamental frequency (f_0), harmonic frequencies (if_0), and multiplet frequencies ($if_0 \pm jf_B$).

$$m(t) = \Sigma A_i \sin(i\omega t + \Phi_{i0}) + \Sigma\Sigma A^{+}_{ij} \sin[(i\omega + j\Omega)t + \Phi^{+}_{ij}] + \Sigma\Sigma A^{-}_{ij} \sin[(i\omega - j\Omega)t + \Phi^{-}_{ij}] \quad (3)$$

where:

$\omega = 2\pi f_0$, f_0 is the fundamental frequency of the light-curve,
$\Omega = 2\pi f_B$, f_B is the Blazhko modulation frequency, and
A_i A^{+} ij A^{-}_{ij} are the Fourier coefficients and Φ_i, Φ^{+}_{ij} and $\Phi^{-}_{ij\,j}$ their phase angles, "i" indices are used for the fundamental and the harmonic frequencies and "j" indices for the side lobes (for example, A^{+}_{32} is the coefficient of the multiplet $(3f_0 + 2f_B)$.

The methodology used herein is similar to the one reported by Kolenberg (2009) where triplet and quintuplet components were detected in the spectrum of SS Fornacis. The spectral analysis was performed with PERIOD04 (Lenz and Breger 2005) to yield a Fourier analysis and multi-frequency sine-wave fitting.

The sine-wave fitting was determined by successive data pre-whitening and Fourier analysis on residuals. For each observed harmonic and triplet, the signal-to-noise ratio has been evaluated to retain only significant signals, that is, with an SNR greater than 3.5. During the PERIOD04 sine-wave fitting process, only the fundamental f_0 and the first main triplet component $f_0 + f_B$ frequencies have been unconstrained; the other frequencies have been entered as combinations of f_0 and $f_0 + f_B$. Table 3 provides the amplitude and phase for each Fourier component obtained with the best sine-wave fitting. The uncertainties of frequencies, amplitudes, and phases have been estimated by Monte Carlo simulations. As it is known that Monte Carlo simulation uncertainties can be underestimated (Kolenberg *et al.* 2009), the uncertainty values have been multiplied by a factor of two. The harmonics of f_0 are significant to the eighth order. The residuals after subtraction of the best fit based on f_0 and harmonics up to the eighth order is provided in Figure 8a. The large residuals close to the phase of maximum light (0.8 to 1.1) are due to amplitude and phase modulations created by the Blazhko effect. The residuals are reduced significantly when the side peaks (triplets) around the f_0 frequency and harmonics up to the seventh order are included in the fitting process (Figure 8b).

The fundamental pulsation frequency f_0 (2.08747 d^{-1}) is very close to the frequency obtained from a linear regression analysis of time of maxima. The

Blazhko period was also measured from the first side peak frequency $f_0 + f_B$ and f_0 to yield $f_B = (2.12329 - 2.08747) = 0.03582$ d^{-1} and $P_B = 27.917 \pm 0.002$ days. The second side peak frequency $f_0 - f_B$ exhibited a lower amplitude and higher uncertainty and was not used for Blazhko period evaluation. The Blazhko period found with the sine-wave fitting method (27.919 ± 0.002 days) is equal to the value found with the brightness at maximum analysis (27.92 ± 0.03 days). Table 4 lists the harmonic and significant amplitude ratios. One useful parameter to quantify the Blazhko effect is the amplitude ratio $A^{\pm}_{11} / A_1$, where $A^{\pm}_{11}$ is the amplitude of the largest side lobe at $f_0 + f_B$ or $f_0 - f_B$ and A_1 is the amplitude of f_0. The most common and maximum values for this ratio are 0.15 and 0.4, respectively (Alcock *et al.* 2003). With an amplitude ratio $A_{11}^{+} / A_1 = 0.34$, V1820 Orionis can be ranked as strongly modulated.

The triplet ratios $R_i = A^{+}_{i1} / A^{-}_{i1}$ and asymmetries $Q_i = (A^{+}_{i1} - A^{-}_{i1}) / (A^{+}_{i1} + A^{-}_{i1})$ are also provided in Table 4. The asymmetry in the side lobes observed for V1820 Orionis is not unexpected on the basis of Szeidl and Jurcsik (2009), which showed that this asymmetry is related to the phase difference between the Blazhko amplitude and phase modulations. If the Blazhko effect were limited to amplitude modulation, the ratios R_i and Q_i would be equal to 1 and 0, respectively. The asymmetry ratios Q_i around 0.35 are a sign that V1820 Orionis is amplitude- and phase-modulated.

Besides the harmonics and triplets, some quintuplet components ($kf_0 + 2f_B$) and a peak at the Blazhko period itself were found. And finally, two modulation peaks appear in the spectrum around f_0 and $2f_0$ with a separation of 0.028 d^{-1}. They correspond to a second Blazhko modulation f_{B2} ($1/f_{B2} = 34.72 \pm 0.01$ days). This phenomenon of multi-periodic modulation has also been detected by Sódor *et al.* (2011) in the spectrum of CZ Lacertae. In the case of CZ Lac, the modulation components of the two frequencies (f_B and f_{B2}) have similar amplitudes, which is not the case for V1820 Orionis. The second modulation frequency f_{B2} has weaker components than f_B, but they remain significant as their SNR are 9.2 and 6.0, respectively. A spectral analysis on M_{max} values provides the same two Blazhko modulation frequencies f_B and f_{B2}, which are in a 5:4 resonance ratio. The corresponding beating period is 139 days, which is visible on the multi-frequency sine-wave fitting obtained with PERIOD04 (Figure 9). For clarity, Figure 9 only includes the last observation season (2011–2012). A 5:4 resonance ratio was also found between the two modulation frequencies of CZ Lac during the 2004 observation season (Sódor *et al.* 2011) but the next year this resonance ratio changed to a value of 4:3.

4. Light curve variations over Blazhko cycle

In order to investigate the light curve variations over the Blazhko cycle, the complete dataset was subdivided into ten temporal subsets corresponding to different Blazhko phase intervals Ψ_i (i = 0,9). The ephemeris derived previously

during the analysis of light curve maxima was used to define the epoch of the Blazhko zero phase (HJD = 2454029.2047). The data points are relatively well distributed over the subsets with the number of data points in each subset varying between 1,144 and 3,045. The light curves for each subset are presented in Figure 10. The strong hump observed during JD 2455942, as described previously, is highlighted in red in the panel of subset (Ψ = 0.5–0.6).

For each subset, the amplitude A_i and phase Φ_i of of the fundamental and harmonic frequencies up to the fourth order have been evaluated with the Least-Square Fit module of PERIOD04. The amplitudes and epoch-independent phase differences ($\Phi_{k1} = \Phi_k - k\Phi_1$) over the Blazhko cycle are provided in Table 4 and exhibited in Figures 11a and 11b. As expected, the amplitude of the fundamental frequency is clearly lower at a Blazhko phase around 0.5, that is, when the light curve amplitude variation on the pulsation cycle is weaker. The maximum and minimum Φ_1 phase values (2.234 and 1.253 radians) are found in subsets Ψ (0.4–0.5) and Ψ (0.1–0.2), respectively. The difference between maximum and minimum Φ_1 phase is a measure of the phase modulation strength and is equal to (2.234 – 1.253) = 0.981 radian or 0.156 cycle, which corresponds roughly to the value of 15 % noted for the peak to peak deviation of (O–C). The phase variation of harmonic component Φ_{41} is the largest, with a value of 3.6 radians, while Φ_{21} varies only by 0.37 radians over the Blazhko cycle. The phase variation of harmonic component Φ_{41} is very large as compared to Φ_{k1} values of 1 and 0.5 radians observed for RZ Lyrae (Jurcsik *et al.* 2012) and SS Fornacis (Kolenberg *et al.* 2009), respectively.

Figure 12 provides a graph of the A_1 coefficient versus the Φ_1 for the different subsets. This graph is similar to the graph of the Magnitude at Maximum versus (O–C) given in Figure 7. In order to compare the two graphs, the Φ_1 axis of Figure 12 was inverted. Indeed, for the sine-wave fitting [$A_i \sin(\omega_i t + \Phi_i)$], a larger Φ_i phase corresponds to a time advance, that is, a lower value of (O–C). With the Φ_1 axis inverted, the loop of A_1 values exhibits a counter-clockwise progression as in Figure 7.

5. Conclusions

The strong and irregular Blazhko behavior of V1820 Ori has been exhibited by two different methods: (1) measurement of light curve maxima, and (2) Fourier analysis. The latter method, Fourier analysis, has been feasible due to the large number of regular observations over the pulsation period which was not limited to the times of light curve maxima. Both methods yield the same results for the fundamental pulsation period (0.4790486 day ± 0.0000018) and the Blazhko period (27.917 days ± 0.002). The irregularities of the Blazhko effect are probably explained by variations of the strength of a shockwave phenomenon generating the hump in the ascending branch of the light curve. This erratic behavior generally occurs around a Blazhko phase of 0.5. Measured

ratios of Fourier amplitudes and their asymmetries also confirm strong Blazhko amplitude and phase modulations. A second weaker Blazhko modulation with a period 34.70 ±0.02 days has also been identified. The two modulation frequencies are in a 5:4 resonance ratio.

6. Acknowledgements

Dr. Arne Henden, Director of AAVSO, and the AAVSO are acknowledged for the use of AAVSOnet telescopes at Cloudcroft, New Mexico. The authors thank Dr. Katrien Kolenberg for helpful suggestions in the Fourier analysis and the referee Dr. Johanna Jurcsik for constructive comments which have helped to clarify and improve the paper.

References

Alcock, C., *et al.* 2003, *Astrophys. J.*, **598**, 597.

de Ponthière, P. 2010, LESVEPHOTOMETRY, automatic photometry software (http://www.dppobservatory.net).

Diffraction Limited. 2004, MAXIMDL image processing software (http://www.cyanogen.com).

Jurcsik, J., *et al.* 2012, *Mon. Not. Roy. Astron. Soc.*, **423**, 993.

Kolenberg, K., *et al.* 2009, *Mon. Not. Roy. Astron. Soc.*, **396**, 263.

Kukarkin, B., *et al.* 2011, *New Catalogue of Suspected Variable Sars* (NSV database, Version 2011 March, http://www.sai.msu.su/gcvs/gcvs/nsv/nsv.dat).

Le Borgne, J. F., *et al.* 2012, *Astron. J.*, **144**, 39.

Lenz, P., and Breger, M. 2005, *Commun. Asteroseismology*, **146**, 53.

Reinsch, C. H. 1967, *Numer. Math.*, **10**, 177.

Samus, N. N., *et al.* 2011 *General Catalogue of Variable Stars* (GCVS database, Version 2011 January, http://www.sai.msu.su/gcvs/gcvs/index.htm).

Smith, H. 1995, *RR Lyrae Stars*, Cambridge Univ. Press, Cambridge.

Sódor, Á., *et al.* 2011, *Mon. Not. Roy. Astron. Soc.*, **411**, 1585.

Szeidl, B., and Jurcsik, J. 2009 *Commun. Asteroseismology*, **160**, 17.

Vanmunster, T. 2007, PERANSO, period analysis software (http://www.cbabelgium.com and http://www.peranso.com).

Wils, P., Lloyd, C., and Bernhard, K. 2006, *Mon. Not. Roy. Astron. Soc.*, **368**, 1757.

Zacharias, N., Monet, D., Levine, S., Urban, S., Gaume, R., and Wycoff, G. 2011, The Naval Observatory Merged Astrometric Dataset (NOMAD, http://www.usno.navy.mil/USNO/astrometry/optical-IR-prod/nomad/).

Table 1. Comparison stars for V1820 Ori.

Identification	*R. A. (2000)* *h m s*	*Dec. (2000)* ° ′ ″	*B*	*V*	*B-V*	
GSC 125-41	05 54 57.4	+04 56 42.5	13.83	13.31	0.52	C1
GSC 125-341	05 54 29.6	+04 53 59.1	14.94	13.65	1.29	C2

Table 2. List of measured maxima of V1820 Ori.

Maximum HJD	*Error*	*O–C (day)*	*E*	*VMagnitude*	*Error*	*Filter*	*Location*[a]	*Remark*[b]
2454075.9173	0.0033	0.0235	0	12.367	0.007	C	1	
2454076.8783	0.0035	0.0264	2	12.330	0.006	C	1	
2454079.7429	0.0020	0.0167	8	12.083	0.005	C	1	
2454085.9515	0.0011	–0.0024	21	11.851	0.005	C	1	
2454104.6673	0.0028	0.0306	60	12.342	0.005	C	1	
2454110.8696	0.0007	0.0053	73	11.902	0.004	C	1	
2454114.6902	0.0008	–0.0065	81	11.844	0.003	C	1	
2454126.6093	0.0023	–0.0636	106	12.393	0.004	C	1	*
2454135.7878	0.0015	0.0130	125	12.158	0.004	C	1	
2454136.7440	0.0018	0.0111	127	12.122	0.004	C	1	
2454137.6982	0.0009	0.0072	129	12.021	0.003	C	1	
2454149.6405	0.0012	–0.0267	154	12.118	0.004	C	1	
2454162.6332	0.0023	0.0317	181	12.299	0.004	C	1	
2454439.9682	0.0039	–0.00205	760	12.348	0.005	V	1	
2454748.9571	0.0035	0.00096	1405	12.132	0.007	V	1	
2454749.9218	0.0053	0.00757	1407	12.046	0.043	V	1	
2454770.8990	0.0036	–0.09334	1451	12.370	0.021	C	1	*
2454832.7977	0.0025	0.00818	1580	12.288	0.009	V	1	
2455245.7039	0.0019	–0.02490	2442	12.356	0.011	V	1	
2455813.8853	0.0011	0.00570	3628	11.827	0.008	V	2	
2455824.8744	0.0027	–0.02330	3651	12.203	0.010	V	2	
2455825.8249	0.0034	–0.03090	3653	12.242	0.009	V	2	
2455845.9745	0.0025	–0.00131	3695	11.798	0.016	V	2	
2455859.8570	0.0033	–0.01120	3724	12.428	0.009	V	2	
2455861.7776	0.0045	–0.00679	3728	12.444	0.009	V	2	
2455871.8475	0.0023	0.00310	3749	11.870	0.017	V	2	
2455872.8024	0.0017	–0.00009	3751	11.886	0.008	V	2	
2455873.7629	0.0018	0.00231	3753	11.923	0.010	V	2	
2455881.8771	0.0048	–0.02730	3770	12.225	0.018	V	2	
2455883.8157	0.0026	–0.00490	3774	12.281	0.010	V	2	
2455884.7742	0.0037	–0.00449	3776	12.288	0.010	V	2	
2455885.7271	0.0035	–0.00969	3778	12.298	0.009	V	2	
2455886.6856	0.0027	–0.00928	3780	12.325	0.009	V	2	
2455887.6455	0.0032	–0.00748	3782	12.326	0.009	V	2	

table continued on next page

Table 2. List of measured maxima of V1820 Ori, cont.

Maximum HJD	*Error*	*O–C (day)*	*E*	*VMagnitude*	*Error*	*Filter*	*Location*[a]	*Remark*[b]
2455894.8573	0.0022	0.01860	3797	12.137	0.010	V	2	
2455895.8119	0.0023	0.01511	3799	12.080	0.010	V	2	
2455896.7562	0.0016	0.00131	3801	11.981	0.020	V	2	
2455896.7649	0.0020	0.01001	3801	11.924	0.009	V	2	
2455897.7287	0.0028	0.01572	3803	11.998	0.009	V	2	
2455898.6824	0.0016	0.01132	3805	11.955	0.009	V	2	
2455899.6376	0.0015	0.00842	3807	11.970	0.010	V	2	
2455900.5927	0.0028	0.00543	3809	11.977	0.014	V	2	
2455905.8498	0.0051	–0.00700	3820	12.129	0.026	V	2	
2455906.8131	0.0045	–0.00179	3822	12.171	0.032	V	2	
2455907.7555	0.0041	–0.01749	3824	12.189	0.027	V	2	
2455908.7226	0.0060	–0.00849	3826	12.269	0.032	V	2	
2455909.6812	0.0063	–0.00798	3828	12.373	0.014	V	2	
2455910.6170	0.0051	–0.03028	3830	12.339	0.012	V	2	
2455919.7662	0.0033	0.01701	3849	12.220	0.014	V	2	
2455930.7657	0.0041	–0.00159	3872	11.928	0.023	V	1	
2455931.7210	0.0024	–0.00438	3874	11.965	0.025	V	1	
2455932.6809	0.0024	–0.00258	3876	12.074	0.019	V	1	
2455941.7342	0.0050	–0.05119	3895	12.461	0.010	V	2	*
2455942.6755	0.0028	–0.06799	3897	12.399	0.009	V	2	*
2455943.6482	0.0064	–0.05338	3899	12.502	0.010	V	2	*
2455943.7167	0.0074	0.01512	3899	12.533	0.010	V	2	
2455944.6666	0.0084	0.00692	3901	12.514	0.009	V	2	
2455945.6294	0.0025	0.01163	3903	12.466	0.016	V	1	
2455945.6433	0.0072	0.02553	3903	12.446	0.009	V	2	
2455946.6153	0.0072	0.03943	3905	12.442	0.018	V	1	
2455946.6215	0.0066	0.04563	3905	12.411	0.009	V	2	
2455947.5790	0.0064	0.04504	3907	12.347	0.010	V	2	
2455948.5257	0.0031	0.03364	3909	12.228	0.010	V	2	
2455953.7740	0.0017	0.01241	3920	11.822	0.015	V	1	
2455954.2495	0.0026	0.00886	3921	11.838	0.015	V	3	
2455955.6847	0.0015	0.00692	3924	11.681	0.014	V	2	
2455956.6423	0.0012	0.00643	3926	11.734	0.013	V	1	
2455957.5987	0.0013	0.00473	3928	11.729	0.020	V	1	
2455964.2835	0.0037	–0.01714	3942	12.284	0.014	V	3	
2455978.6990	0.0030	0.02692	3972	12.177	0.009	V	1	
2455979.6582	0.0022	0.02803	3974	12.066	0.009	V	1	
2455980.6063	0.0012	0.01803	3976	11.953	0.009	V	1	
2455989.6865	0.0029	–0.00368	3995	12.018	0.020	V	1	

[a]*Locations: 1—Cloudcroft; 2—Chile; 3—Lesve.* [b]*Remarks: *—hump*

Table 3. Multi–frequency fit results for V1820 Ori. The frequency uncertainties on f_0, $f_0 + f_B$, and $f_0 + f_{B2}$ are 4×10^{-7}, 2×10^{-6}, and 7×10^{-6}, respectively. The values displayed in italics correspond to components not exceeding a SNR greater than 3.5.

Parameter	*f* (d^{-1})	A_i *(mag)*	Φ*(cycle)*	σ(Φ)	*SNR*
f_0	2.087466	0.335	0.245768	0.001	82.1
$2f_0$	4.174932	0.126	0.851262	0.002	34.8
$3f_0$	6.262398	0.062	0.459455	0.003	19.8
$4f_0$	8.349864	0.031	0.070836	0.006	11.6
$5f_0$	10.43733	0.020	0.703054	0.010	8.3
$6f_0$	12.5248	0.014	0.296387	0.014	6.1
$7f_0$	14.61226	0.011	0.914742	0.016	5.4
$8f_0$	16.69973	0.007	0.506391	0.028	3.3
f_B	0.035824	0.026	0.113932	0.007	5.8
$f_0 + f_B$	2.12329	0.114	0.08408	0.002	28.0
$f_0 - f_B$	2.051642	0.056	0.16969	0.003	13.8
$2f_0 + f_B$	4.210756	0.078	0.672295	0.003	21.8
$2f_0 - f_B$	4.139108	0.040	0.756026	0.005	11.2
$3f_0 + f_B$	6.298222	0.065	0.335476	0.003	20.7
$3f_0 - f_B$	6.226574	0.032	0.435456	0.006	10.2
$4f_0 + f_B$	8.385687	0.041	0.972183	0.005	15.4
$4f_0 - f_B$	8.31404	0.019	0.089832	0.010	7.2
$5f_0 + f_B$	10.47315	0.024	0.599442	0.008	9.9
$5f_0 - f_B$	10.40151	0.011	0.722088	0.017	4.8
$6f_0 + f_B$	12.56062	0.016	0.183182	0.012	7.1
$6f_0 - f_B$	12.48897	0.007	0.299414	0.027	3.2
$7f_0 + f_B$	14.64809	0.012	0.783367	0.016	5.6
$f_0 + 2f_B$	2.159114	0.014	0.494921	0.015	3.3
$3f_0 + 2f_B$	6.334046	0.021	0.081559	0.009	6.7
$4f_0 + 2f_B$	8.421511	0.023	0.818861	0.009	8.5
$f_0 + f_{B2}$	2.116266	0.028	0.90776	0.007	7.0
$2f_0 + f_{B2}$	4.203732	0.024	0.509457	0.008	6.7

Table 4. V1820 Ori Harmonic, Triplet amplitudes, ratios, and asymmetry parameters.

k	A_i/A_1	A_{i1}^{+}/A_1	A_{i1}^{-}/A_1	R_i	Q_i
1	1.00	0.34	0.17	2.01	0.34
2	0.37	0.23	0.12	1.96	0.32
3	0.18	0.19	0.10	2.02	0.34
4	0.09	0.12	0.06	2.14	0.36
5	0.06	0.07	0.03	2.08	0.35
6	0.04	0.05	0.02	2.20	0.37
7	0.03	—	—	—	—
8	0.02	—	—	—	—

Table 5. V1820 Ori. Fourier coefficients over Blazhko cycle.

Ψ *(cycle)*	A_1 *(mag.)*	A_2 *(mag.)*	A_3 *(mag.)*	A_4 *(mag.)*	Φ_1 *(rad.)*	Φ_{21} *(rad.)*	Φ_{31} *(rad.)*	Φ_{41} *(rad.)*
0.0–0.1	0.466	0.223	0.149	0.108	1.411	2.225	4.642	0.873
0.1–0.2	0.432	0.188	0.134	0.070	1.253	2.134	4.667	0.910
0.2–0.3	0.367	0.156	0.100	0.039	1.368	2.219	4.604	0.814
0.3–0.4	0.320	0.150	0.080	0.032	1.752	2.269	4.897	1.293
0.4–0.5	0.240	0.100	0.028	0.016	2.234	2.180	5.353	2.206
0.5–0.6	0.219	0.094	0.042	0.016	2.227	2.323	5.948	4.482
0.6–0.7	0.231	0.055	0.018	0.016	1.567	2.485	5.091	2.699
0.7–0.8	0.326	0.112	0.047	0.014	1.344	2.503	5.267	2.544
0.8–0.9	0.401	0.172	0.098	0.055	1.266	2.269	4.809	1.052
0.9–1.0	0.462	0.211	0.149	0.099	1.275	2.362	4.777	1.051

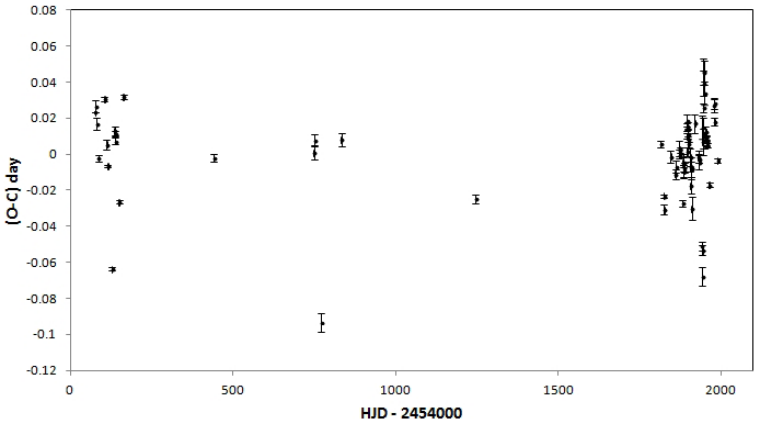

Figure 1. V1820 Ori (O–C).

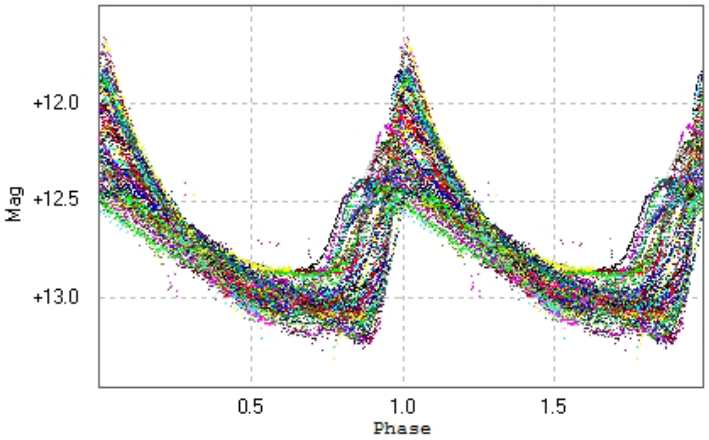

Figure 2. V1820 Ori light curve folded with pulsation period.

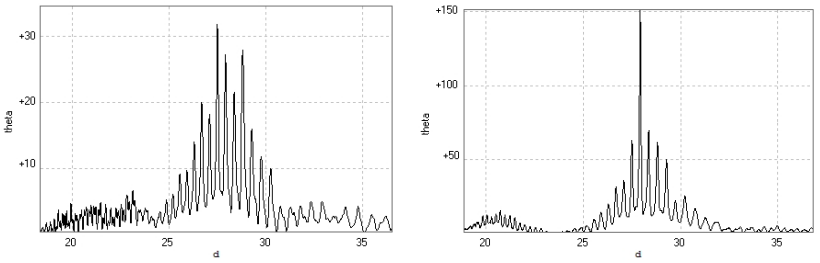

Figure 3a (left). V1820 Ori (O–C) periodogram. Figure 3b (right). V1820 Ori magnitude at maximum periodogram.

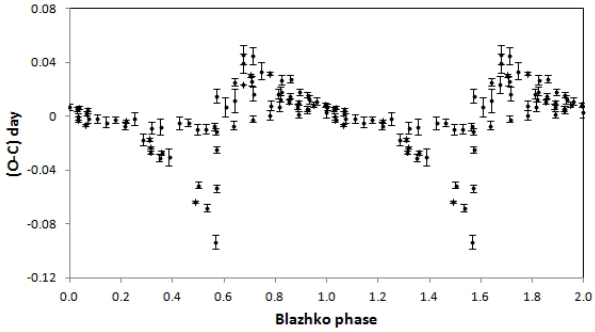

Figure 4. V1820 Ori O–C (days) versus Blazhko phase.

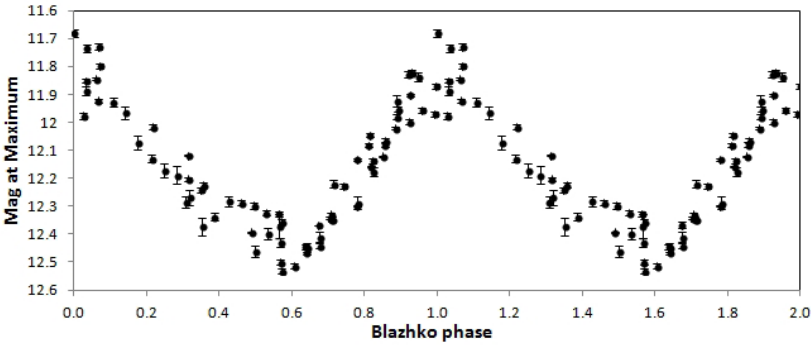

Figure 5. V1820 Ori magnitude at maximum versus Blazhko phase.

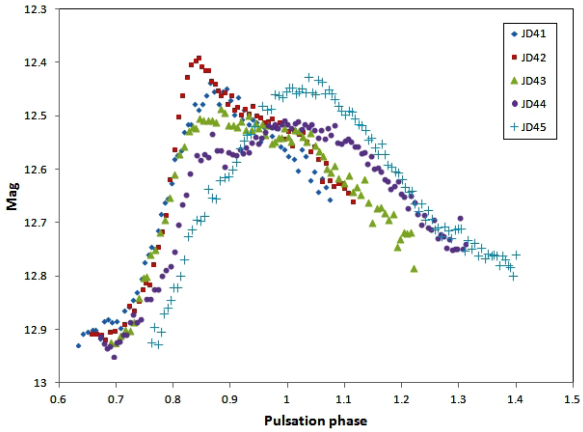

Figure 6. V1820 Ori hump evolution for nights JD 2455941 to 2455945.

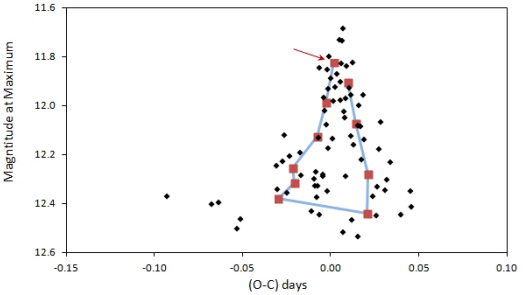

Figure 7. V1820 Ori magnitude at maximum versus O–C (days) values. Individual values and their means are represented as small diamonds and large squares, respectively. The point corresponding to the bin nearest to 0.0 Blazhko phase is indicated by an arrow.

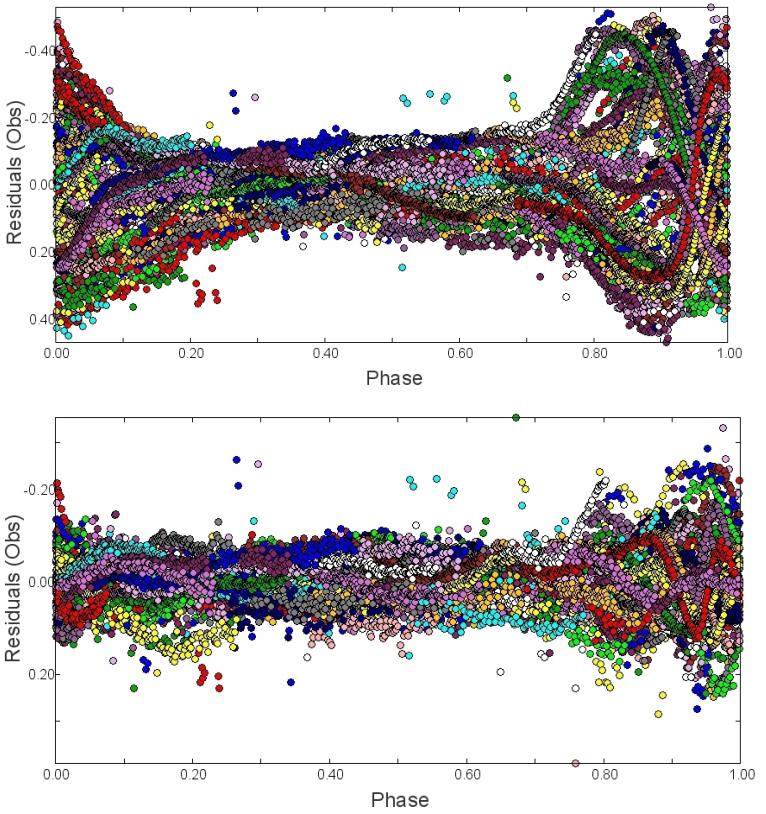

Figure 8a (top). V1820 Ori, residuals after harmonics whitening. Figure 8b (bottom). V1820 Ori residuals after triplet whitening.

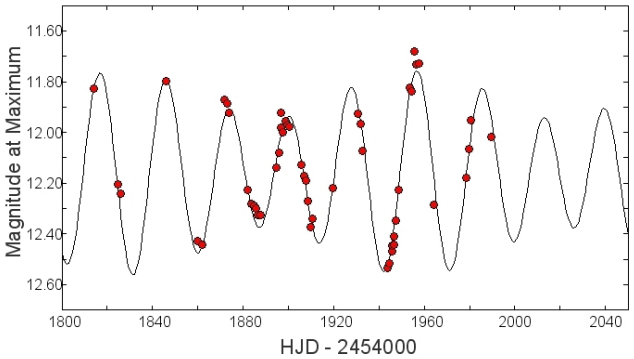

Figure 9. V1820 Ori magnitude at maximum curve fitting.

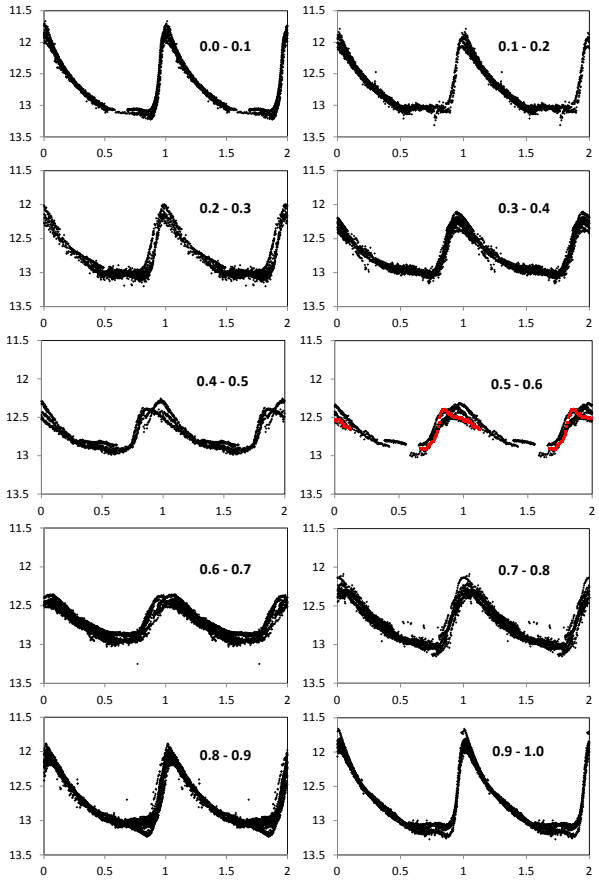

Figure 10. V1820 Ori light curve for different Blazhko subsets.

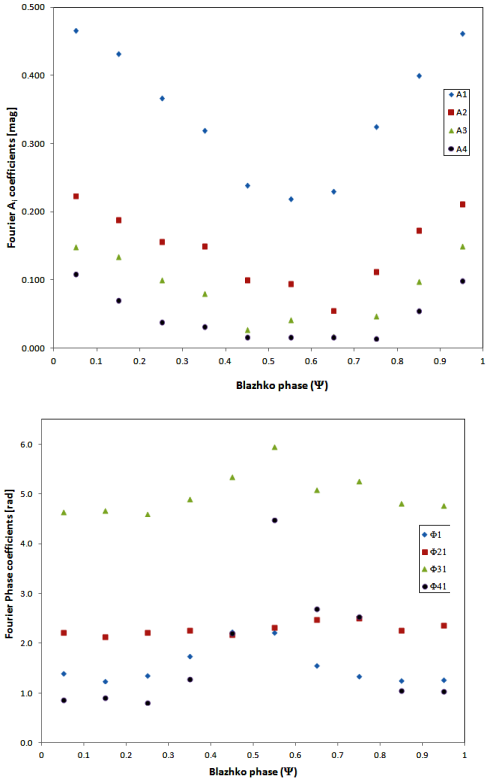

Figure 11a (top). V1820 Ori Fourier A_i amplitude (magnitude) variations versus Blazhko Ψ_i subsets. Figure 11b (bottom). V1820 Ori Fourier Φ_1 and Φ_{k1} phase (rad.) variations versus Blazhko Ψ_i subsets.

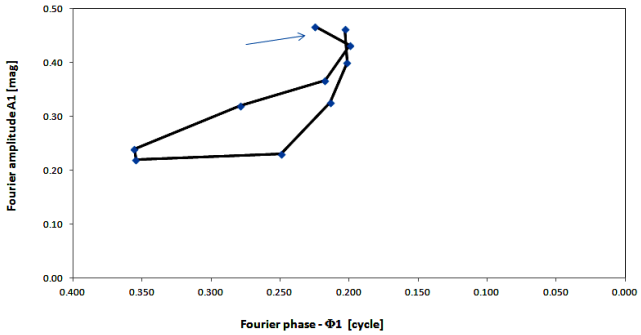

Figure 12. V1820 Ori Fourier amplitude A_1 versus phase Φ_1 for different Blazhko subsets. The point corresponding to the bin nearest to 0.0 Blazhko phase is indicated by an arrow.

Period Changes in RRc Stars

John R. Percy
Paul Jx Tan
Department of Astronomy and Astrophysics, University of Toronto, Toronto, ON M5S 3H4, Canada; john.percy@utoronto.ca

Received March 30, 2012; revised April 12, 2012; accepted April 12, 2012

Abstract We have used (O–C) analysis to study period changes in forty RRc stars in the GEOS (Groupe Européen d'Observation Stellaire) database of times of maximum of RR Lyrae stars. We find that many of the stars show approximately-linear period changes which are in agreement with the predictions of stellar evolution models. Other stars show period changes that are non-linear and/or larger than predicted by evolution models. Further long-term systematic, sustained observations may help to clarify the nature of the non-evolutionary changes.

1. Introduction

The period of a pulsating variable star may change for various reasons, including the evolution of the star; the pulsation period depends strongly on the radius of the star, and this may increase or decrease as a result of evolution. The change is very slow, but it is still observable because its effects on the observed times of maximum brightness are *cumulative*.

RR Lyrae stars have periods of about half a day, and visual amplitudes generally between 0.5 and 1.5 magnitudes. They are in the helium-burning phase of evolution, and lie on the horizontal branch in the Hertzsprung-Russell (HR) diagram. Their evolution is relatively rapid; they remain in this phase for only a few tens of millions of years. Their period changes have been studied for up to a century, especially those RR Lyrae stars in globular star clusters—for example, Jurcsik *et al.* (2012). For more information on RR Lyrae stars, see Smith (1995), or the mini-essays on RR Lyrae stars on the AAVSO's *Variable Star of the Season* webpage (http://www.aavso.org/vsots_archive).

RR Lyrae stars are subdivided into RRab stars which are pulsating in the fundamental mode, RRc stars which are pulsating in the first overtone, and RRd stars which are pulsating in both modes. RRc stars tend to lie on the blue (hot) side of the instability strip in the HR diagram. Some RR Lyrae stars show the *Blazhko effect* which is a slow, quasi-periodic change in the amplitude and shape of the light curve.

Percy *et al.* (2012) recently analyzed the period changes of fifty-nine RRab and RRc stars as a pilot research project and as an educational project, using times of maximum from the GEOS database. Le Borgne *et al.* (2007) had

analyzed the period changes of some of the RRab stars a few years earlier. Walker (2010a, 2010b, 2010c, 2011) has carried out detailed analyses of the RRab stars RR Lyr, AR Her, BD Dra, and RW Dra (also EF Cnc, which is classified in the *General Catalogue of Variable Stars* (GCVS; Kholopov *et al.* 1985) as an eclipsing variable). Walker's four RRab stars have (O–C) diagrams with a complex mixture of period changes and Blazhko effect.

The period changes of RRc stars are more difficult to measure, because RRc stars have sinusoidal light curves with rounded maxima, whereas the RRab stars have light curves with sharp, easy-to-measure maxima. In the present paper, we analyze the period changes of forty RRc stars.

Since many of the times of maxima of RR Lyrae stars are measured by AAVSO observers, one important purpose of this paper is to provide observers with feedback on how their measurements are used in astronomical research. Another important purpose of this paper is to demonstrate how undergraduate students (such as co-author Tan) can carry out useful research with archival variable star data.

2. Data and analysis

We used times of maximum t(max) in a database of the Groupe Européen d'Observation Stellaire (GEOS), and the standard (O–C) method of analysis (see, for example, Percy 2007): we compare the observed time of maximum (O) with the calculated time (C), where C = t(0) + NP where t(0) is an initial epoch (time of maximum), P is the period (assumed to be constant), and N is an integer. A parabola is fit to the (O–C) diagram, and the rate of period change is proportional to the quadratic term in the best-fit parabola. The GEOS database is at: http://dbrr.ast.obs-mip.fr

The number of times of maximum in the database ranged from one to several hundred. For a satisfactory fit to the parabola, we require at least several dozen times of maximum, well-distributed in time with no lengthy gaps. That is because, if the gap is too long, it is often not possible to know the correct values of N corresponding to each time of maximum. We therefore examined all RRc stars in the database with at least one or two dozen times of maximum, and analyzed those without significant gaps. They are listed in Table 1. For completeness, the following stars were also examined, but not found suitable for analysis because of insufficient or poorly-distributed times of maximum: NU And, RW Ari, BS Boo, AK Com, AN Com, AR Com, AY Com, AZ Com, CE Com, CS Com, DQ Com, DR Com, DY Com, FI Com, FL Com, HY Com, V791 Cyg, V835 Cyg, V926 Cyg, V997 Cyg, EG Del, V410 Her, V458 Her, V806 Her, BB Leo, BR Leo, BX Leo, LO Lyr, LQ Lyr, LR Lyr, V518 Mon, V535 Mon, V558 Oph, V980 Oph, V2598 Oph, V2652 Oph, RU Psc, SX UMa, and AU Vir. The following stars in the table are suspected of being eclipsing binaries: UU Cam, BB CMi, V508 Cyg, KN Per, and perhaps V789 Cyg (see,

for example, Hubscher *et al.* 2010). The sinusoidal light curve of an RRc star can be mistaken for that of a W UMa binary with equal minima.

The times of maximum have been determined by a wide variety of observers, using a wide variety of instruments and methods. Also, the database does not state how each time of maximum was measured from the light curve, but we presume that most were measured using Pogson's method, or by fitting a low-order polynomial to the light curve maximum. There is a significant benefit to using the *whole* light curve to determine the time of maximum, where this is possible.

Analysis was done with a least-squares routine, written in Python, based on the Levenberg-Marquardt algorithm (as implemented in the module scipy.optimize.leastsq); it gives the coefficients of the parabola, and their standard errors. *SciPy.org* is community-developed, open-source software for science, mathematics, and engineering.

3. Results

The results of the analysis are contained in Table 1, which lists: the name of the star, the number of times of maximum, the rate of period change in days per day, the characteristic evolution time τ, and the elements used for the analysis. We define τ as P/dP/dt; it is a measure of rate of evolution, but not necessarily the length of time that the star spends in the instability strip. The stars marked * have period changes which are significant at the 2σ level or better.

The stars in Table 1 are classified RRc in the GEOS database and in the GCVS. The stars with longer-than-average periods have amplitudes which are consistent with the RRc classification.

Some stars with fewer than twenty t(max) gave useful results, if the t(max) were well-distributed in time. The errors are large in some cases, but they still provide an upper limit to the rate of period change during the interval of observation.

Figures 1 through 4 show a selection of (O–C) diagrams. TV Boo (Figure 1) is well fit by a parabola, representing a period increase. AE Boo (Figure 2) can be fit by a parabola to yield an upper limit to the rate of period change, if dP/dt is constant. HY Com (Figure 3) is distinctly non-parabolic; it has a wavelike appearance. It can still be fit by a parabola to yield an upper limit to any underlying linear period change. SX UMa (Figure 4) is extremely complex, and is discussed below.

4. Notes on individual stars

The following comments apply to the (O–C) given in the GEOS database. TV Boo: an extra cycle was added to the t(max) at JD 2417703.3900. CQ Boo: the t(max) at JD 2435868.6300 was not used, because of the long gap following

it. UY Cam: the t(max) at JD 2435565.2390 was not used because of the long gap following it. DY Com: unusually large scatter. RV CrB: very large, non-parabolic excursions in the (O–C) diagram. VZ Dra: there are four t(max) for which the cycle number had to be adjusted. LR Lyr: there are two t(max) for which the cycle number had to be adjusted, and the t(max) at JD 2436272.565 was not used because of the long gap preceding it. V535 Mon: the cycle number of the first t(max) was adjusted by one, and the last three t(max) were not used because of the long gap preceding them. ET Mus: one cycle was added to the t(max) at JD 2436732.3060. V2598 Oph: the data are sparse, but all t(max) are CCD measurements. SS Psc: the t(max) at JD 2392862.4750 was not used because of the large gap following it.

SX UMa is an unusual case; its (O–C) diagram (Figure 4) is extremely complex. The discontinuities occur because one or more cycles need to be (but have not been) added at those times. Even with such cycles added, however, the (O–C) diagram can only be represented by a number of different periods at different epochs. These periods are given in various publications and editions of the GCVS. The following are taken from the GEOS database: max = 2416200.486 + 0.3071148E (before JD2418800); max = 2418800.213 + 0.3071345E (JD2418800-22500); max = 2422653.5032 + 0.30711855E (JD2422500-26000); max = 2426400.418 + 0.3071555E (JD2426000-29500); max = 2430000.250 + 0.3071301E (JD2429500-34000); max = 2438508.751 + 0.3071363E (JD2434000-39000), where E is an integer.

Three other stars have distinctly non-parabolic (O–C) diagrams: RV CrB, RU Psc, and HY Com. These four stars all have relatively long periods: 0.307 day (SX UMa), 0.332 day (RV CrB), 0.390 day (RU Psc), and 0.449 day (HY Com).

5. Discussion and conclusions

The shorter-period stars (P less than 0.275 day) seem to have smaller rates of period change, and therefore longer evolution times; for four out of five, the period change is close to zero. These stars are of special interest, because there are very few stars in globular clusters with such short periods. The longer-period stars (P greater than 0.275 day) are equally divided into increasing and decreasing periods, though the longest-period stars generally tend to have decreasing periods. The rates range from ±1 to ±1000 × 10^{-10} day per day, or 0.04 to 40 days per million years—another commonly-used unit.

It is not simple to compare our observed period changes with those predicted by models of stellar evolution. Our stars are few in number; the number and range of the t(max) is limited; and their accuracy is not as great as for RRab stars. Furthermore: the predicted period changes depend on the mass and metallicity of the stars, and our stars (unlike those in a globular cluster) are field stars which have a range of metallicities and presumably of masses. The

rates of period change, and the time that the star spends in the instability strip in the HR diagram, are especially sensitive to the mass of the star (Lee 1991). Lee predicts rates of ±0.2 d/Myr, including an allowance for scatter in the observed values, with a majority of the rates expected to be positive. Lee attributes the negative period changes to "random error," though it is not clear how such an error would arise, observationally.

About half of our values are significantly greater than the expected rates, and the same has been found in other studies. We note that some of our stars show distinctly non-parabolic (O–C) diagrams, and this is also not in agreement with evolutionary models. One suggested explanation is random mixing events which arise from composition instabilities in the cores of the stars (Sweigart and Renzini 1979). Observations of non-parabolic (O–C) diagrams may therefore shed light on the processes at work in these stars.

If the non-parabolic period changes are random, they may—over a long enough time—average out to the evolutionary rate of period change. One might then expect to see smaller average period changes for those RR Lyrae stars that have been observed for the longest time. In Table 1, the stars which have been observed for the shortest time tend to have large errors associated with the rate of period change. However, it is indeed true that the stars with the longest datasets (typically 30,000 days or more) have smaller rates of period change. Some pulsating variables show random cycle-to-cycle period fluctuations, but Percy *et al.* (2007) did not find such fluctuations in the one RR Lyrae star (XZ Dra) which they studied.

The strength of our data would improve if there were more measurements of t(max), if their time span were longer, and if they were more accurate (CCD measurements instead of visual, for instance). However, the data are sufficient to show that: (i) many of the stars show period changes whose nature and size are consistent with predictions of evolutionary models; (ii) some stars show period changes which do not agree, in nature and size, with predictions; (iii) systematic measurements of t(max) in these stars have both scientific and educational value.

The power of (O–C) analysis increases as the *square* of the length of the dataset, so further systematic, sustained observations of these stars would be scientifically valuable. To quote Lee (1991), referring to the comparison between observations and theory: "Observations of the RR Lyrae stars over the next century will undoubtedly help to clarify this problem further."

6. Acknowledgements

We thank GEOS and all of the observers who made the measurements on which this study is based. We also thank both Professor Christine Clement and the referee for providing helpful comments. This work was supported by the Ontario Work-Study Program.

References

Hubscher, J., Lehmann, P. B., Monninger, G., Steinbach, H., and Walter, F. 2010, *Inf. Bull. Var. Stars*, No. 5941, 1.
Jurcsik, J., *et al.* 2012, *Mon. Not. Roy. Astron. Soc*., **419**, 2173.
Kholopov, P. N., *et al.* 1985, *General Catalogue of Variable Stars*, 4th ed., Moscow.
Le Borgne, J. F., *et al.* 2007, *Astron. Astrophys.*, **476**, 307.
Lee, Y. -W. 1991, *Astrophys. J.*, **367**, 524.
Percy, J. R. 2007, *Understanding Variable Stars*, Cambridge Univ. Press, Cambridge.
Percy, J. R., Bandara, K., and Cimino, P. 2007, *J. Amer. Assoc. Var. Star Obs.*, **35**, 343.
Percy, J. R., MacNeil, D., Meema-Coleman, L., and Morenz, K., 2012, arxiv.org/abs/1202.5773.
Smith, H. 1995, *The RR Lyrae Stars*, Cambridge Univ. Press, Cambridge.
Sweigart, A. V., and Renzini, A. 1979, *Astron. Astrophys.*, **71**, 66.
Walker, E. N. 2010a, *The Observatory*, **130**, 1.
Walker, E. N. 2010b, *The Observatory*, **130**, 159.
Walker, E. N. 2010c, *The Observatory*, **130**, 225.
Walker, E. N. 2011, *The Observatory*, **131**, 155.

Table 1. Rates of period change, and characteristic evolution times for RRc stars.

Star	*N*	*dP/dt (d/d)*	*τ(MY)*	*Elements*
NT And	53	2.24e–09 ± 1.55e–09	0.430 ± 0.298	2438642.4300 + 0.351661E
TV Boo*	97	1.82e–10 ± 1.50e–11	4.71 ± 0.389	2424609.5150 + 0.31255936E
AE Boo	57	7.87e–11 ± 5.22e–11	11.0 ± 7.26	2430388.2003 + 0.3148921E
BS Boo	20	–1.42e–08 ± 1.12e–08	0.0569 ± 0.0449	2437669.62 + 0.296149E
CQ Boo*	48	–2.07e–09 ± 7.11e–10	0.372 ± 0.128	2450948.5480 + 0.281883E
UY Cam*	54	1.02e–10 ± 1.87e–11	7.18 ± 1.32	2435565.2390 + 0.26704234E
ST CVn*	66	1.71e–10 ± 4.10e–11	5.26 ± 1.26	2440390.467 + 0.329051E
RZ Cep*	426	–1.32e–10 ± 1.61e–11	6.38 ± 0.777	2442635.374 + 0.3086853E
EZ Cep*	103	1.49e–10 ± 1.97e–11	6.95 ± 0.917	2426631.3700 + 0.378999E
U Com	36	–2.48e–11 ± 2.88e–11	32.4 ± 37.6	2424961.445 + 0.2927382E
AK Com	16	–3.85e–08 ± 4.5e–08	0.0258 ± 0.0301	2437737.63 + 0.36299E
AR Com	21	–2.01e–08 ± 4.07e–08	0.0397 ± 0.0806	2437764.45 + 0.291303E
AY Com	22	4.21e–08 ± 6.14e–08	0.0231 ± 0.0336	2437696.51 + 0.35455E
AZ Com	19	–5.04e–09 ± 6.57e–08	0.217 ± 2.83	2437696.59 + 0.39983E
CE Com*	19	5.73e–08 ± 2.14e–08	0.0145 ± 0.00542	2437668.44 + 0.304579E
CS Com*	22	–9.61e–08 ± 4.31e–08	0.00873 ± 0.00392	2437752.37 + 0.30645E
DQ Com	27	–5.83e–09 ± 3.33e–08	0.15 ± 0.859	2437764.24 + 0.320379E
DY Com*	19	8.73e–08 ± 3.99e–08	0.0112 ± 0.00511	2437785.28 + 0.35667E
FI Com	17	3.32e–08 ± 2.94e–08	0.0292 ± 0.0259	2437668.55 + 0.35344E
FL Com	26	2.25e–08 ± 2.7e–08	0.0442 ± 0.053	2437669.5 + 0.363775E
RV CrB*	282	8.61e–11 ± 3.92e–11	10.5 ± 14.5	2442926.3340 + 0.331565E
V791 Cyg*	54	–4.71e–09 ± 1.48e–09	0.197 ± 0.062	2433999.3804 + 0.33804949E

table continued on next page

Table 1. Rates of period change, and characteristic evolution times for RRc stars, cont.

Star	*N*	*dP/dt (d/d)*	*τ(MY)*	*Elements*
V926 Cyg	19	4.16e–11 ± 1.67e–10	20.2 ± 81.2	2433749.1992 + 0.30697965E
VZ Dra*	302	–4.57e–10 ± 7.38e–11	1.93 ± 0.311	2443534.7546 + 0.321025E
LS Her	95	1.49e–11 ± 2.23e–11	42.4 ± 63.4	2428004.9470 + 0.23080771E
BB Leo*	25	6.74e–08 ± 2.56e–08	0.0128 ± 0.00488	2437731.561 + 0.316028E
BR Leo*	18	–8.82e–08 ± 3.58e–08	0.0108 ± 0.00439	2437647.32 + 0.348384E
BX Leo*	17	–1.7e–09 ± 3.7e–10	0.584 ± 0.127	2438406.72 + 0.36286E
TV Lyn	74	2.87e–11 ± 1.76e–11	22.9 ± 14.1	2440950.9220 + 0.24065119E
LQ Lyr*	39	–7.97e–09 ± 3.58e–09	0.119 ± 0.0533	2429373.559 + 0.3451239E
LR Lyr	27	3.59–09 ± 4.93e–09	0.258 ± 0.355	2436272.565 + 0.338471E
V518 Mon	34	–1.03e–09 ± 5.78e–10	0.931 ± 0.526	2434769.522 + 0.34874473E
V535 Mon*	31	–5.48e–09 ± 5.43e–10	0.166 ± 0.0165	2434795.334 + 0.3328635E
ET Mus*	50	5.97e–09 ± 1.83e–09	0.105 ± 0.0322	2438536.2770 + 0.2296741E
V980 Oph*	16	–3.97e–10 ± 6.12e–11	2.39 ± 0.369	2435640.418 + 0.34696946E
V2598 Oph*	13	1.7e–09 ± 1.42e–10	0.623 ± 0.0518	2444374.383 + 0.38749054E
DH Peg	162	–1.16e–11 ± 3.46e–11	60.3 ± 180	2444463.5710 + 0.2555104E
SS Psc*	95	–7.76e–11 ± 1.90e–11	10.2 ± 2.49	2419130.3050 + 0.28779276E
T Sex*	52	4.02e–10 ± 9.79e–11	2.21 ± 0.538	2441384.3000 + 0.324698E
ER Sge*	55	1.29e–09 ± 1.60e–10	0.885 ± 0.11	2442585.9470 + 0.418431E
SX UMa	150	—	—	—

** Period change significant at the 2-sigma level or better.*

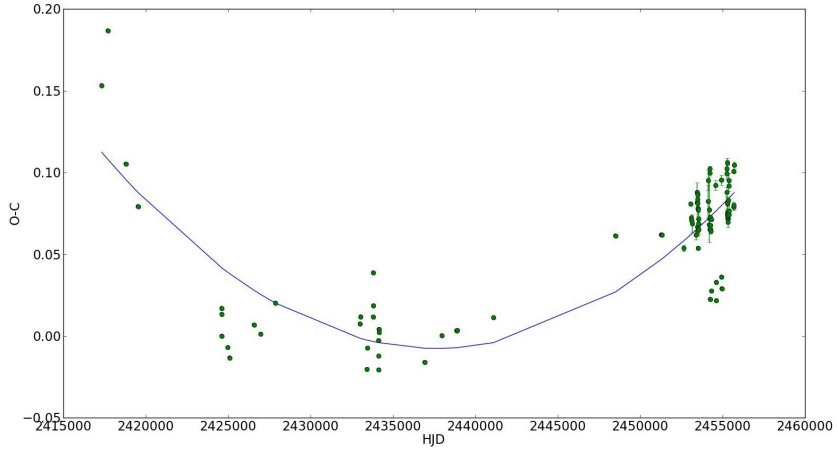

Figure 1. The (O–C) diagram of TV Boo. The diagram is parabolic, and corresponds to a period increase at a rate of $+1.82 \times 10^{-10}$ day/day.

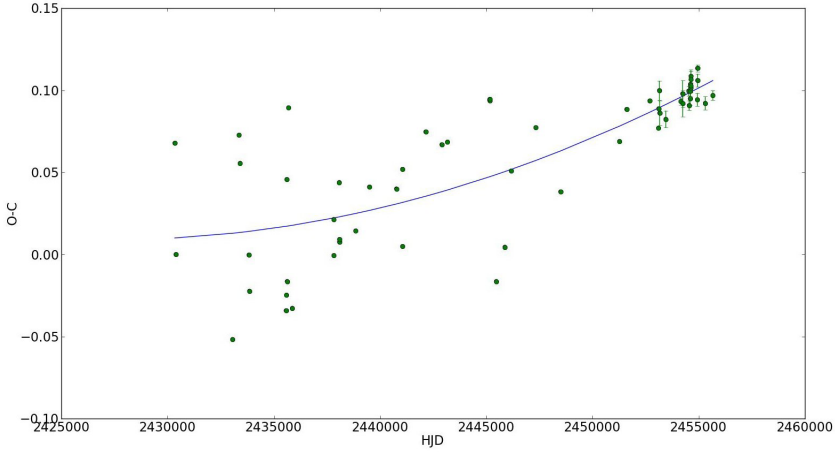

Figure 2. The (O–C) diagram of AE Boo. The diagram is rather scattered, but yields a period increase of $+7.87 \times 10^{-11}$ day/day with a σ which is comparable with the period change. It does, however, set a 3σ upper limit to the rate of period change.

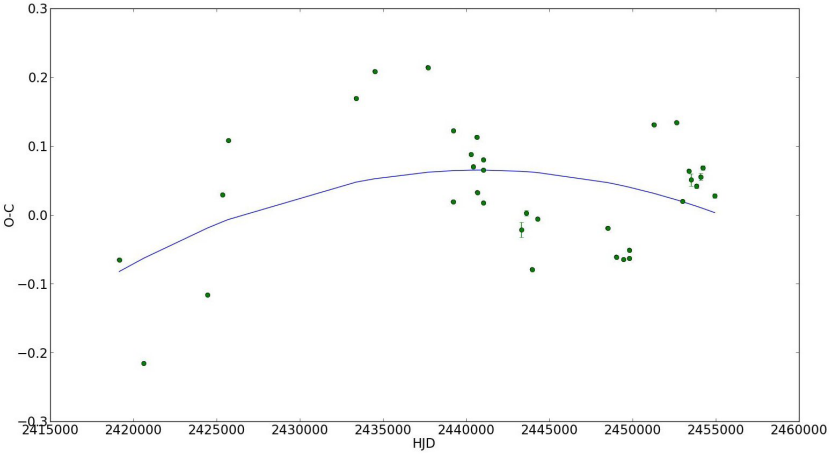

Figure 3. The (O–C) diagram of HY Com. The diagram does not appear to be sinusoidal, rather, it appears wavelike.

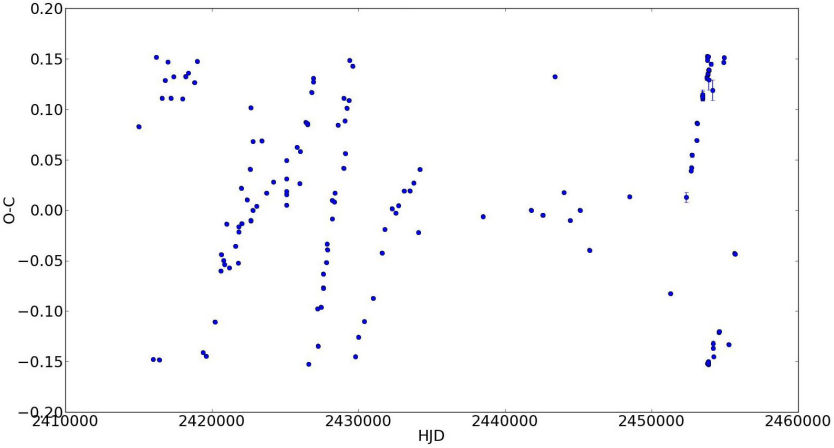

Figure 4. The (O–C) diagram of SX UMa. The diagram is very complex, and there are epochs at which extra cycles need to be added. See text for further discussion.

Recent Maxima of 61 Short Period Pulsating Stars

Gerard Samolyk
P.O. Box 20677, Greenfield WI 53220; gsamolyk@wi.rr.com

Received January 7, 2013; accepted January 7, 2013

Abstract This paper contains times of maxima for 61 short period pulsating stars (primarily RR Lyrae and δ Scuti stars). This represents a portion of the CCD observations received by the AAVSO Short Period Pulsator (SPP) section in 2011 along with some earlier data.

1. Recent observations

This accompanying list contains times of maxima calculated from CCD observations made by participants in the AAVSO's Short Period Pulsator (SPP) Section. This list will be web-archived and made available through the AAVSO ftp site at ftp:ftp.aavso.org/public/datasets/gsamoj411b.txt. The error estimate is included. RR Lyr stars in this list, along with data from earlier AAVSO publications, are included in the GEOS database at: http://rr-lyr.ast.obs-mip.fr/dbrr/dbrr-V1.0_0.php. This database does not include δ Scuti stars. These observations were reduced by the writer using the PERANSO program (Vanmunster 2007). Column F indicates the filter used.

The linear elements in the *General Catalogue of Variable Stars* (GCVS; Kholopov *et al.* 1985) were used to compute the O–C values for most stars. For a few exceptions where the GCVS elements are missing or are in significant error, light elements from another source are used: VY CrB (Antipin 1996), DG Hya (Samolyk 2010), AH Leo (Schmidt *et al.* 1995), and VY LMi (Henden and Vidal-Sainz 1997).

References

Antipin, S. V. 1996, *Inf. Bull. Var. Stars,* No. 4343, 1.

Henden, A. A., and Vidal-Sainz, J. 1997, *Inf. Bull. Var. Stars,* No. 4535, 1.

Kholopov, P. N., *et al.* 1985, *General Catalogue of Variable Stars*, 4th ed., Moscow.

Samolyk, G. 2010 *J. Amer. Assoc. Var. Star Obs.*, **38**, 12 .

Schmidt, E. G., Chab, J. R., and Reiswig, D. E. 1995, *Astron. J.*, **109**, 1239.

Vanmunster, T. 2007, PERANSO period analysis software (http://www.peranso.com).

Table 1. Recent times of maxima of stars in the AAVSO Short Period Pulsator program.

Star	*JD(max) Hel. 2400000 +*	*Cycle*	*O–C*	*F*	*Observer*	*Error*
SW And	56156.9224	85974	–0.4028	V	R. Sabo	0.0009
SW And	56165.7721	85994	–0.3988	V	R. Sabo	0.0012
SW And	56173.7282	86012	–0.4036	V	R. Sabo	0.0018
SW And	56183.9025	86035	–0.4018	V	R. Sabo	0.0012
XX And	55930.5875	23304	0.2510	V	R. Sabo	0.0020
XX And	55943.5967	23322	0.2508	V	R. Sabo	0.0018
XX And	56169.8182	23635	0.2523	V	G. Samolyk	0.0021
XX And	56208.8501	23689	0.2559	V	R. Sabo	0.0014
ZZ And	56158.9461	56499	0.0297	V	R. Sabo	0.0016
ZZ And	56212.7292	56596	0.0232	V	R. Sabo	0.0011
AT And	56164.7728	22404	–0.0058	V	G. Samolyk	0.0025
AT And	56167.8568	22409	–0.0063	V	R. Sabo	0.0020
TZ Aur	55937.6845	92003	0.0125	V	K. Menzies	0.0009
TZ Aur	55938.8599	92006	0.0129	V	R. Sabo	0.0015
TZ Aur	56040.6955	92266	0.0130	V	R. Sabo	0.0006
TZ Aur	56213.8152	92708	0.0125	V	K. Menzies	0.0006
TZ Aur	56249.8496	92800	0.0129	V	K. Menzies	0.0006
BH Aur	55936.7427	28909	0.0007	V	G. Samolyk	0.0012
BH Aur	55936.7441	28909	0.0021	V	R. Sabo	0.0013
BH Aur	55964.5671	28970	0.0036	V	K. Menzies	0.0019
BH Aur	56173.9129	29429	0.0042	V	R. Sabo	0.0021
RS Boo	55962.9554	37612	–0.0076	V	R. Sabo	0.0013
RS Boo	56040.6882	37818	–0.0065	V	R. Sabo	0.0011
RS Boo	56061.8211	37874	–0.0046	V	R. Sabo	0.0010
ST Boo	56059.7761	59262	0.0994	V	R. Sabo	0.0016
ST Boo	56102.6970	59331	0.0822	V	R. Sabo	0.0008
SW Boo	55997.8409	26146	0.3752	V	K. Menzies	0.0012
SW Boo	56055.8736	26259	0.3793	V	R. Sabo	0.0010
SZ Boo	56006.8747	54257	0.0098	V	K. Menzies	0.0009
TV Boo	52763.6631	90076	0.0512	V	G. Lubcke	0.0013
TV Boo	56005.8676	100449	0.0775	V	K. Menzies	0.0011
TV Boo	56020.8994	100497	0.1064	V	R. Sabo	0.0017
TV Boo	56028.7226	100522	0.1157	V	R. Sabo	0.0017
TV Boo	56090.9164	100721	0.1101	V	R. Sabo	0.0031
TW Boo	55932.0214	54560	–0.0697	V	R. Sabo	0.0011
TW Boo	56042.7346	54768	–0.0693	V	R. Poklar	0.0011
UU Boo	56066.7075	43732	0.2502	V	R. Sabo	0.0011

Table continued on following pages

Table 1. Recent times of maxima of stars in the AAVSO Short Period Pulsator program, cont.

Star	*JD(max) Hel. 2400000 +*	*Cycle*	*O–C*	*F*	*Observer*	*Error*
UY Cam	55928.7325	76256	–0.0872	V	R. Poklar	0.0034
UY Cam	56195.7742	77256	–0.0879	V	G. Samolyk	0.0032
RW Cnc	55930.9037	29925	–0.3404	V	K. Menzies	0.0011
RW Cnc	55935.8343	29934	–0.3346	V	R. Sabo	0.0021
RW Cnc	55962.6417	29983	–0.3399	V	R. Sabo	0.0018
RW Cnc	55969.7686	29996	–0.3266	V	R. Sabo	0.0018
RW Cnc	55975.7902	30007	–0.3242	V	R. Sabo	0.0020
RW Cnc	55986.7198	30027	–0.3386	V	R. Sabo	0.0011
RW Cnc	56009.7135	30069	–0.3272	V	R. Sabo	0.0018
RW Cnc	56061.6917	30164	–0.3329	V	R. Sabo	0.0010
TT Cnc	55961.6644	28427	0.1213	V	R. Sabo	0.0018
TT Cnc	55996.5749	28489	0.0979	V	N. Simmons	0.0013
TT Cnc	56010.6696	28514	0.1064	V	R. Sabo	0.0017
TT Cnc	56260.8363	28958	0.1016	V	K. Menzies	0.0013
VZ Cnc	55929.8441	89886	0.0196	V	G. Samolyk	0.0010
VZ Cnc	55934.8402	89914	0.0215	V	R. Sabo	0.0013
VZ Cnc	56039.6981	90502	0.0016	V	R. Sabo	0.0018
VZ Cnc	56054.6808	90586	0.0017	V	R. Sabo	0.0011
SS CVn	56020.7876	34269	–0.3536	V	K. Menzies	0.0018
RZ Cap	56185.6846	11972	–0.0014	V	G. Samolyk	0.0017
YZ Cap	51451.6199	28238	0.0199	V	G. Samolyk	0.0051
YZ Cap	52504.7154	32089	0.0352	V	G. Samolyk	0.0052
AN Cap	56185.6913	4672	0.0004	V	G. Samolyk	0.0016
RR Cet	56258.7249	41729	0.0096	V	R. Poklar	0.0016
RX Cet	56225.6336	28063	0.3216	V	R. Poklar	0.0036
RX Cet	56283.5717	28164	0.3168	V	G. Samolyk	0.0019
RZ Cet	56193.8411	43648	–0.1885	V	G. Samolyk	0.0015
RZ Cet	56236.7251	43732	–0.1958	V	R. Poklar	0.0019
UU Cet	56227.7121	24781	–0.1571	V	R. Poklar	0.0021
VY CrB	56094.6126	30928	–0.1315	V	K. Menzies	0.0021
XX Cyg	55712.7225	83471	0.0022	V	K. Menzies	0.0005
XX Cyg	56064.8558	86082	0.0026	V	G. Samolyk	0.0005
XZ Cyg	55698.8139	24805	–2.1196	V	G. Samolyk	0.0009
XZ Cyg	55713.7486	24837	–2.1193	V	G. Samolyk	0.0010
XZ Cyg	55719.8130	24850	–2.1220	V	G. Samolyk	0.0012
XZ Cyg	56061.8335	25583	–2.1926	V	G. Samolyk	0.0009
DM Cyg	56086.8546	32164	0.0715	V	G. Samolyk	0.0013

Table continued on following pages

Table 1. Recent times of maxima of stars in the AAVSO Short Period Pulsator program, cont.

Star	*JD(max) Hel. 2400000 +*	*Cycle*	*O–C*	*F*	*Observer*	*Error*
DM Cyg	56112.8858	32226	0.0714	V	R. Sabo	0.0015
DM Cyg	56120.8640	32245	0.0723	V	R. Sabo	0.0012
DM Cyg	56152.7829	32321	0.0819	V	R. Sabo	0.0030
DM Cyg	56157.8133	32333	0.0739	V	R. Sabo	0.0010
DM Cyg	56168.7320	32359	0.0763	V	R. Sabo	0.0014
DM Cyg	56208.6164	32454	0.0740	V	R. Sabo	0.0015
DM Cyg	56261.5181	32580	0.0733	V	K. Menzies	0.0010
RW Dra	55657.8715	36757	0.1803	V	R. Sabo	0.0006
RW Dra	55692.8947	36836	0.2131	V	R. Sabo	0.0006
RW Dra	56081.7503	37714	0.1876	V	G. Samolyk	0.0016
RW Dra	56096.8480	37748	0.2261	V	R. Sabo	0.0010
RW Dra	56146.9016	37861	0.2300	V	R. Sabo	0.0007
RW Dra	56210.6560	38005	0.2045	V	R. Sabo	0.0010
XZ Dra	55713.7789	28931	–0.1298	V	G. Samolyk	0.0013
XZ Dra	56076.8746	29693	–0.1248	V	R. Sabo	0.0014
XZ Dra	56129.7762	29804	–0.1144	V	R. Sabo	0.0028
SV Eri	53000.8150	24444	0.6668	V	G. Samolyk	0.0039
SV Eri	53322.7803	24895	0.7100	V	G. Samolyk	0.0023
SV Eri	55146.6423	27450	0.8221	V	G. Samolyk	0.0029
SS For	56185.7957	35357	–0.1445	V	G. Samolyk	0.0016
RR Gem	55928.8997	36677	–0.4662	V	R. Sabo	0.0011
RR Gem	55929.6928	36679	–0.4677	V	R. Poklar	0.0010
RR Gem	55931.6759	36684	–0.4712	V	R. Sabo	0.0009
RR Gem	55961.8696	36760	–0.4731	V	R. Sabo	0.0013
RR Gem	55964.6537	36767	–0.4701	V	K. Menzies	0.0009
RR Gem	55965.8462	36770	–0.4696	V	R. Sabo	0.0017
RR Gem	55970.6103	36782	–0.4732	V	N. Simmons	0.0007
RR Gem	55985.7089	36820	–0.4724	V	R. Sabo	0.0010
VX Her	55648.8954	74441	0.0046	V	G. Samolyk	0.0010
VX Her	55654.8135	74454	0.0029	V	K. Menzies	0.0020
VX Her	55969.9237	75146	–0.0049	V	N. Simmons	0.0008
VX Her	56058.7193	75341	–0.0070	V	R. Sabo	0.0016
VX Her	56058.7194	75341	–0.0069	V	G. Samolyk	0.0012
VZ Her	56059.9200	43765	0.0718	V	R. Sabo	0.0008
VZ Her	56112.7588	43885	0.0713	V	R. Sabo	0.0009
AR Her	56049.7174	31055	–1.3492	V	R. Poklar	0.0016
AR Her	56054.8888	31066	–1.3480	V	R. Sabo	0.0016

Table continued on following pages

Table 1. Recent times of maxima of stars in the AAVSO Short Period Pulsator program, cont.

Star	*JD(max) Hel. 2400000 +*	*Cycle*	*O–C*	*F*	*Observer*	*Error*
AR Her	56062.8644	31083	–1.3629	V	G. Samolyk	0.0012
AR Her	56081.6828	31123	–1.3456	V	G. Samolyk	0.0021
AR Her	56126.7858	31219	–1.3653	V	R. Sabo	0.0017
DL Her	56028.8900	30121	0.0390	V	R. Sabo	0.0021
DL Her	56105.8197	30251	0.0571	V	R. Sabo	0.0029
DL Her	56121.7700	30278	0.0335	V	R. Sabo	0.0017
DY Her	55605.8963	149137	–0.0243	V	K. Menzies	0.0012
DY Her	55646.7653	149412	–0.0289	V	K. Menzies	0.0012
DY Her	55713.6509	149862	–0.0274	V	N. Simmons	0.0006
DY Her	55975.9851	151627	–0.0276	V	R. Sabo	0.0012
DY Her	56039.8966	152057	–0.0276	V	R. Sabo	0.0009
DY Her	56066.7988	152238	–0.0276	V	R. Sabo	0.0008
DY Her	56085.6743	152365	–0.0283	V	G. Samolyk	0.0013
DY Her	56099.7930	152460	–0.0296	V	R. Sabo	0.0007
DY Her	56106.7804	152507	–0.0279	V	R. Sabo	0.0009
DY Her	56109.6040	152526	–0.0282	V	K. Menzies	0.0005
LS Her	55629.8955	119688	0.0353	V	K. Menzies	0.0011
LS Her	56085.6908	121663	–0.0146	V	G. Samolyk	0.0033
V365 Her	56184.5269	44276	–0.2092	V	K. Menzies	0.0018
SZ Hya	56000.7178	28519	–0.2480	V	R. Poklar	0.0015
SZ Hya	56007.6615	28532	–0.2885	V	R. Poklar	0.0026
SZ Hya	56283.8522	29046	–0.2392	V	G. Samolyk	0.0010
DG Hya	56001.7278	4809	0.0097	V	R. Poklar	0.0022
DH Hya	55981.7371	50727	0.0814	V	R. Poklar	0.0012
XZ Lac	56182.6388	29029	0.0230	V	K. Menzies	0.0011
RR Leo	55963.8890	28003	0.1174	V	R. Sabo	0.0008
RR Leo	55969.7716	28016	0.1189	V	N. Simmons	0.0010
SS Leo	56008.7359	22715	–0.0794	V	R. Poklar	0.0013
SS Leo	56020.6340	22734	–0.0818	V	K. Menzies	0.0009
SS Leo	56055.7087	22790	–0.0824	V	R. Sabo	0.0007
ST Leo	56005.6300	58752	–0.0216	V	K. Menzies	0.0008
ST Leo	56014.7121	58771	–0.0212	V	R. Poklar	0.0010
ST Leo	56037.6559	58819	–0.0206	V	K. Menzies	0.0007
TV Leo	55991.7273	28164	0.1166	V	R. Poklar	0.0020
WW Leo	56008.5450	35044	0.0414	V	K. Menzies	0.0011
AA Leo	55999.7311	27400	–0.0901	V	R. Sabo	0.0012
VY LMi	55963.6418	10408	0.0072	V	K. Menzies	0.0016

Table continued on following pages

Table 1. Recent times of maxima of stars in the AAVSO Short Period Pulsator program, cont.

Star	*JD(max) Hel. 2400000 +*	*Cycle*	*O–C*	*F*	*Observer*	*Error*
SZ Lyn	55570.6471	144740	0.0245	V	R. Poklar	0.0008
SZ Lyn	55601.6239	144997	0.0239	V	G. Samolyk	0.0007
SZ Lyn	55639.7115	145313	0.0224	V	G. Samolyk	0.0011
SZ Lyn	55654.6578	145437	0.0224	V	N. Simmons	0.0010
SZ Lyn	55932.6119	147743	0.0230	V	R. Poklar	0.0010
SZ Lyn	55932.7321	147744	0.0226	V	R. Poklar	0.0007
SZ Lyn	55935.6269	147768	0.0246	V	G. Samolyk	0.0008
SZ Lyn	55936.5888	147776	0.0222	V	N. Simmons	0.0006
SZ Lyn	55958.5270	147958	0.0231	V	G. Samolyk	0.0006
SZ Lyn	55958.6474	147959	0.0229	V	G. Samolyk	0.0006
SZ Lyn	55969.6165	148050	0.0233	V	N. Simmons	0.0005
SZ Lyn	55995.6533	148266	0.0246	V	N. Simmons	0.0007
SZ Lyn	55999.6306	148299	0.0243	V	R. Poklar	0.0007
RR Lyr	56185.6431	23396	–0.2143	V	G. Samolyk	0.0018
RZ Lyr	56076.9016	29132	–0.0350	V	R. Sabo	0.0020
RZ Lyr	56093.7780	29165	–0.0297	V	R. Sabo	0.0010
RZ Lyr	56093.7806	29165	–0.0271	V	K. Menzies	0.0011
RZ Lyr	56096.8460	29171	–0.0291	V	R. Sabo	0.0016
RZ Lyr	56115.7562	29208	–0.0349	V	R. Sabo	0.0012
RZ Lyr	56160.7298	29296	–0.0506	V	R. Sabo	0.0008
RZ Lyr	56164.8245	29304	–0.0458	V	R. Sabo	0.0015
RZ Lyr	56180.6776	29335	–0.0412	V	R. Sabo	0.0013
AV Peg	55716.7874	30551	0.1339	V	K. Menzies	0.0008
AV Peg	56102.8760	31540	0.1420	V	R. Sabo	0.0008
AV Peg	56111.8564	31563	0.1438	V	R. Sabo	0.0012
AV Peg	56164.9459	31699	0.1422	V	R. Sabo	0.0015
AV Peg	56170.8037	31714	0.1444	V	K. Menzies	0.0015
AV Peg	56183.6860	31747	0.1444	V	R. Sabo	0.0008
AV Peg	56223.5041	31849	0.1443	V	K. Menzies	0.0006
BF Peg	56115.8573	26531	–0.1091	V	R. Sabo	0.0029
BH Peg	56256.6193	26352	–0.1082	V	K. Menzies	0.0061
DF Ser	56054.8451	60185	0.0918	V	R. Sabo	0.0011
DF Ser	56076.7354	60235	0.0924	V	R. Sabo	0.0013
DF Ser	56086.8055	60258	0.0932	V	G. Samolyk	0.0015
DF Ser	56100.8151	60290	0.0933	V	R. Sabo	0.0016
DF Ser	56111.7548	60315	0.0881	V	R. Sabo	0.0006
RV UMa	55929.9506	23190	0.1282	V	G. Samolyk	0.0019

Table continued on next page

Table 1. Recent times of maxima of stars in the AAVSO Short Period Pulsator program, cont.

Star	*JD(max) Hel. 2400000 +*	*Cycle*	*O–C*	*F*	*Observer*	*Error*
RV UMa	55931.8213	23194	0.1267	V	R. Sabo	0.0013
RV UMa	55938.8391	23209	0.1236	V	R. Sabo	0.0014
RV UMa	55944.9241	23222	0.1238	V	G. Samolyk	0.0013
RV UMa	55968.7941	23273	0.1227	V	G. Samolyk	0.0016
RV UMa	56040.8752	23427	0.1226	V	R. Sabo	0.0013
AE UMa	55931.7145	236318	–0.0019	V	G. Samolyk	0.0007
AE UMa	55931.8061	236319	0.0037	V	G. Samolyk	0.0008

Two New Cool Variable Stars in the Field of NGC 659

Steven P. Souza
Department of Astronomy, Williams College, Williamstown, MA, 01267; ssouza@williams.edu

Received December 11, 2012; revised December 20, 2012; accepted December 20, 2012

Abstract From data taken in the course of a program to monitor variations in Hα emission by hot, massive stars, we report the incidental finding that the very red stars USNO-B1.0 1508-0065037 and USNO-B1.01507-0066512 are irregular variables with brightness ranges to date of 0.2 and 0.8 magnitude, respectively.

1. Introduction

Since summer 2010 we have been monitoring variations in Hα emission in early type stars in open cluster fields by means of narrowband photometry (Souza *et al.* 2011). While our focus is on Be and other hot stars, the temporal coverage and homogeneity of the observations provide opportunities for discovery of variables of other types. NGC 659 is a young (~35 MY) open cluster in Cassiopeia at a distance of ~4,900 pc (WEBDA; Inst. Astron., Univ. Vienna 2012). As home to at least five Be stars, it is a prime target of the program.

2. Observations and reduction

As a result of this monitoring, two stars have shown themselves to be irregular variables. USNO-B1.0 1508-0065037 (R.A. $01^h\ 44^m\ 37.56^s$, Dec. +60° 49' 53.5" (J2000)), has a brightness range of 0.2 magnitude. USNO-B1.0 1507-0066512, (R.A. $01^h\ 44^m\ 26.90^s$, Dec. +60° 44' 35.3" (J2000)), has a brightness range of 0.8 magnitude. Basic observational data for both stars, designated Star 1 and Star 2, are given in Table 1, and a finding chart for NGC 659 is provided in Figure 1. Observations were obtained with an Apogee U9000 CCD on the 0.6-m DFM Engineering telescope at Williams College, through matched 5 nm-wide 645-nm continuum and 656-nm Hα filters from Astrodon Imaging. The NGC 659 field was observed on twenty-six nights during 2010–2012. Useful data are obtained for stellar objects down to R ≈ 15. Each observation consists of multiple exposures to enable removal of cosmic ray artifacts.

We employ a semi-automated reduction pipeline described in Souza *et al.* (2013). Since photometric nights are extremely rare at our location, corrections for seeing, transparency, and airmass variations are critical. We use inhomogeneous ensemble photometry (Bhatti *et al.* 2010; Richmond 2012),

which employs all stars in the field, except those identified as variable, as reference stars. The magnitude scale is roughly set by determining an offset between mean measured narrowband magnitudes for a nonvariable early B star in the field and its R magnitude (from NOMAD; USNO 2012). This offset is then applied to all other objects in the field. While reasonable for early-type stars, this method—along with the possibility that Hα may be in emission in any given star—renders the narrowband magnitudes reported here unsuitable for comparison with other observations, for these cool stars.

3. Results and discussion

Figure 2 is the light curve for Star 1. Since the 645-nm and 656-nm light curves track each other well and differ only by a constant offset (656 nm – 645 nm = –0.055 ± 0.028), we plot the mean of 645-nm and 656-nm magnitudes as a function of Heliocentric Julian Date (HJD). Uncertainties are estimated by Ensemble 0.7 (Richmond 2012) from nonvariable stars of similar magnitude. Experience indicates that these error bars correspond to roughly ±2 standard deviations. Brightening occurs at about HJD – 2450000 = 5650, 5850, and 6220. The brightness range over the observed period is ~0.2 magnitude, and there is no evidence of periodicity.

Figure 3 is the light curve for Star 2, plotted similarly. Both stars are plotted with a magnitude range of 1.0 so that they may be more directly compared. For Star 2, 656 nm – 645 nm = –0.104 ± 0.062. Brightening occurs at about HJD – 2450000 = 5650 and 6010, and there is an overall dimming trend. The brightness range over the observed period is ~0.8 magnitude, and there is again no evidence of periodicity.

For both stars, variability over the observed period is significant and irregular. Brightening of both stars near HJD – 2450000 = 5650 is coincidental. A few of the ~330 stars measured in the field show such a feature, with no positional dependence and consistent with chance. Neither star is identified as variable in the GCVS, the VSX database, or elsewhere as found using VizieR identifier and positional searches. Star 1 has been classified as a carbon star (Aaronson *et al.* 1990), and with (B–V) ≈ 2.7, it is very red. Star 2, with (B–V) ≈ 2.3, is also very red, but has not been spectrally classified. Similarities in color and variability between this star and Star 1 make it tempting to speculate that it may also be a carbon star.

It is very unlikely that either of these stars is a member of NGC 659. From their colors and apparent magnitudes they must be much less distant than the cluster, so the ~0.65 magnitude of interstellar reddening at the cluster (WEBDA 2012) is not likely to be a major factor affecting their colors. If they are indeed carbon stars or stars of other evolved moderate- to low-mass type, NGC 659 is far too young to have produced them.

4. Acknowledgements

We gratefully acknowledge support from the Division III Research Funding Committee of Williams College, and the Office of the Dean of Faculty of Williams College. We would also like to thank the students who obtained some of the early data: S. Wilson (Williams College), E. Boettcher (Haverford College), A. Davis (Williams College), and Y. Teich (Vassar College). We thank an anonymous referee for several helpful suggestions.

This work made use of the following software and resources: astrometry.net (Lang *et al.* 2010); Aperture Photometry Tool 2.1.8 (Laher *et al.* 2012); Ensemble 0.7 (Richmond 2012); GCVS online edition (Samus *et al.* 2012); VSX AAVSO Variable Star Index (Watson *et al.* 2012); VizieR catalog access tool, CDS, Strasbourg, France (http://vizier.u-strasbg.fr); WEBDA database, Institute for Astronomy, University of Vienna (http://www.univie.ac.at/webda); NOMAD catalog, U.S. Naval Observatory (http://www.nofs.navy.mil/nomad).

References

Aaronson, M., Blanco, V. M., Cook, K. H., Olszewski, E. W., and Schechter, P. L. 1990, *Astrophys. J., Suppl. Ser.*, **73**, 841.

Bhatti, W. W., Richmond, M. W., Ford, H. C., and Petro, L. D. 2010, *Astrophys. J., Suppl. Ser.*, **186**, 233.

Institute for Astronomy, University of Vienna. 2012, WEBDA database (http://www.univie.ac.at/webda).

Laher, R. R., Gorjian, V., Rebull, L. M., Masci, F. J., Fowler, J. W., Helou, G., Kulkarni, S. R., and Law, N. M. 2012, *Publ. Astron. Soc. Pacific*, **124**, 737, (Aperture Photometry Tool 2.1.8, http://www.aperturephotometry.org).

Lang, D., Hogg, D. W., Mierle, K., Blanton, M., and Roweis, S. 2010, *Astron. J.*, **139**, 1782 (astronomy.net, http://astrometry.net).

Richmond, M. 2012, Ensemble 0.7 (http://spiff.rit.edu/ensemble).

Samus, N. N., *et al.* 2012, *General Catalogue of Variable Stars*, published online (http://www.sai.msu.su/gcvs/cgi-bin/search.htm).

Souza, S. P., Boettcher, E., Wilson, S., and Hosek, M. 2011, *Bull. Amer. Astron. Soc*., **43**, 322.01.

Souza, S. P., Davis A. B., and Teich Y. G. 2013, *Bull. Amer. Astron. Soc*., **45**, PM354.22.

U.S. Naval Observatory. 2012, NOMAD catalog (http://www.nofs.navy.mil/nomad).

Watson, C., Henden, A. A., and Price, A. 2012, AAVSO International Variable Star Index VSX (http://www.aavso.org/vsx).

Table 1. Identifications and basic observational data. Identifications and positions are from VizieR; magnitudes are from NOMAD (USNO 2012) as accessed through VizieR.

Parameter	*Star 1*	*Star 2*
USNO B1.0 identifier	1508-0065037	1507-0066512
NOMAD identifier	1508-0067389	1507-0069147
GSC 2.3 identifier	NAJ5009439	NAJ5008235
R.A. (J2000)	$01^h\ 44^m\ 37.56^s$	$01^h\ 44^m\ 26.90^s$
Dec. (J2000)	+60° 49' 53.5"	+60° 44' 35.3"
B	17.90	17.21
V	15.21	14.97
R	13.98	13.95

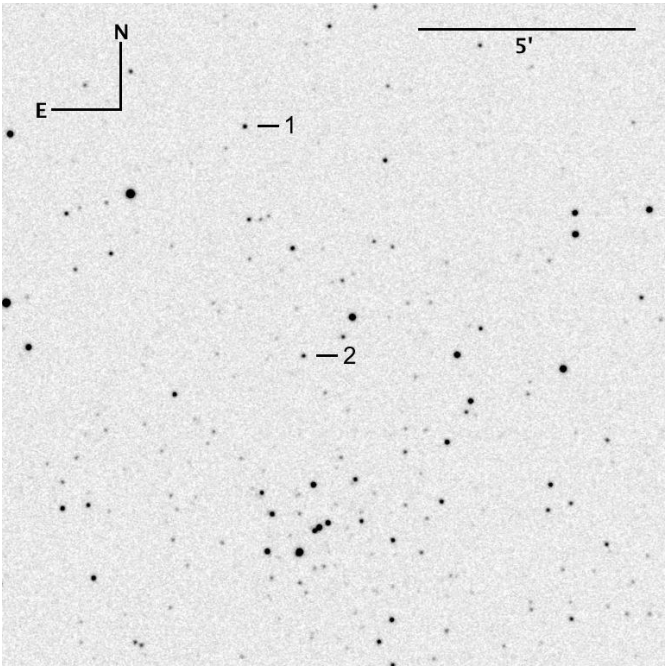

Figure 1. The field of NGC 659, from a 656-nm image taken 11 December 2011. The positions of Star 1 and Star 2 are indicated.

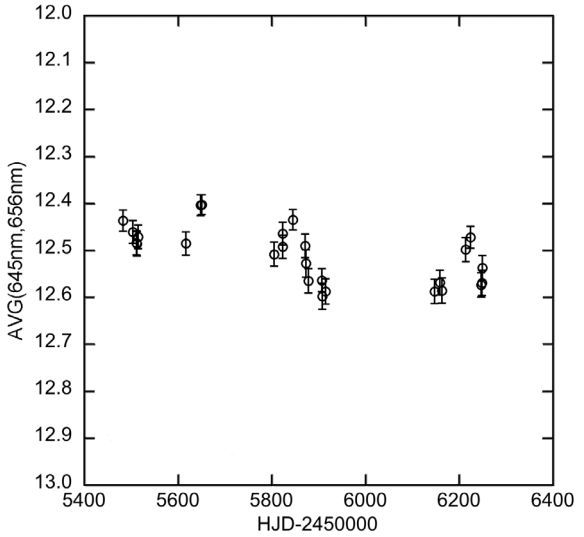

Figure 2. The light curve for Star 1 (USNO-B1.0 1508-0065037), plotted as the average of narrowband (5-nm wide) magnitudes at 645 nm and 656 nm. Figures 2 and 3 are plotted with the same 1.0 magnitude range so that they may be more directly compared.

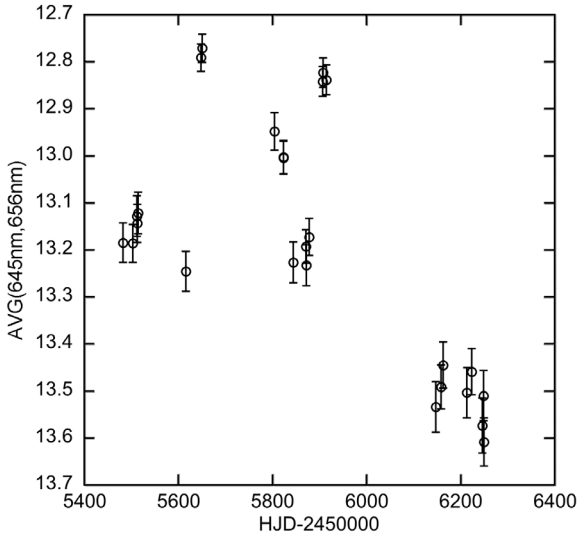

Figure 3. The light curve for Star 2 (USNO-B1.0 1507-0066512), plotted as in Figure 2.

Simultaneous CCD Photometry of Two Eclipsing Binary Stars in Pegasus—Part 1: KW Pegasi

Kevin B. Alton
UnderOak Observatory, 70 Summit Avenue, Cedar Knolls, NJ 07927; kbalton@optonline.net

Received December 5, 2012; revised January 3, 2013; accepted January 3, 2013

Abstract The coincidental location of BX Peg and KW Peg in the same field-of-view captured by the primary imaging system at UnderOak Observatory (UO) provided an opportunity to study both variable stars from the same exposures. Herein new findings for the eclipsing binary KW Peg will be presented while those from BX Peg will be discussed in a separate paper (Part 2). KW Peg, described as an "Algol type" eclipsing variable (P = 0.816402 d), is only reported in a single work published over twenty years ago. Photometric data collected in three bandpasses (B, V, and I_c), produced eight new times of minimum for KW Peg. These were used to update the linear ephemeris and further analyze potential changes in orbital periodicity by examining the available history of eclipse timings. In addition, synthetic fitting of light curves by Roche modeling was accomplished with programs employing the Wilson-Devinney code. Results from the present study provide a reasonable case for classifying KW Peg as a short-period RS CVn eclipsing binary rather than Algol-like. The primary star in KW Peg would appear to be a late stage G9V-K0V dwarf whereas the secondary is a slightly cooler K0-K1 companion. The eclipse-timing diagram for KW Peg is quite simple and indicates that, on average, the orbital period for this system has remained fairly constant over the past two decades.

1. Introduction

KW Peg was first detected as a variable by De Young (1991). The shape of the corresponding light curve suggested a semi-detached Algol-type eclipsing binary; however, aside from times-of-minimum from a number of different sources, no comprehensive analysis of this variable target is reported in the literature. The initial reported (De Young 1991) orbital period (0.816384 d) closely agrees with that published by Kreiner (2004).

2. Observations and data reduction

2.1. Astrometry

Images of KW Peg were automatically matched against the standard star fields (UCAC3) provided in MPO CANOPUS v10.3.0.2 (Minor Planet Observer 2010) and then rotated and scaled as necessary. Plate constants were

internally calculated which convert X/Y coordinates of a detected object to a corresponding right ascension and declination.

2.2. Photometry

A summary of CCD photometric session dates (UTC) is tabulated below for campaigns conducted in 2008 and 2011.

2008	2011	
October	October	November
8, 10, 12, 13, 16, 18, 19, 20, 24, 27, 31	6, 7, 8, 9, 10	3, 8

Equipment included a 0.2-m catadioptic telescope with an SBIG ST 402ME CCD camera mounted at the primary focus. Automated multi-bandwidth imaging was performed with SBIG photometric B, V, and I_c filters manufactured to match the Bessell prescription. Since accurate timing for each image is critical, the computer clock was updated automatically (Dimension 4; http://www.thinkman.com/dimension4/) via the U.S. Naval Observatory Time Server immediately prior to each session. In general, image acquisition (lights, darks, and flats) was performed using CCDSOFT v5 (Software Bisque 2011) while calibration and registration were accomplished with AIP4WIN v2.3.1 (Berry and Burnell 2005). MPO CANOPUS provided the means for further photometric reduction using the same five non-varying comparison stars to ultimately calculate ephemerides and orbital periods. No color or air mass corrections were applied since images were only taken above 30° altitude (airmass < 2.0), which minimizes error due to differential refraction and color extinction. The exposure time for all filters was 45 seconds during the 2008 campaign but increased in 2011 to 90 seconds for B and 60 seconds for V and I_c. Instrumental readings were reduced to catalogue-based magnitudes using the MPOSC3 reference star fields built into MPO CANOPUS. Almost all stars in MPOSC3 also have $BVRI_c$ magnitudes derived from 2MASS J–K magnitudes; these have an internal consistency of ±0.05 mag. for V, ±0.08 mag. for B, ±0.03 mag. for I_c, and ±0.05 mag. for B–V (Warner 2007).

2.3 Light curve analyses

Roche-type modeling was performed using BINARY MAKER 3 (Bradstreet and Steelman 2002), WDWINT v5.6a (Nelson 2009a), and PHOEBE v.31a (Prša and Zwitter 2005), the latter two of which employ the Wilson-Devinney (W-D) code (Wilson and Devinney 1971; Wilson 1979). BINARY MAKER 3 (BM3) is a commercial application whereas PHOEBE (http://phoebe.fiz.uni-lj.si/) and WDWINT (http://members.shaw.ca/bob.nelson/software1.htm) are freely available GUI implementations of the W-D modeling code. 3-D spatial renderings of KW Peg were also produced by BM3 once each model fit was finalized. Times of minimum (ToM) were estimated using the method of Kwee and van Woerden (1956) as implemented in MINIMA V25c (Nelson 2007).

3. Results and discussion

3.1. Photometry

Five stars in the same FOV as KW Peg were selected to calculate the relative change in flux and derive catalogue-based (MPOSC3) magnitudes using the "Comp Star Selector" feature in MPO CANOPUS (Table 1). The difference in magnitude over time from each comparison star against the averaged magnitude yielded a narrow range of values with no obvious trend; variability was generally within ±0.015 mag. for V and I_c filters and ±0.03 for B passband.

3.2. Ephemerides

3.2.1 Light curves from 2008 campaign

Photometric observations in B (n = 878), V (n = 884), and I_c (n = 891) filters were folded to produce light curves that spanned 23 days (Figure 1). These observations included four new ToM values in each bandpass. No meaningful color dependencies emerged; therefore the timings from all three filters were averaged for each session (Table 2). Initially seeded with the orbital period (0.816402 d) posted at the Mt. Suhora Astronomical Observatory website (Kreiner 2004), the Fourier analysis routine (FALC) in MPO CANOPUS provided a period solution for all the data. The corresponding linear ephemeris (Equation 1) from the 2008 campaign alone was determined to be:

$$\text{Min. I (hel.)} = 2454766.5239\ (10) + 0.8164109\ (1)\ E \qquad (1)$$

3.2.2 Light curves from 2011 campaign

Photometric observations in B (n = 634), V (n = 645), and I_c (n = 652) passbands were folded by filter to produce light curves that spanned 32 days of imaging (Figure 2). These observations included four new ToM values in each bandpass (Table 2). As described above with the 2008 light curves, Fourier analysis yielded the following linear ephemeris (Equation 2) for the 2011 data collected at UO:

$$\text{Min. I (hel.)} = 2455873.5661\ (16) + 0.8164109\ (1)\ E \qquad (2)$$

Each of these periods was calculated using fairly short sampling times (< 33 days). Fourier analysis of pooled (2008 and 2011) light curve data extends the baseline period to 1,126 days, thereby improving the robustness of the period estimate. The resulting linear ephemeris (Equation 3) compares favorably with the limited number of values reported since De Young (1991).

$$\text{Min. I (hel.)} = 2455873.5661\ (16) + 0.8164020\ (1)\ E \qquad (3)$$

As is standard practice at UnderOak Observatory (UO), all period determinations were independently confirmed using PERANSO v2.5 (CBA Belgium Observatory 2011) by applying periodic orthogonals (Schwarzenberg-Czerny 1996) to fit

observations and analysis of variance (ANOVA) to evaluate fit quality. In toto, five new primary (p) and three new secondary (s) minima were recorded during this investigation. These eight minima along with additional values cited in AAVSO, IBVS, OEJV, BBSAG, and B.R.N.O. publications were used to prepare these data for period analysis (Table 3). The reference epoch (Kreiner 2004) used to calculate eclipse timing (ET) residuals was defined by the following linear ephemeris (Equation 4):

$$\text{Min. I (hel.)} = 2452500.1930\ (2) + 0.81640201\ (8)\ E \qquad (4)$$

The progression of orbital periodicity over time can be visualized by plotting the difference between the observed eclipse times and those predicted by the reference epoch against the period cycle number (Figure 3). More commonly called an observed minus computed (O–C) diagram, this generalized term fails to exactly inform the reader about which variables are being analyzed. Going forward in this paper the term eclipse timing or ET diagram will be used instead. The ET diagram for KW Peg (Figure 3) proved to be a quite simple in that nearly all observations fall within a straight line relationship. Accordingly, the latest linear ephemeris (Equation 5) was calculated from linear least squares fitting of data acquired between 1990 and 2011:

$$\text{Min. I (hel.)} = 2455873.5657\ (2) + 0.81640193\ (8)\ E \qquad (5)$$

As expected from this binary system which has exhibited a constant orbital period thus far, values obtained from the reference epoch in 2002 (Kreiner 2004), pooled (2008 and 2011) light curve data, and that predicted from the ET diagram using all data (1990–2011) are internally consistent (P = 0.816402 d).

3.3 Spectral classification

Folded light curves from 2008 and 2011 were similar enough in each filter to combine prior to modeling with BM3 and PHOEBE. In retrospect, the similarity between these two epochs is not unexpected, given that evidence from the ET diagram (Figure 3) suggests no remarkable changes have occurred over the past twenty-one years. The associated light curve shapes are consistent with a detached binary. Minima appear to be equally separated and, unless our vantage point is coincidently staring directly down the semi-major axis of an elliptical system, this finding suggests a circular orbit for this system. Both peaks had very similar widths, further arguing against an elliptical orbit. No source was found in the literature which posited a spectral class for this binary system. It was therefore necessary to piece together assorted data produced at UO and from several other survey catalogues in order to make an informed guess regarding the classification, and by inference, its temperature. The effective temperature ($Teff_1$) of the primary was initially estimated from B–V magnitudes determined at UO during quadrature (0.25P and 0.75P). This color index (0.733) corresponds to the effective temperature (5462 K; log = 3.737) of

a G8 main sequence star (Flower 1996; Harmanec 1988). Similar color index data calculated from other surveys (Table 4) suggest a potentially cooler system ranging between G8 and K2V. Therefore, Roche modeling of this system was initiated using a $Teff_1$ value (5260 K) midway between G8 and K2 spectral classes estimated for KW Peg (Table 4).

3.4 Roche modeling of combined KW Peg light curve data from the 2008 and 2011 campaigns

Before attempting to model light curve data from KW Peg additional assumptions had to be made regarding the physical makeup of this binary system. As mentioned before, the light curve shape suggests that KW Peg is most likely a detached binary in which stellar companions move around each other in a circular orbit (Min I and Min II separated by 0.5P). In the absence of any mass ratio data in the literature derived from radial velocity experiments, a starting point for q (m_1/m_2) was guesstimated as follows. Unlike many contact binaries, in well-detached systems the poor correlation between q, Ω_1, Ω_2, and other parameters precludes the possibility of deriving a reliable photometric mass ratio (Terrell and Wilson 2005). Assuming that KW Peg is on the main sequence, its putative spectral class (G9V-K0V) provides a hint regarding its mass (usually measured in solar masses, $M_\odot$). The relationship between spectral class and mass have been conveniently tabulated by Harmanec (1988) and in this case, the primary star in KW Peg is estimated to be less massive than Sol ($\sim$0.93 $M_\odot$). The comparative intensity of Min I and Min II in each bandpass also suggests that the size or luminosity of the secondary is probably not greatly different than the primary star, so q = 1 was initially adopted for modeling purposes.

Phased V-band light curve data that had been normalized with respect to flux were used for preliminary Roche modeling by BM3. Starting points for the Roche potentials ($\Omega_1 \approx 5.3$ and $\Omega_2 \approx 4.9$) were adopted according to the strategy proposed by Kang (2010) in which V364 Cas (Nelson 2009b) was used as the reference for a similarly shaped light curve from a detached system. Values for $Teff_1$ (5260 K) and a mass ratio (q = 1) were held constant while iteratively adjusting the effective temperature of the cooler secondary ($Teff_2$), inclination (i), and surface potentials (Ω_1 and Ω_2) until a reasonable fit to the model was obtained. Bolometric albedo ($A_{1,2}$ = 0.5) and gravity darkening coefficients ($g_{1,2}$ = 0.32) for cooler stars with convective envelopes were assigned according to Rucinski (1969) and Lucy (1967), respectively. Following any Teff change to either star, new logarithmic limb darkening coefficients (x_1, x_2, y_1, y_2) were interpolated according to van Hamme (1993). Thereafter, model fitting in PHOEBE employed phased data which had been transformed into catalogue-based magnitudes. A_1, A_2, g_1, g_2, and $Teff_1$ were fixed parameters whereas values for Ω_1 (5.2), Ω_2 (5.1), i (80°) and T_2 (5000 K), initially obtained from BM3 along with passband specific luminosity, phase shift, x_1, x_2, y_1, and y_2, were iteratively

adjusted using differential corrections (DC) to achieve a simultaneous minimum residual fit of all (B, V, and I_c) photometric observations. It should be noted that light curves from KW Peg are noisier in all passbands compared to other binary systems that have been imaged with similar or lower apparent magnitudes using the same equipment at UO. Since light curves from KW Peg and BX Peg (Alton 2013), a known W UMa binary, were reduced using the same ensemble of stars (Table 1), a direct comparison of residual mean error from the best fit Roche models (B, V, and I_c) consistently revealed higher (~17%) photometric variability for KW Peg. Although not compelling, it led this investigator to consider the possibility that this detached binary belongs to the short period RS CVn group of eclipsing stars. This observation may be related to the well-documented coronal and/or chromospheric activity of these variables (Heckert *et al.* 1998; Budding and Zeilik 1987).

The reader should, however, be advised that a large number of assumptions are required to nominate KW Peg as a potential member of the short-period RS CVn group of binaries. A defining characteristic (Hall 1976) of RS CVn systems is excess emission centered on the Ca II (H and K) and Hα lines so that a high resolution spectroscopic study is ultimately needed to unambiguously define the mass ratio, rotational velocity, and classification of this system. Nonetheless, the best fit unspotted model values for $Teff_1$ (5260 K) and $Teff_2$ (5047 K) are consistent with a well detached binary composed of a G9-K0V primary and a K0-K1 secondary. These spectral classes are fairly typical of those observed in other short-period RS CVn variables. At least during 2008 and 2011, the light curves from KW Peg are quite similar but do exhibit asymmetry relative to the clean unspotted curve fits, suggesting the putative spot has been stable for an extended period of time. By contrast, many other RS CVn stars feature prominent cool spots on the primary and/or evidence of coronal flares which can result in dramatic out-of-eclipse distortions in the light curves (Hilditch 2001) which change over much shorter time scales (Hempelmann *et al.* 1997).

Finding a spotted solution that matched the out-of-eclipse portion of the light curve and meaningfully enhanced the overall model fit proved to be less than completely successful. One approach which improved the curve fit was to position a hot spot on the secondary facing the primary star (Figure 4). Mathematical goodness-of-fit aside, this hot spot solution is difficult to defend considering the following factors. Since KW Peg appears to be a well-detached system, mass transfer which could lead to a hot spot formed by direct impact of an accretion stream is highly unlikely. Furthermore, the straight line relationship in the ET diagram for KW Peg (Figure 3) rather than a parabolic response strongly argues against this possibility since the orbital period is not changing significantly. Secondly, although persistent (months to years) cool spots have been documented for some RS CVn stars, flares or hot spots tend to be much more transient (Osten *et al.* 2000). Unless by mere coincidence, a hot spot is unlikely to persist at the same location as suggested by the similarity

between the 2008 and 2011 light curves. Large crown-like polar spots are more commonly observed as enduring features in other RS CVn stars (Hatzes *et al.* 1996). This addition to the model (Figure 4) was not as effective as a hot spot at minimizing model error, but at least could be rationalized based on the known behavior of other RS CVn systems. Hence, only the clean synthetic light curve fits and those with a single cool spot are reproduced in Figures 5 (B mag.), 6 (V mag.), and 7 (I_c mag.). For the sake of completeness, a comparison of all light curve parameters and geometric elements obtained from Roche modeling is summarized in Table 5. Other multiple starspot combinations were attempted but none led to a convincing improvement over these synthetic curves.

4. Conclusions

CCD-based photometric data collected in B, V, and I_c produced eight new times of minimum for KW Peg. The linear ephemeris for this system was updated and potential changes in orbital periodicity assessed through the analysis of observed versus predicted eclipse timings. The ET diagram for KW Peg is relatively simple and indicates that the orbital period for this system has remained fairly constant over the past two decades. In addition, results from the present study provide a reasonable case for classifying KW Peg as a short-period RS CVn eclipsing binary rather than Algol-like but further observations will need to be made to confirm that classification. The primary star in KW Peg is proposed to be a G9V-K0V dwarf whereas its secondary companion is slightly cooler (K0-K1). The addition of a single cool or hot spot on either star failed to fully account for the out-of-eclipse asymmetry observed in all 2008 and 2011 light curves. Public access to any light curve data associated with this research can be obtained by request (mail@underoakobservatory.com)

5. Acknowledgements

This research has made use of the SIMBAD database, operated at Centre de Donnees astronomiques de Strasbourg, France. Times of minimum data published by B.R.N.O., IBVS, AAVSO, BAV-M, and BBSAG proved invaluable to the assessment of potential period changes. The diligence and dedication shown by all associated with these organizations is very much appreciated. Last, and certainly not least, I would like to thank Professor Dirk Terrell and an unknown referee for their selfless assistance in reviewing this study report and suggesting changes that have significantly improved the quality of this manuscript.

References

Agerer, F., and Hübscher, J. 2003, *Inf. Bull. Var. Stars*, No. 5484, 1.
Alton, K. B. 2013, *J. Amer. Assoc. Var. Star Obs.*, **41**, in press.
Beob. der Schweizerischen Astron. Ges. (BBSAG). 1994, *BBSAG Bull.*, No. 106, 1.
Berry, R., and Burnell, J. 2005, *Handbook of Astronomical Image Processing*, Willmann-Bell, Richmond.
Bradstreet, D. H., and Steelman, D. P. 2002, *Bull. Amer. Astron. Soc.*, **34**, 1224.
Brát, L., Zejda, M., and Svoboda, P. 2007, *Open Eur. J. Var. Stars*, **74**, 1 (*B.R.N.O. Contrib.*, No. 34).
Brát, L., *et al.* 2011, *Open Eur. J. Var. Stars*, **137**, 1 (*B.R.N.O. Contrib.*, No. 37).
Budding, E., and Zeilik, M. 1987, *Astrophys. J.*, **319**, 827.
CBA Belgium Observatory. 2011, Flanders, Belgium (http://www.cbabelgium.com/).
De Young, J. A. 1991, *Inf. Bull. Var. Stars*, No. 3579, 1.
Diethelm, R. 2010, *Inf. Bull. Var. Stars*, No. 5920,1.
Diethelm, R. 2012, *Inf. Bull. Var. Stars*, No. 6011, 1.
Dvorak, S.W. 2006, *Inf. Bull. Var. Stars*, No. 5677, 1.
Flower, P. J. 1996, *Astrophys. J.*, **469**, 355.
Hall, D. S. 1976, in *Multiple Periodic Variable Stars*, ed. W. S. Fitch, IAU Symp. 29, Reidel, Dordrecht, 287.
Harmanec, P. 1988, *Bull. Astron. Inst. Czechoslovakia*, **39**, 329.
Hatzes, A. P., Vogt, S. S., Ramseyer, T. F., and Misch, A. 1996, *Astrophys. J.*, **469**, 808.
Heckert, P. A., Maloney, G. V., Stewart, M. C., Ordway, J. I., Hickman, A., and Zeilik, M. 1998, *Astron. J.*, **115**, 1145.
Hempelmann, A., Hatzes, A. P., Kürster, M., and Patkós, L. 1997, *Astron. Astrophys.*, **317**, 125.
Hilditch, R. W. 2001, *An Introduction to Close Binary Stars*, Cambridge Univ. Press, New York.
Hübscher, J. 2005, *Inf. Bull. Var. Stars*, No. 5643, 1.
Hübscher, J. 2011, *Inf. Bull. Var. Stars*, No. 5984, 1.
Hübscher, J., and Lehmann, P. B. 2012, *Inf. Bull. Var. Stars*, No. 6026, 1.
Hübscher, J., Paschke, A., and Walter, F. 2005, *Inf. Bull. Var. Stars*, No. 5657, 1.
Hübscher, J., Paschke, A., and Walter, F. 2006, *Inf. Bull. Var. Stars*, No. 5731,1.
Hübscher, J., and Walter, F. 2007, *Inf. Bull. Var. Stars*, No. 5761, 1.
Kang, Y.-W. 2010, *J. Astron. Space Sci.*, **27**, 75.
Kotková, L., and Wolf, M. 2006, *Inf. Bull. Var. Stars*, No. 5676, 1.
Krajci, T. 2005, *Inf. Bull. Var. Stars*, No. 5592, 1.
Kreiner, J. M. 2004, *Acta Astron.*, **54**, 207.

Kwee, K. K., and Van Woerden, H. 1956, *Bull. Astron. Inst. Netherlands*, **12**, 327.
Lucy, L. B. 1967, *Z. Astrophys.*, **65**, 89.
Minor Planet Observer. 2010, MPO Software Suite (http://www.minorplanetobserver.com), BDW Publishing, Colorado Springs.
Nelson, R. H. 2007, Minima©2002–2006: Astronomy Software by Bob Nelson (http://members.shaw.ca/bob.nelson/software1.htm).
Nelson, R. H. 2009a, WDwint56a: Astronomy Software by Bob Nelson (http://members.shaw.ca/bob.nelson/software1.htm).
Nelson, R. H. 2009b, *Inf. Bull. Var. Stars*, No. 5884, 1.
Osten, R. A., Brown, A., Ayres, T. R., Linsky, J. L., Drake, S. A., Gagné, M., and Stern, R. A. 2000, *Astrophys. J.*, **544**, 953.
Parimucha, Š., Dubovský, P., Baludanský, D., Pribulla, T., Hambalek, L., Vanko, M., and Ogloza, W. 2009, *Inf. Bull. Var. Stars*, No. 5898, 1.
Pribulla, T., *et al.* 2005, *Inf. Bull. Var. Stars*, No. 5668, 1.
Prša, A. and Harmanec, P. 2010, *PHOEBE Manual: Adopted for PHOEBE 0.32*, Villanova Univ., Dept. of Astronomy and Astrophysics, Villanova, PA (http://phoebe.fmf.uni-lj.si/docs/phoebe_manual.pdf).
Prša, A., and Zwitter, T. 2005, *Astrophys. J.*, **628**, 426.
Ruciński, S. M. 1969, *Acta Astron.*, **19**, 245.
Samolyk, G. 2008, *J. Amer. Assoc. Var. Star Obs.*, **36**, 186.
Samolyk, G. 2010, *J. Amer. Assoc. Var. Star Obs.*, **38**, 183.
Schwarzenberg-Czerny, A. 1996, *Astrophys. J., Lett. Ed.*, **460**, L107.
Software Bisque 2011, Santa Barbara Instrument Group, Santa Barbara, CA.
Terrell, D., and Wilson, R. E. 2005, *Astrophys. Space Sci.*, **296**, 221.
van Hamme, W. 1993, *Astron. J.*, **106**, 2096.
Warner, B. 2007, *Minor Planet Bull.*, **34**, 113.
Wilson, R. E. 1979, *Astrophys. J.*, **234**, 1054.
Wilson, R. E., and Devinney, E. J. 1971, *Astrophys. J.*, **166**, 605.
Zasche, P., Uhlar, R., Kucáková, H., and Svoboda, P. 2011, *Inf. Bull. Var. Stars*, No. 6007, 1.
Zejda, M. 2004, *Inf. Bull. Var. Stars*, No. 5583, 1.
Zejda, M., Mikulásek, Z., and Wolf, M. 2006, *Inf. Bull. Var. Stars*, No. 5741, 1.

Table 1. Astrometric coordinates (J2000) and MPOSC3 catalogue magnitudes (V, B, and I_c) for KW Peg and five comparison stars used in this photometric study.

Star Identification	*R.A.* h m s	*Dec.* ° ′ ″	*MPOSC3*[a] *B mag.*	*MPOSC3 V mag.*	*MPOSC3* I_c *mag.*	*MPOSC3 (B–V)*
KW Peg	21 39 10.59	26 42 34.4	12.65–13.05[b]	11.9–12.3	11.08–11.44	0.805
C1	21 38 57.74	26 36 51.4	13.154	12.694	12.145	0.460
C2	21 39 00.59	26 38 10.4	13.327 (13.51)[c]	12.678 (12.77)[c]	11.95	0.649
C3	21 39 02.87	26 38 43.0	13.384 (13.37)[c]	12.287 (12.34)[c]	11.16 (11.20)[c]	1.097
C4	21 39 07.72	26 44 37.4	13.219	12.736	12.164	0.483
C5	21 39 00.86	26 44 58.8	13.88	13.044	12.151	0.836

Notes: a. MPOSC3 is a hybrid catalogue which includes a large subset of the Carlsberg Meridian Catalog (CMC-14) as well as the Sloan Digital Sky Survey (SDSS). b. Range of magnitudes in light curves for each variable. c. AAVSO comparison star magnitudes in parentheses.

Table 2. New times of minimum for KW Peg acquired at UnderOak Observatory.

Mean Computed Time of Minimum (HJD–2400000)[a]	*Error ±*	*UT Date of Observations*	*Type of Minimum*[a]
54755.5016	0.0010	16 Oct 2008	s
54757.5431	0.0007	18 Oct 2008	p
54759.5844	0.0008	20 Oct 2008	s
54766.5239	0.0010	27 Oct 2008	p
55842.5411	0.0019	08 Oct 2011	p
55844.5806	0.0011	10 Oct 2011	s
55868.6681	0.0013	03 Nov 2011	p
55873.5661	0.0016	08 Nov 2011	p

Note: a. s= secondary; p = primary.

Table 3. Recalculated eclipse timing residuals $(ETR)_2$ for KW Peg following simple linear least squares fit of residuals $(ETR)_1$ from the reference epoch and cycle number occurring between 1990 Sept 24 and 2011 Nov 08.

Time of Minimum (HJD–2400000)	*Type*	*Cycle Number*	$(ETR)_1$[a]	$(ETR)_2$	*Reference**
48158.5685	p	–5318	0.00138918	0.00034626	1
48160.6075	s	–5315.5	–0.00061584	0.00034606	1
48225.5099	p	–5236	–0.00217564	0.00033970	1
48225.5122	p	–5236	0.00012436	0.00033970	1
49250.5040	s	–3980.5	–0.00079919	0.00023922	2
52240.5777	p	–318	0.00053918	–0.00005392	3
52505.4998	s	6.5	0.00018694	–0.00007989	4
52510.3966	s	12.5	–0.00142512	–0.00008037	4
52521.4223	p	26	0.00284774	–0.00008145	5
52602.6530	s	125.5	0.00154774	–0.00008942	3
52878.5966	s	463.5	0.00126836	–0.00011647	6
52886.3522	p	473	0.00104927	–0.00011723	7
52887.5769	s	474.5	0.00114626	–0.00011735	6
52920.6400	p	515	–0.00003515	–0.00012059	3
52982.2775	s	590.5	–0.00088690	–0.00012663	8
53208.4209	s	867.5	–0.00084367	–0.00014880	9
53212.5011	s	872.5	–0.00265373	–0.00014920	9
53221.4850	s	883.5	0.00082416	–0.00015008	10
53228.4284	p	892	0.00480708	–0.00015076	10
53250.4661	p	919	–0.00034719	–0.00015292	10
53255.3663	p	925	0.00144075	–0.00015340	10

table continued on next page

Table 3. Recalculated eclipse timing residuals $(ETR)_2$ for KW Peg following simple linear least squares fit of residuals $(ETR)_1$ from the reference epoch and cycle number occurring between 1990 Sept 24 and 2011 Nov 08, cont.

Time of Minimum (HJD–2400000)	*Type*	*Cycle Number*	*$(ETR)_1$[a]*	*$(ETR)_2$*	*Reference**
53257.4052	s	927.5	–0.00066428	–0.00015360	10
53360.2722	s	1053.5	–0.00031753	–0.00016369	11
53589.6806	s	1334.5	–0.00088234	–0.00018618	3
53601.5201	p	1349	0.00078851	–0.00018734	12
53613.3551	s	1363.5	–0.00204064	–0.00018850	12
53617.4407	s	1368.5	0.00149931	–0.00018890	13
53627.6449	p	1381	0.00072419	–0.00018990	14
53659.4834	p	1420	–0.00045420	–0.00019302	12
53928.4864	s	1749.5	–0.00191649	–0.00021940	15
53966.4520	p	1796	0.00099004	–0.00022312	16
54002.3717	p	1840	–0.00099840	–0.00022664	16
54297.5015	s	2201.5	–0.00052501	–0.00025557	15
54384.4495	p	2308	0.00062092	–0.00026410	17
54755.5016	s	2762.5	–0.00191929	–0.00030047	18
54757.5431	p	2765	–0.00142432	–0.00030067	18
54759.5844	s	2767.5	–0.00116267	–0.00030087	18
54766.5239	p	2776	–0.00111309	–0.00030155	18
55000.4237	s	3062.5	–0.00046562	–0.00032448	19
55000.4243	s	3062.5	0.00013438	–0.00032448	19
55000.4254	s	3062.5	0.00123437	–0.00032448	19
55121.6584	p	3211	–0.00145411	–0.00033637	20
55146.5584	s	3241.5	–0.00171541	–0.00033881	21
55481.2842	s	3651.5	–0.00073951	–0.00037162	22
55842.5411	p	4094	–0.00169561	–0.00040704	18
55844.5806	s	4096.5	–0.00320063	–0.00040724	18
55850.7070	p	4104	0.00015096	–0.00040784	23
55857.2382	p	4112	0.00013488	–0.00040848	24
55868.6681	p	4126	0.00040674	–0.00040960	18
55873.5661	p	4132	–0.00000532	–0.00041008	18

Note: a. Eclipse Timing Residuals $(ETR)_1$ from linear elements (Kreiner 2004) for KW Peg.

** References: (1) De Young 1991; (2) BBSAG 1994; (3) Samolyk 2008; (4) Agerer and Hübscher 2003; (5) Zejda 2004; (6) Hübscher 2005; (7) Krajci 2005; (8) Kotková and Wolf 2006; (9) Pribulla et al. 2005; (10) Hübscher et al. 2005; (11) Zejda et al. 2006; (12) Hübscher et al. 2006; (13) Brát et al. 2007; (14) Dvorak 2006; (15) Parimucha et al. 2009; (16) Hübscher and Walter 2007; (17) Zasche et al. 2011; (18) Alton 2013 (present study); (19) Brát et al. 2011; (20) Diethelm 2010; (21) Samolyk 2010; (22) Hübscher 2011; (23) Diethelm 2012; (24) Hübscher and Lehmann 2012.*

Table 4. Spectral classification of KW Peg based upon data from various survey catalogs and present study.

Stellar Attribute	*Tycho-2*	*USNO-B1.0*	*USNO-A2.0*	*All Sky Combined*	*MPOSC3*	*2MASS*	*SDSS-DR8*	*Present Study*
(B–V)	0.903	0.728	0.945	0.785	0.805	0.804	0.838	0.733
Teff[a] (K)	5040	5470	4953	5320	5269	5272	5188	5574
Spectral Class[b]	K1	G8	K2	G9	G9	G9	K0	G8

Notes: a. Interpolated from Flower (1996). b. Estimated from Harmanec (1988).

Table 5. Selected geometrical and physical elements for KW Peg obtained during Roche model light curve fitting.

Parameter	*Unspotted Fit*	*Cool Spot 1*	*Hot Spot 2*
T_1 (K)[a]	5260	5260	5260
T_2 (K)	5046 ±25	5094 ±24	5128 ±25
q (m_2/m_1)[b]	0.911 ±0.021	0.911 ±0.015	0.914 ±0.016
A[a]	0.5	0.5	0.5
g[a]	0.32	0.32	0.32
Ω_1[b]	5.322 ±0.054	5.258 ±0.089	5.232 ±0.066
Ω_2[b]	5.126 ±0.098	5.125 ±0.073	5.131 ±0.075
i°[b]	78.3 ±0.21	78.3 ±0.17	78.4 ±0.20
$A_{S1} = T_{S1}/T$[d]	—	0.909 ±0.007	1.107 ±0.011
Θ_{S1} (spot co-latitude)[d]	—	6 ±1.28	32.5 ±10
φ_{S1} (spot longitude)[d]	—	354.9 ±8.3	0 ±8
r_{S1} (angular radius)[d]	—	38.7 ±0.71	13.47 ±0.44
r_1(back)[e]	0.2315 ±0.0092	0.2351 ±0.0067	0.2368 ±0.0074
r_1(side)[e]	0.2281 ±0.0091	0.2315 ±0.0066	0.2331 ±0.0073
r_1(pole)[e]	0.2256 ±0.0090	0.2289 ±0.0065	0.2304 ±0.0072
r_1(point)[e]	0.2328 ±0.0093	0.2366 ±0.0068	0.2384 ±0.0074
r_2(back)[e]	0.2284 ±0.0091	0.2285 ±0.0065	0.2288 ±0.0071
r_2(side)[e]	0.2245 ±0.0090	0.2247 ±0.0064	0.2250 ±0.0070
r_2(pole)[e]	0.2219 ±0.0089	0.2221 ±0.0064	0.2224 ±0.0069
r_2(point)[e]	0.2299 ±0.0092	0.2301 ±0.0066	0.2304 ±0.0072
$\chi 2$ (B)[c]	0.013134	0.013362	0.012997
$\chi 2$ (V)[c]	0.013006	0.013194	0.012617
$\chi 2$ (I_c)[c]	0.054050	0.052406	0.052273

Notes: a. Fixed elements during DC. b. Variability (±S.D.) from heuristic $\chi 2$ scanning in PHOEBE. *c. $\chi 2$ from* PHOEBE *(Prša and Zwitter 2005). d. Error estimates from* WDWINT *v5.6a (Nelson 2009a). e. Formal error estimates from numerical methods according to* PHOEBE *0.32 manual (Prša and Harmanec 2010).*

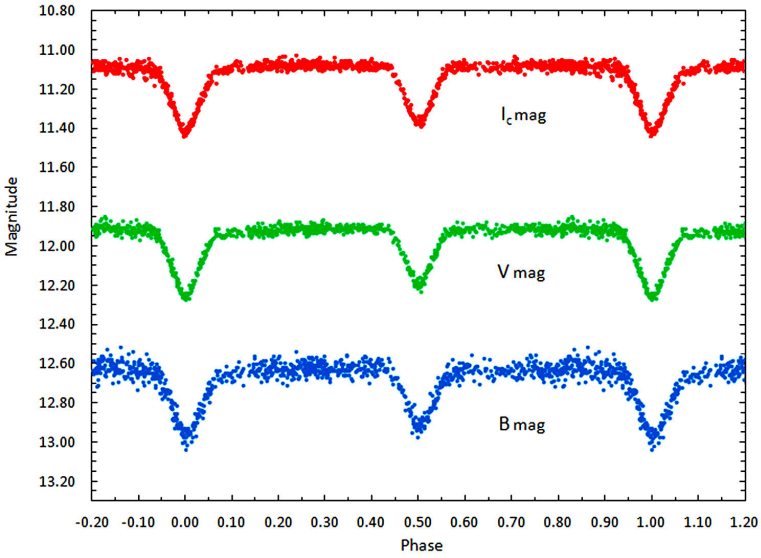

Figure 1. Folded CCD light curves for KW Peg obtained between October 8 and October 31, 2008. The top (I_c), middle (V), and bottom curve (B) shown above were reduced to magnitudes from the MPOSC3 catalogue using MPO CANOPUS.

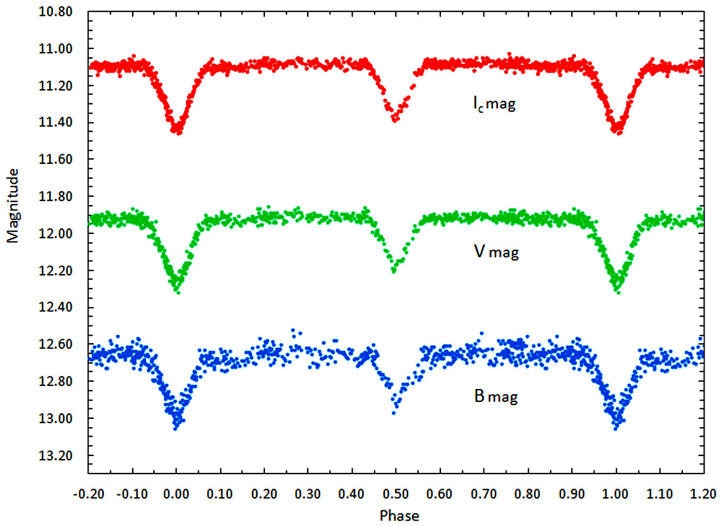

Figure 2. Folded CCD light curves for KW Peg obtained between October 6 and November 8, 2011. The top (I_c), middle (V), and bottom curve (B) shown above were reduced to magnitudes from the MPOSC3 catalogue using MPO CANOPUS.

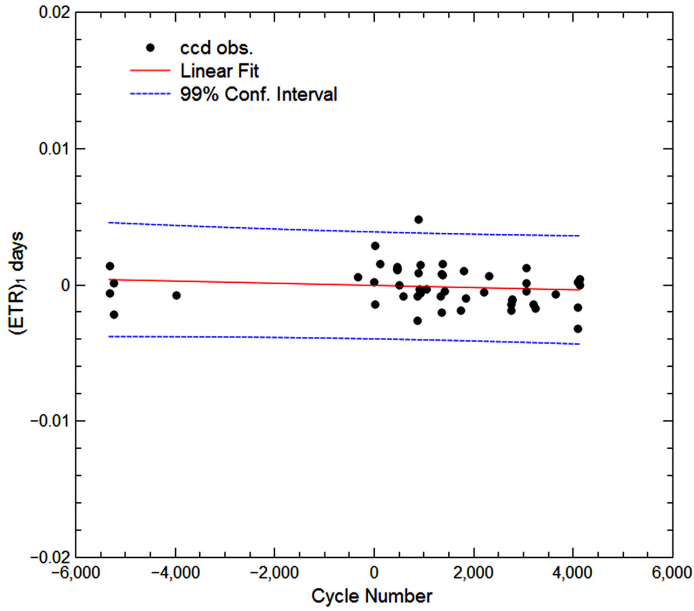

Figure 3. Linear regression fit of all CCD time-of-minimum residuals $(ETR)_1$ reported for KW Peg between 1990 and 2011. The eclipse timing residuals $(ETR)_2$ after curve fitting do not exhibit any other underlying periodicity that can be determined at this point.

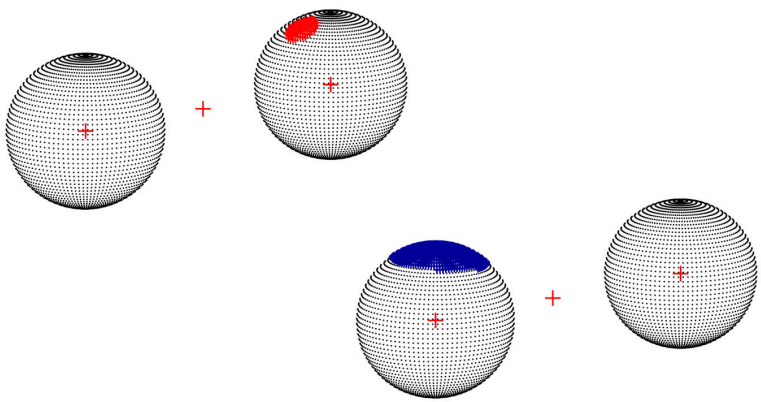

Figure 4. 3-D spatial representations of KW Peg showing the location of a putative hot spot on secondary star (top) or alternatively, a cool polar crown on the primary star (bottom).

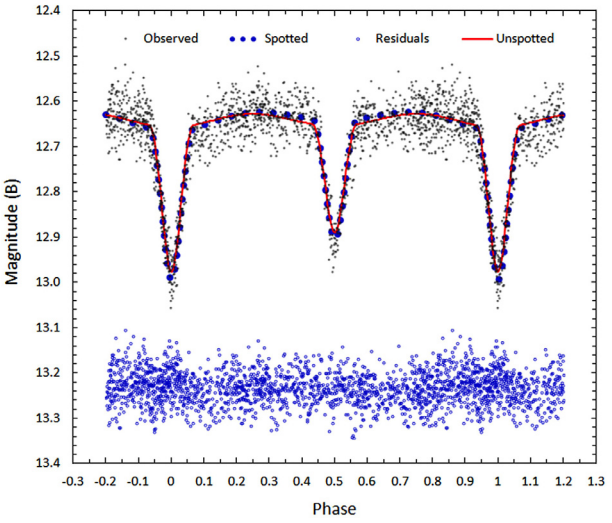

Figure 5. Synthetic fit of B bandpass light curve for KW Peg (2008 and 2011) collected at UO using an unspotted (solid-line) and spotted (dotted-line) Roche model which incorporates a cool polar crown on the more massive star. Spotted residuals are offset by a constant value to keep the y-axis on scale.

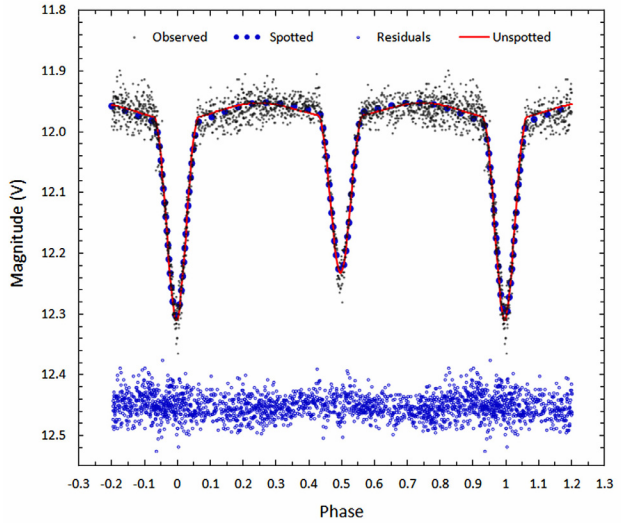

Figure 6. Synthetic fit of V bandpass light curve for KW Peg (2008 and 2011) collected at UO using an unspotted (solid-line) and spotted (dotted-line) Roche model which incorporates a cool polar crown on the more massive star. Spotted residuals are offset by a constant value to keep the y-axis on scale.

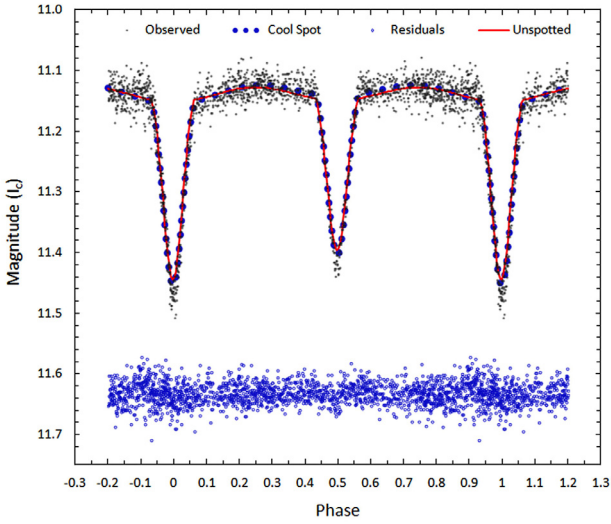

Figure 7. Synthetic fit of I_c bandpass light curve for KW Peg (2008 and 2011) using an unspotted (solid-line) and spotted (dotted-line) Roche model which incorporates a cool polar crown on the more massive star. Spotted residuals are offset by a constant value to keep the y-axis on scale.

Very Short-Duration UV–B Optical Flares in RS CVn-type Star Systems

Gary A. Vander Haagen
Stonegate Observatory, 825 Stonegate Road, Ann Arbor, MI; garyvh2@gmail.com

Received February 11, 2013; revised March 13, 2013; accepted March 15, 2013

Abstract Very short-duration UV–B optical flares were observed during a high-cadence search for conventional flares on three RS CVn type stars: AR Lac, II Peg, and UX Ari. A statistical criterion was developed for isolating these short-duration optical flares from random photon events. Five flares, ranging in duration from 30 to 85ms with peaks 0.29–0.51 mag. above the mean, were detected within the 132 hours of monitoring time. The time resolution of the observations was 5ms for AR Lac and 10ms for II Peg and UX Ari.

1. Introduction

A flare survey was conducted of known RS CVn-type flare stars AR Lac, II Peg, and UX Ari from August 15, 2012, through December 28, 2012. The optical system consisted of a 43cm corrected Dall-Kirkham scope, a high-speed silicon photomultiplier (SPM), and a data acquisition system capable of sub-millisecond data collection times. The SPM was chosen for the remote controlled application because it has comparable sensitivity to a standard single channel vacuum photomultiplier yet a more robust mechanical and electrical design with the disadvantage of higher dark counts (Vander Haagen 2012).

The optical train is shown in Figures 1 and 2. The incoming beam is split approximately 80/5 with the reflected portion passing through the UV–B filter, an *f*-stop yielding a 57 arc-second field, and onto the SPM detector. A wide bandwidth pulse amplifier amplifies the SPM signal, producing a 2–3volt pulse of approximately 50ns for each converted photon. These photon pulses are sent to a PC-based data acquisition system where they are gated and counted based upon the collection rate. A 10ms gate was used for most of the measurements, generating a 100Hz data collection rate or 100 samples/second (100s/sec). The balance of the incoming beam passes straight through to a conventional CCD camera used for initial alignment and guiding. The SPM is mounted within the housing on a miniature X-Y stage for precise alignment to the center of the CCD camera. This allows automated flips and realignment to the small field of view SPM.

Each data set was also time-stamped at one-second intervals using a GPS time signal. Data sets can be timed between the 1-second intervals using synchronized tics provided by the data acquisition system. Each of the acquisition system files consists of one million data sets. Files of this size are too large for

spreadsheet analysis but are easily analyzed using signal processing software such as SIGVIEW (SignalLab 2013). The files can be reviewed and processed using a variety of filters, time domain transforms, and statistical tools.

2. Flare search

The search's initial objective was collection of rapid cadence data on three known flare stars for profiling of the rise and fall structure and possible oscillation detection during the flare sequences (Mathioudakis *et al.* 2003). However, when reviewing over 476Ksec of data another unusual phenomenon became apparent. Very short flares of 10 to 100ms duration were observed unconnected with conventional flaring activity. These very short flares generally had a build up of one or more points at 3σ or higher with a peak at 4–10σ. A similar 50ms-duration flare was reported for EV Lac in the UV–B band by Zhilyaev *et al.* (1990).

A criterion was developed to isolate these short-duration flares in the database of 6.6×10^7 data sets: flares must consist of a minimum of three consecutive data points, two at or above 3σ and one at or above 5σ. Since the minimum number of photons per gate was 400, normal distribution statistics were used to compute the standard deviation. Statistics were collected 600 seconds prior to the event where possible using digital signal processing software (SignalLab 2013). This process is similar in direction to that followed by flare searches (Byrne *et al.* 1994). The probability of this sequence being a random event can be represented by Equation (1), where N is the number of photons gated each measurement and σ is for the positive events only.

$$\Pi_{3,3,5\sigma} = P_r(3\sigma)^2 5\sigma = (1.35 \times 10^{-3})^2 \times (2.9 \times 10^{-7})\ N = 5.2 \times 10^{-13}\ N \qquad (1)$$

With N ranging from 400 to 2000 the probability of the event sequence being random ranges from approximately 2×10^{-10} to 10^{-9}. This criterion was used for each of the data sets to isolate potential short-duration flares.

3. AR Lac

AR Lac is a RS CVn-type eclipsing binary system with flaring reported from the X-ray to the optical region (Kovari and Pagano 2000). AR Lac was observed in the B band. The total monitoring time was179Ksec, or 49.7 hours. Sampling occurred at 200s/sec (5ms gating period) with two short-duration flares observed that meet the detection criterion, or 0.04 flares/hour. Figure 3 shows a flare that occurred on September 5, 2012. This flare had strong leading intensity points with maxima at 6σ, approximately 85ms in duration with peak 0.42 mag. above mean. The Figure 4 flare occurred on September 15, 2012, with duration of 30ms and 0.32 mag. above mean.

4. II Peg

A second RS CVn-type eclipsing binary system, II Peg, was studied with UV–B optical flaring reported by Henry and Newsom (1996). II Peg and UX Ari were observed in the UV–B band using an Edmund 500nm short pass filter. When combined with the response of the SPM the resultant band pass is approximately 380 to 500nm. Sampling was at 100s/sec (10ms gating period) for a total of 205Ksec, or 69.4 hours. Two short flares were recorded, or 0.03 flare/hour. The Figure 5 flare occurred on November 6, 2012, with duration of 50ms and 0.36 mag. above mean. The periodicity produced by peaks 2, 3, and 4 of Figure 5 generate a strong 6.3–7+ Hz component on the power spectral density spectrum (PSD) of Figure 6. Figure 7 shows the November 8, 2012, flare with duration of approximately 70ms and 0.51 mag. above mean.

5. UX Ari

The third target was UX Ari, a member of a subset of RS CVn stars with flares reported by Henry and Newsom (1996). Sampling was at 100s/sec (10ms gating period) for a total of 92Ksec, or 25.6 hours. With one detected flare the resultant rate was 0.04 flare/hour. Figure 8 shows the December 13, 2012, flare with duration of 60ms and peak 0.29 mag. above mean.

6. Discussion and conclusions

The potential for atmospheric scintillation as source or inducer of the short duration peaks was investigated. There was no simultaneous secondary reference to rule out this contribution. Fourier PSD transforms were made of each data set. A wide range of noise amplitude and cutoff frequencies were present across the data sets. Where short-duration peaking occurred, digital band pass filters were employed to isolate the frequency domain signature of the event. No signature that was narrow or consistent enough could be identified. Such a signature might allow correlation with the frequency domain noise spectra to give indication of possible contribution to the peaking events. This area of investigation did not prove fruitful.

In conclusion, very short optical flares were observed during a high cadence search for conventional flares on three RS CVn type stars. A statistical criterion was developed for isolating these short optical flares from random photon events in the 6.6×10^7 data sets. Five flares, ranging in duration from 30 to 85ms with peaks 0.29–0.51 mag. above the mean, were detected within the 476Ksec, or 132 hours, of monitoring time. Whether the criterion is too restrictive or permits occasional random events to be classified as flares will require additional collaboration. With collaborative support a theoretical analysis of the short flare events could be developed.

References

Byrne, P. B., Lanzafame, A. C., Sarro, L. M., and Ryans, R. 1994, *Mon. Not. Roy. Astron. Soc.*, **270**, 427.

Henry, G. W., and Newsom, M. S. 1996, *Publ. Astron. Soc. Pacific*, **108**, 242.

Kovari, Zs., and Pagano, I. 2000, in *Workshop on the Sun and Sun-Like Stars, 9–11 August 1999*, eds. I. Jankovics, J. Kovacs, and I. J. Vincze, Szombathely, Hungary, 7.

Mathioudakis, M., Seiradakis, J. H., Williams, D. R., Avgoloupis, S., Bloomfield, D. S., and McAteer, R. T. J. 2003, *Astron. Astrophys.*, **403**, 1101.

SignalLab. 2013, Sigview 2.6.0 software for DSP applications (http://www.sigview.com/index.htm).

Vander Haagen, G. A. 2012, in *The Society for Astronomical Sciences 31st Annual Symposium on Telescope Science*, eds. B. D. Warner, R. K. Buchleim, J. L. Foote, and D. Mais, The Society for Astronomical Sciences, Rancho Cucamonga, CA, 165.

Zhilyaev, B. E., Romanjuk, Ya. O., and Svyatogorov, O. A. 1990, in *Flare Stars in Star Clusters, Associations, and the Solar Vicinity*, eds. L. V. Mirzoyan, B. R. Pettersen, and M. K. Tsvetkov, Kluwer Academic, Dordrecht, The Netherlands, 35.

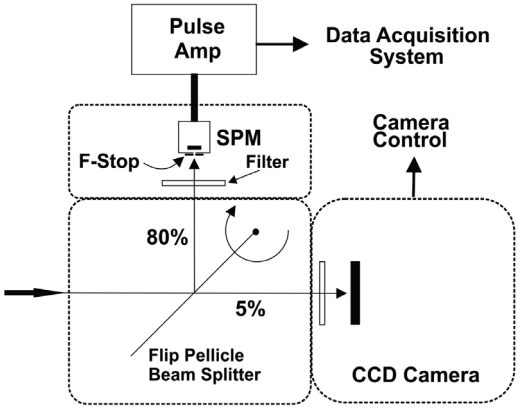

Figure 1. Optical train showing pellicle beam splitter with reflective and pass-through beams. Reflected path passes through the narrow band filter, aperture, and onto the silicon photomultiplier. The pellicle can be flipped to allow 100% light transmission for initial target alignment using the CCD camera. The SPM is mounted on a X-Y stage for precise centering of detector to the centerline of the CCD camera. Guiding is provided with pellicle in position shown.

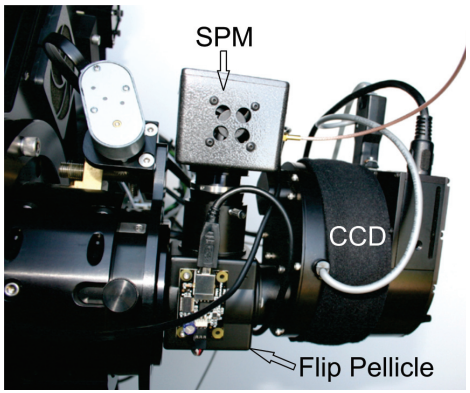

Figure 2. The optical train photo shows the SPM detector assembly mounted top center with SBIG CCD camera to the right in the same relative positions as the Figure 1 diagram. The flip pellicle is automated with its housing and motor controller visible directly below the SPM.

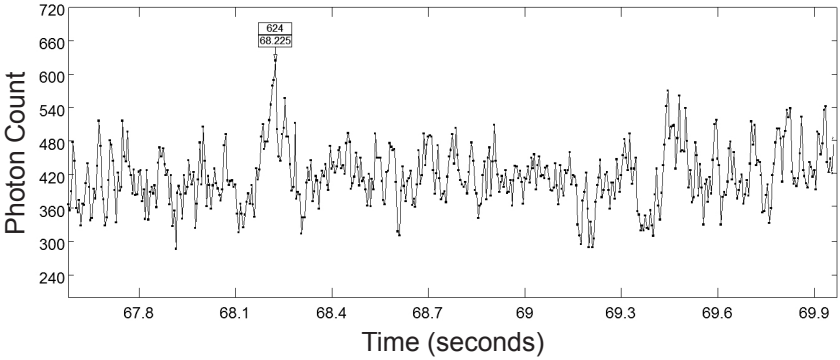

Figure 3. September 5, 2012, AR Lac sampled at 200 s/sec (5ms gating period) mean 424, σ 33, data leading to maxima 545, 579, 589, and 624 (6σ). A 3σ peak was 0.23 mag. above the mean. Flare length was 85ms with peak 0.42 mag. above mean. X-axis is seconds from start of data collection run. Annotation box on graph shows peak count (upper value) and time at peak (lower value).

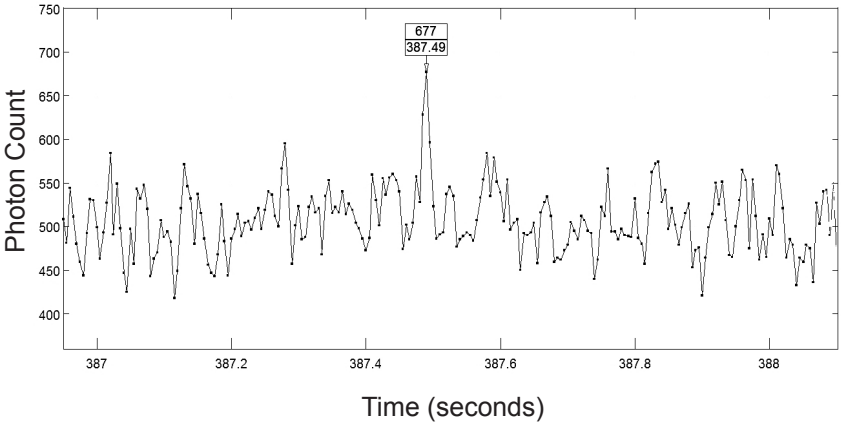

Figure 4. September 15, 2012, AR Lac sampled at 200s/sec, mean 502, σ 31, data points 628, 677 (5.6σ), 596. A 3σ peak was 0.18 mag. above the mean. Flare duration 30ms with peak 0.32 mag. above mean. Annotation box on graph shows peak count (upper value) and time at peak (lower value).

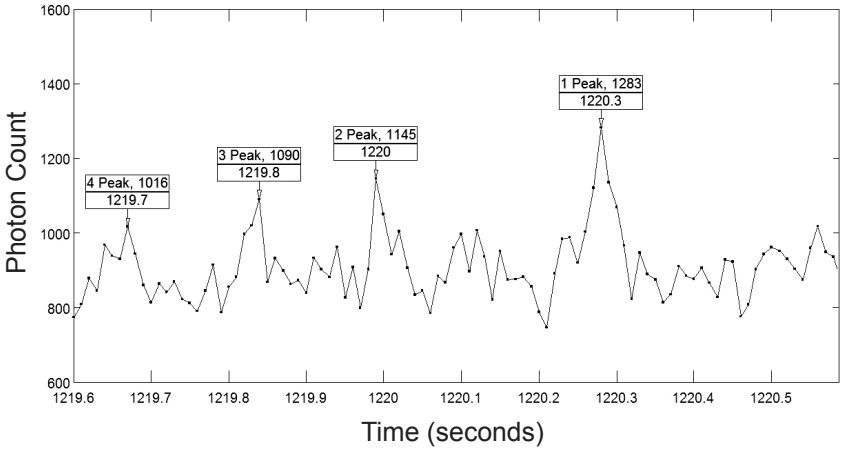

Figure 5. November 6, 2012, II Peg sampled at 100s/sec (10ms gating period), mean 921, σ 35, data point sequence on peak one 1121, 1283 (10.3σ), 1135, 1068. A 3σ peak was 0.12 mag above the mean. Peak 1 flare duration 50ms with peak 0.36 mag. above mean. Note periodicity of peaks 2, 3, and 4. Annotation box on graph shows peak count (upper value) and time at peak (lower value).

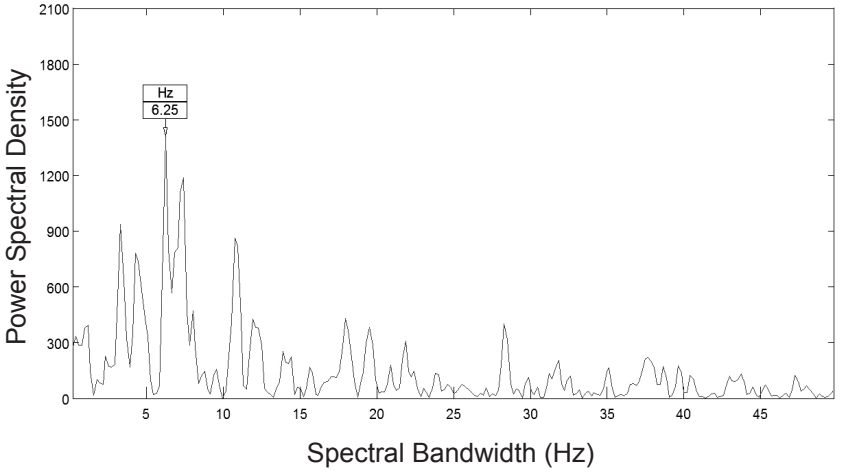

Figure 6. Power spectral density (PSD) curve of II Peg, November 6, 2012. Note 6.25–7+ Hz signal produced by peaks 2, 3, and 4 of Figure 5 data. The spectral bandwidth is 50 Hz as dictated by a sampling rate of 100 Hz.

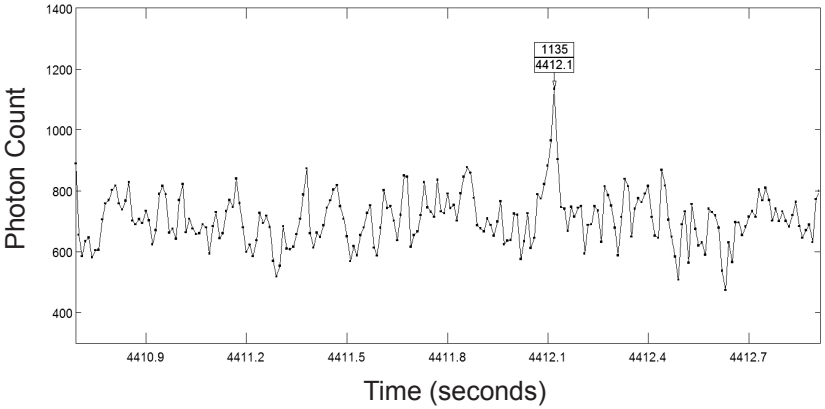

Figure 7. November 8, 2012, II Peg sampled at 100 s/sec, mean 710, σ 68, data point sequence 882, 964, 1135 (6.3σ), 903. A 3σ peak was 0.27 mag. above the mean. Flare duration 70 ms with peak 0.51 mag. above mean. Annotation box on graph shows peak count (upper value) and time at peak (lower value).

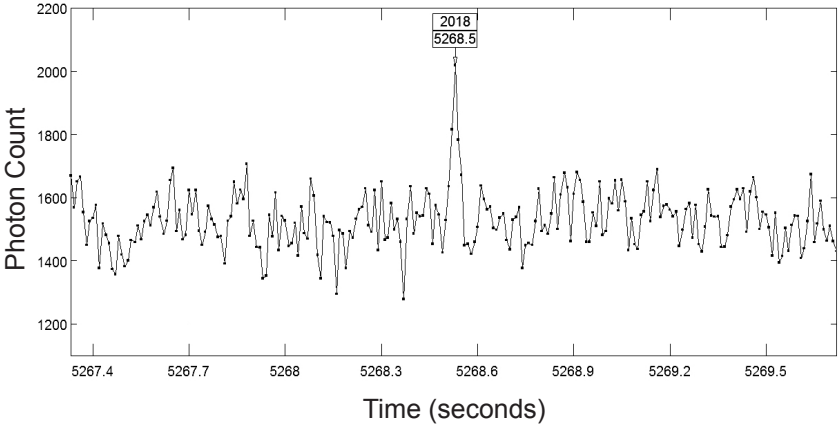

Figure 8. December 13, 2012, UX Ari sampled at 100s/sec, mean 1542, σ 80, data point sequence 1815, 2018 (6σ), 1783. A 3σ peak was 0.16 mag. above the mean. Flare duration 60 ms with peak 0.29 mag. above mean. Annotation box on graph shows peak count (upper value) and time at peak (lowervalue).

Recent Minima of 273 Eclipsing Binary Stars

Gerard Samolyk
P.O. Box 20677, Greenfield, WI 53220; gsamolyk@wi.rr.com

Received December 13, 2012; accepted December 13, 2012

Abstract This paper continues the publication of times of minima for eclipsing binary stars from observations reported to the AAVSO Eclipsing Binary Section. Times of minima from observations made from January 2012 through December 2012, along with some unpublished times of minima from older data, are presented.

1. Recent observations

The accompanying list contains times of minima calculated from recent CCD observations made by participants in the AAVSO's eclipsing binary program. This list will be web-archived and made available through the AAVSO ftp site at ftp://ftp.aavso.org/public/datasets/gsamoj411a.txt. This list, along with the eclipsing binary data from earlier AAVSO publications, is also included in the Lichtenknecker database administrated by the Bundesdeutsche Arbeitsgemeinschaft für Veränderliche Sterne e.V. (BAV) at: http://www.bav-astro.de/LkDB/index.php?lang=en. These observations were reduced by the observers or the writer using the method of Kwee and Van Worden (1956). A colon (:) following a time of minimum in Table 1 indicates that the light curve was of substandard quality. Column F in Table 1 indicates the filter used. A blank indicates that no filter was used. The standard error is included when available.

The linear elements in the *General Catalogue of Variable Stars* (GCVS, Kholopov *et al.* 1985) were used to compute the O–C values for most stars. For some exceptions where the GCVS elements are missing or are in significant error, light elements from another source are used: CD Cam (Baldwin and Samolyk 2007), AC CMi (Samolyk 2008), CW Cas (Samolyk 1992a), DV Cep (Frank and Lichtenknecker 1987), Z Dra (Danielkiewicz-Krośniak and Kurpińska-Winiarska 1996), DF Hya (Samolyk 1992b), DK Hya (Samolyk 1990), EF Ori (Baldwin and Samolyk 2005), and GU Ori (Samolyk 1985). Light elements for QX And, V376 And, CV Boo, UZ CMi, V520 Cas, EX Del, V829 Her, DU Leo, EX Leo, FS Leo, V453 Mon, V1123 Tau, HX UMa, and MS Vir are from Kreiner (2004, 2011). O–C values listed in this paper can be directly compared with values published in the *AAVSO Observed Minima Timings of Eclipsing Binaries* series.

References

Baldwin, M. E., and Samolyk, G. 2005, *Observed Minima Timings of Eclipsing Binaries No. 10*, AAVSO, Cambridge, MA.

Baldwin, M. E., and Samolyk, G. 2007, *Observed Minima Timings of Eclipsing Binaries No. 12*, AAVSO, Cambridge, MA.

Danielkiewicz-Krośniak, E., and Kurpińska-Winiarska, M., eds. 1996, *Rocznik Astron.* (SAC 68), **68**, 1.

Frank, P., and Lichtenknecker D. 1987, *BAV Mitt.,* No. 47, 1.

Kreiner, J. M. 2004, *Acta Astron.*, **54**, 207 (http://www.as.up.krakow.pl/ephem/).

Kreiner, J. M. 2011, Lichtenknecker-Database of the BAV, http://www.bavdata-astro.de/~tl/cgi-bin/varstars_cgi

Kholopov, P. N., *et al.* 1985, *General Catalogue of Variable Stars*, 4th ed., Moscow.

Kwee, K. K., and Van Woerden, H. 1956, *Bull. Astron. Inst. Netherlands*, **12**, 327.

Samolyk, G. 1985, *J. Amer. Assoc. Var. Star Obs.*, **14**, 12.

Samolyk, G. 1990, *J. Amer. Assoc. Var. Star Obs.*, **19**, 5.

Samolyk, G. 1992a, *J. Amer. Assoc. Var. Star Obs.*, **21**, 34.

Samolyk, G. 1992b, *J. Amer. Assoc. Var. Star Obs.*, **21**, 111.

Samolyk, G. 2008, *J. Amer. Assoc. Var. Star Obs.,* **36**, 171.

Table 1. Recent times of minima of stars in the AAVSO eclipsing binary program.

Star	*HJD 2400000+*	*Cycle*	*O–C (day)*	*F*	*Observer*	*Standard Error (day)*
RT And	54079.5908	20571	–0.0072	I	G. Lubcke	0.0001
RT And	54079.5909	20571	–0.0071	V	G. Lubcke	0.0001
RT And	55889.6465	23449	–0.0107	V	J. A. Howell	0.0001
UU And	56193.8183	9785	0.0719	V	G. Samolyk	0.0001
XZ And	55938.5473	23548	0.1735	V	G. Samolyk	0.0001
XZ And	55938.5473	23548	0.1735	V	N. Simmons	0.0001
XZ And	56163.8555	23714	0.1735	V	G. Samolyk	0.0002
AB And	56143.5548	60363	–0.0304	R	L. Corp	0.0003
AB And	56178.4047	60468	–0.0291	R	L. Corp	0.0005
AB And	56178.5698	60468.5	–0.0299	R	L. Corp	0.0004
AB And	56211.5917	60568	–0.0313	V	N. Simmons	0.0001
AD And	56196.7222	17435	–0.0532	V	G. Samolyk	0.0001
AP And	50744.670	15233	–0.009	—	S. Cook	—
BD And	55930.4946	45297	0.0091	V	K. Menzies	0.0001
BX And	56195.7829	32235	–0.0628	V	G. Samolyk	0.0001
CN And	54014.8352	26875	–0.1016	V	V. Petriew	0.0005
DS And	56164.8282	19814	0.0038	V	G. Samolyk	0.0003

Table continued on following pages

Table 1. Recent times of minima of stars in the AAVSO eclipsing binary program, cont.

Star	HJD 2400000+	Cycle	O–C (day)	F	Observer	Standard Error (day)
GK And	54028.8551	7657	–0.2827	V	V. Petriew	0.0003
QX And	56164.8537	8891.5	0.0024	V	G. Samolyk	0.0006
V376 And	53990.8126	1866	–0.0050	V	V. Petriew	0.0004
CZ Aqr	55854.6059	14469	–0.0507	V	J. A. Howell	0.0001
CZ Aqr	56193.6656	14862	–0.0533	V	G. Samolyk	0.0001
XZ Aql	56167.6886	6668	0.1687	V	G. Samolyk	0.0002
OO Aql	56064.5375	34435	0.0539	R	L. Corp	0.0006
OO Aql	56127.8861	34560	0.0540	V	R. Sabo	0.0001
OO Aql	56139.5432	34583	0.0550	R	L. Corp	0.0006
V342 Aql	56167.7013	4969	–0.1724	V	G. Samolyk	0.0001
V343 Aql	56180.6598	15037	–0.0525	V	G. Samolyk	0.0002
V346 Aql	55848.5902	12591	–0.0104	V	J. A. Howell	0.0001
V346 Aql	56181.6058	12892	–0.0100	V	G. Samolyk	0.0001
V873 Aql	53144.7609	40533	0.0268	V	S. Dvorak	0.0005
RS Ari	50438.678	3001	–0.0932	—	S. Cook	—
RX Ari	55946.5527	17043	0.0671	V	G. Samolyk	0.0001
SS Ari	55937.5314	41649.5	–0.2940	V	G. Samolyk	0.0001
SS Ari	55966.5572	41721	–0.2968	V	G. Samolyk	0.0001
SS Ari	56233.6916	42379	–0.3062	V	R. Poklar	0.0001
SS Ari	56247.7005	42413.5	–0.3041	V	B. Manske	0.0003
SS Ari	56254.6013	42430.5	–0.3051	V	K. Menzies	0.0001
SX Aur	55929.6979	13030	0.0174	V	G. Samolyk	0.0006
SX Aur	56235.8478	13283	0.0170	V	K. Menzies	0.0004
TT Aur	56167.8992	26206	–0.0106	V	G. Samolyk	0.0003
WW Aur	55934.5791	9104.5	0.0023	V	G. Samolyk	0.0002
AP Aur	56006.5804	23821	1.3783	V	K. Menzies	0.0001
BF Aur	50849.644	6456	0.006	—	S. Cook	—
CL Aur	55944.6038	18465	0.1513	V	G. Samolyk	0.0003
EP Aur	55942.5369	50140	0.0138	V	G. Samolyk	0.0002
EP Aur	56020.5468	50272	0.0106	V	K. Menzies	0.0002
EP Aur	56187.8046	50555	0.0132	V	K. Menzies	0.0001
HP Aur	56194.8784	9445	0.0602	V	G. Samolyk	0.0002
IM Aur	55929.5163	12358	–0.1142	V	G. Samolyk	0.0001
KO Aur	50453.690	10506	0.042	—	S. Cook	—
TU Boo	55982.4782	70666.5	–0.1389	R	L. Corp	0.0001
TU Boo	55982.6412	70667	–0.1381	R	L. Corp	0.0001
TU Boo	56062.7386	70914	–0.1395	V	R. Sabo	0.0002
TY Boo	56052.7372	68019.5	0.0843	V	R. Poklar	0.0002

Table continued on following pages

Table 1. Recent times of minima of stars in the AAVSO eclipsing binary program, cont.

Star	*HJD 2400000+*	*Cycle*	*O–C (day)*	*F*	*Observer*	*Standard Error (day)*
TY Boo	56062.7259	68051	0.0828	V	R. Sabo	0.0002
TZ Boo	56093.6001	55393	0.0636	V	K. Menzies	0.0003
TZ Boo	56123.6137	55494	0.0639	V	K. Menzies	0.0001
UW Boo	56045.6652	13577	–0.0064	V	K. Menzies	0.0002
UW Boo	56050.6887	13582	–0.0064	V	R. Poklar	0.0002
VW Boo	55945.9194	72366	–0.1993	V	K. Menzies	0.0001
VW Boo	55990.7623	72497	–0.2010	V	K. Menzies	0.0002
BW Boo	50574.647	3064	–0.019	—	S. Cook	—
CV Boo	51702.6935	–942	0.0006	V	J. A. Howell	0.0003
Y Cam	55966.6554	3934	0.4014	V	G. Samolyk	0.0004
SV Cam	55307.7150	21436	0.0524	B	M. de Jong	0.0001
SV Cam	55307.7151	21436	0.0525	V	M. de Jong	0.0001
AT Cam	50841.5920	17755	–0.0875	—	S. Cook	—
CD Cam	55928.7154	4143	0.0015	V	R. Poklar	0.0009
CD Cam	56195.7954	4492.5	–0.0009	V	G. Samolyk	0.0005
TX Cnc	50477.651	32559	0.020	—	S. Cook	—
YZ CVn	52441.6202	6506	–0.0061	V	S. Dvorak	0.0006
SX CMa	55980.7037	17168	0.0358	V	R. Poklar	0.0003
TU CMa	55976.6614	25713	–0.0104	V	R. Poklar	0.0001
TZ CMa	55962.6464	15087	–0.2104	V	G. Samolyk	0.0002
UU CMa	55963.6850	5246	–0.1031	V	R. Poklar	0.0001
UZ CMi	50491.604	–3643.5	0.001	—	S. Cook	—
XZ CMi	55963.6512	23357	–0.0040	V	G. Samolyk	0.0003
XZ CMi	55989.6983	23402	–0.0033	V	R. Poklar	0.0001
XZ CMi	55996.6438	23414	–0.0035	V	N. Simmons	0.0002
AC CMi	55969.6841	4602	0.0025	V	R. Poklar	0.0002
AG CMi	50127.282	9269	–0.052	—	S. Cook	—
AK CMi	55961.6701	22725	–0.0226	V	R. Poklar	0.0002
RW Cap	56189.5919	3987	–0.6223	V	G. Samolyk	0.0004
RZ Cas	56039.7146	10742	0.0650	V	M. de Jong	0.0001
ZZ Cas	50360.657	13609	0.003	—	S. Cook	—
AB Cas	54059.6027	8300	0.0875	V	G. Lubcke	0.0001
AB Cas	54059.6027	8300	0.0875	I	G. Lubcke	0.0001
AB Cas	56194.6881	9862	0.1160	V	G. Samolyk	0.0002
AE Cas	52585.7598	35797	0.0770	V	S. Dvorak	0.0003
BZ Cas	50717.169	9979	0.191	—	S. Cook	—
CW Cas	55936.5228	44860.5	–0.0652	V	G. Samolyk	0.0001
CW Cas	56261.5968	45880	–0.0731	V	K. Menzies	0.0001

Table continued on following pages

Table 1. Recent times of minima of stars in the AAVSO eclipsing binary program, cont.

Star	HJD 2400000+	Cycle	O–C (day)	F	Observer	Standard Error (day)
IR Cas	56195.5899	20320	0.0086	V	G. Samolyk	0.0001
IS Cas	56194.6082	14889	0.0671	V	G. Samolyk	0.0002
MS Cas	52592.7172	14937	0.0361	V	S. Dvorak	0.0003
OR Cas	55887.6642	9374	–0.0253	V	J. A. Howell	0.0002
V364 Cas	56208.5781	14176.5	–0.0234	V	N. Simmons	0.0002
V368 Cas	50425.611	5587	–0.033	—	S. Cook	—
V375 Cas	54061.5755	13180	0.1153	V	G. Lubcke	0.0001
V375 Cas	54061.5759	13180	0.1157	I	G. Lubcke	0.0001
V380 Cas	56186.7937	22502	–0.0684	V	G. Samolyk	0.0005
V520 Cas	52980.551	981	0.0011	V	S. Dvorak	0.0010
U Cep	56196.7859	4675	0.1858	V	G. Samolyk	0.0001
SU Cep	56191.5929	33133	0.0052	V	G. Samolyk	0.0003
VZ Cep	51053.731	6197	–0.001	—	S. Cook	—
WZ Cep	56182.6314	67415	–0.1209	V	G. Samolyk	0.0003
ZZ Cep	55934.6160	13076	–0.0118	V	G. Samolyk	0.0003
AH Cep	51462.603 :	9282	–0.034	—	S. Cook	—
DL Cep	56153.8172	13620	0.0579	V	K. Menzies	0.0001
DV Cep	55962.7031	7917	–0.0044	V	G. Samolyk	0.0002
EG Cep	56068.8841	24741	0.0129	V	G. Samolyk	0.0001
GT Cep	51060.6380	5181	0.1232	—	S. Cook	—
V338 Cep	50686.692 :	3123	0.019	—	S. Cook	—
TT Cet	56253.6352	48786	–0.0686	V	R. Poklar	0.0001
TW Cet	56256.6917	43816.5	–0.0276	V	R. Poklar	0.0001
TX Cet	56243.6698	17765	0.0085	V	R. Poklar	0.0002
RW Com	56061.6512	67577.5	–0.0076	V	G. Samolyk	0.0002
RZ Com	55962.7808	62407.5	0.0453	V	G. Samolyk	0.0001
RZ Com	56086.6737	62773.5	0.0450	V	G. Samolyk	0.0001
SS Com	55935.8322	74935	0.7612	V	K. Menzies	0.0002
CC Com	56064.6237	74907.5	–0.0168	V	G. Samolyk	0.0002
U CrB	56061.7617	11388	0.1212	V	G. Samolyk	0.0001
W Crv	56073.6931	42326	0.0179	V	G. Samolyk	0.0002
RV Crv	56076.7180	20137	–0.0815	V	G. Samolyk	0.0005
V Crt	56013.7219	20820	–0.0020	V	R. Poklar	0.0001
WZ Cyg	52495.5587	19967	0.0531	V	S. Dvorak	0.0001
ZZ Cyg	55837.6453	17240	–0.0592	V	J. A. Howell	0.0003
ZZ Cyg	56196.5826	17811	–0.0618	V	G. Samolyk	0.0002
AE Cyg	56181.5803	11964	–0.0042	V	G. Samolyk	0.0001
BR Cyg	56193.6742	10997	0.0009	V	G. Samolyk	0.0001

Table continued on following pages

Table 1. Recent times of minima of stars in the AAVSO eclipsing binary program, cont.

Star	*HJD 2400000+*	*Cycle*	*O–C (day)*	*F*	*Observer*	*Standard Error (day)*
CG Cyg	56170.6257	26532	0.0706	V	G. Samolyk	0.0001
CV Cyg	50251.655 :	26232	–0.118	—	S. Cook	—
DK Cyg	56170.6884	38605	0.0959	V	K. Menzies	0.0002
DK Cyg	56187.6338	38641	0.0964	V	G. Samolyk	0.0002
GO Cyg	54023.5496	27994	0.0636	V	V. Petriew	0.0001
KR Cyg	56181.7125	32036	0.0196	V	K. Menzies	0.0001
MY Cyg	56196.5526	5580	0.0004	V	G. Samolyk	0.0002
V346 Cyg	56110.6449	7445	0.1604	V	K. Menzies	0.0001
V370 Cyg	52589.5713	23188	–0.0142	V	S. Dvorak	0.0003
V387 Cyg	56166.5990	43992	0.0211	V	K. Menzies	0.0001
V388 Cyg	56186.6269	16569	–0.0978	V	G. Samolyk	0.0001
V401 Cyg	56182.6233	21189	0.0678	V	G. Samolyk	0.0002
V466 Cyg	56173.6401	19689.5	0.0067	V	G. Samolyk	0.0003
V477 Cyg	56170.6226	5105	–0.0283	V	G. Samolyk	0.0002
V726 Cyg	53169.7262	39826	0.0438	V	S. Dvorak	0.0002
V753 Cyg	52486.7722	39233	0.0576	V	S. Dvorak	0.0002
W Del	56189.7074	2676	0.0343	V	G. Samolyk	0.0001
TT Del	55852.5993	3699	–0.0888	V	J. A. Howell	0.0002
EX Del	52575.5268	228	–0.0010	V	S. Dvorak	0.0005
FZ Del	55839.6295	31301	–0.0371	V	J. A. Howell	0.0001
FZ Del	56189.7257	31748	–0.0369	V	B. Manske	0.0001
FZ Del	56193.6419	31753	–0.0367	V	G. Samolyk	0.0001
FZ Del	56200.6909	31762	–0.0367	V	B. Manske	0.0001
GG Del	52470.7094	42095	–0.0201	V	S. Dvorak	0.0004
Z Dra	55982.7064	4522	–0.0188	V	R. Poklar	0.0001
RR Dra	52470.6078	2821	0.0588	V	S. Dvorak	0.0003
BH Dra	56169.5933	8887	–0.0041	V	G. Samolyk	0.0002
BW Dra	50590.631 :	27443.5	0.005	—	S. Cook	—
TZ Eri	55929.6215	5186	0.3039	V	G. Samolyk	0.0002
YY Eri	55946.6093	44681.5	0.1445	V	N. Simmons	0.0003
YY Eri	56261.6775	45661.5	0.1483	V	R. Poklar	0.0002
AE For	52285.5160	–349	0.0004	V	S. Dvorak	0.0001
AE For	53026.5111	458	0.0005	V	S. Dvorak	0.0002
RW Gem	55946.6937	13137	0.0020	V	G. Samolyk	0.0002
RW Gem	56221.7815	13233	0.0020	V	K. Menzies	0.0001
SX Gem	55965.5996	27021	–0.0538	V	R. Sabo	0.0003
TX Gem	56024.5581	12920	–0.0348	V	K. Menzies	0.0001
WW Gem	55936.8285	24198	0.0209	V	G. Samolyk	0.0001

Table continued on following pages

Table 1. Recent times of minima of stars in the AAVSO eclipsing binary program, cont.

Star	HJD 2400000+	Cycle	O–C (day)	F	Observer	Standard Error (day)
WW Gem	56258.6658	24458	0.0274	V	K. Menzies	0.0002
AF Gem	55940.6437	23143	–0.0668	V	R. Poklar	0.0001
AL Gem	55937.7718	21284	0.0765	V	G. Samolyk	0.0001
KM Gem	52965.8942	25315	0.1649	V	S. Dvorak	0.0005
RV Gru	51089.289	64476.5	0.004	—	H. Lund	—
Z Her	56076.8686	10767	–0.0264	V	G. Samolyk	0.0005
RX Her	56058.8464	12869	0.0001	V	G. Samolyk	0.0001
SZ Her	55836.5823	17079	–0.0234	V	J. A. Howell	0.0001
SZ Her	56064.8316	17358	–0.0235	V	G. Samolyk	0.0001
SZ Her	56187.5458	17508	–0.0240	V	K. Menzies	0.0001
TU Her	56062.7443	5294	–0.2183	V	G. Samolyk	0.0001
AD Her	50262.095	1153	0.105	—	S. Cook	—
AK Her	56127.4751	33073	0.0176	R	L. Corp	0.0004
AK Her	56157.4022	33144	0.0167	R	L. Corp	0.0005
CC Her	56075.7361	9462	0.2313	V	G. Samolyk	0.0001
CT Her	55838.5812	7454	0.0115	V	J. A. Howell	0.0004
DI Her	49934.962 :	730	–0.008	—	S. Cook	—
DI Her	56125.4934	1317	–2.4254	R	L. Corp	0.0005
DP Her	51727.6733	13574.5	0.0547	V	G. Lubcke	0.0018
HS Her	51364.669	3789	–0.006	—	S. Cook	—
MS Her	53173.7350	44202.5	0.1169	V	S. Dvorak	0.0006
MT Her	52456.3798	23249	0.0119	V	L. Baldinelli	0.0002
V342 Her	53305.5260	20678	0.0131	V	S. Dvorak	0.0010
V829 Her	53149.6626	1813.5	–0.0073	V	S. Dvorak	0.0004
WY Hya	55958.7023	21491	0.0311	V	R. Poklar	0.0001
DF Hya	55966.6840	39863	–0.0085	V	G. Samolyk	0.0001
DF Hya	55967.6757	39866	–0.0087	V	R. Poklar	0.0001
DF Hya	55987.6760	39926.5	–0.0100	V	R. Poklar	0.0003
DI Hya	55936.9206	40251	–0.0314	V	G. Samolyk	0.0003
DI Hya	55986.7114	40332	–0.0324	V	R. Poklar	0.0002
DK Hya	55997.6879	25203	0.0025	V	R. Poklar	0.0002
EU Hya	52384.6433	23462	–0.0200	V	S. Dvorak	0.0001
RT Lac	50348.078	1079	–0.078	—	S. Cook	—
SW Lac	56127.8023	33838	–0.0992	V	R. Sabo	0.0001
SW Lac	56186.4942	34021	–0.0993	R	L. Corp	0.0001
VX Lac	56166.8116	10152	0.0804	V	K. Menzies	0.0001
CM Lac	56183.5584	18170	–0.0040	V	K. Menzies	0.0001
CN Lac	52503.6476	41163	0.0322	V	S. Dvorak	0.0006

Table continued on following pages

Table 1. Recent times of minima of stars in the AAVSO eclipsing binary program, cont.

Star	*HJD 2400000+*	*Cycle*	*O–C (day)*	*F*	*Observer*	*Standard Error (day)*
CO Lac	56173.6327	18570.5	–0.0045	V	G. Samolyk	0.0002
CO Lac	56258.4532	18625.5	–0.0054	V	K. Menzies	0.0003
EK Lac	52435.7893	12757	–0.0039	V	S. Dvorak	0.0003
EM Lac	53359.5329	38804	0.0553	V	S. Dvorak	0.0003
GX Lac	50737.627 :	1729	–0.008	—	S. Cook	—
Y Leo	55935.7849	6227	–0.0233	V	G. Samolyk	0.0001
Y Leo	55962.7617	6243	–0.0241	V	G. Samolyk	0.0001
UV Leo	55995.6420	29254	0.0356	V	R. Poklar	0.0001
UV Leo	56058.6519	29359	0.0365	V	G. Samolyk	0.0001
UX Leo	52647.8926	15162.5	0.2172	V	S. Dvorak	0.0001
VZ Leo	55995.5824	22783	–0.0620	V	N. Simmons	0.0006
XY Leo	55975.6509	38371	0.0782	V	N. Simmons	0.0001
XZ Leo	56002.6251	22506.5	0.0571	V	R. Poklar	0.0006
AP Leo	56011.4664	38282	–0.0252	R	L. Corp	0.0003
DU Leo	53831.6554	969	0.0006	V	V. Petriew	0.0001
EX Leo	53823.6942	3239	–0.0027	V	V. Petriew	0.0001
FS Leo	53832.6949	2916	–0.0016	V	V. Petriew	0.0001
T LMi	55966.8634	3500	–0.1021	V	G. Samolyk	0.0002
Z Lep	55957.6660	28714	–0.1775	V	R. Poklar	0.0001
RR Lep	55959.6742	27946	–0.0387	V	R. Poklar	0.0001
SX Lyn	50586.614 :	2545	0.000	—	S. Cook	—
UV Lyn	52667.8611	29872	0.0491	V	S. Dvorak	0.0003
UZ Lyr	55837.5617	6423	–0.0243	V	J. A. Howell	0.0009
FL Lyr	55840.6419	8089	–0.0015	V	J. A. Howell	0.0003
AT Mon	55983.6607	14478	0.0091	V	R. Poklar	0.0002
AV Mon	51587.559 :	3581	–0.084	—	S. Cook	—
FS Mon	50502.560	8421	–0.018	—	S. Cook	—
MX Mon	52607.7686	32745	–0.0974	V	S. Dvorak	0.0001
V453 Mon	53068.6918	1112	–0.0017	V	S. Dvorak	0.0002
V527 Mon	52372.622	23097	–0.019	V	S. Dvorak	0.0006
V456 Oph	52503.5653	10439	0.0135	V	S. Dvorak	0.0001
V506 Oph	52437.6864	8939.5	0.0274	V	S. Dvorak	0.0002
V508 Oph	56073.8037	31878	–0.0228	V	G. Samolyk	0.0002
V566 Oph	50234.045	20501	0.037	—	S. Cook	—
V788 Oph	52493.6080	28275	–0.0229	V	G. Lubcke	0.0010
V788 Oph	52494.6980	28277	–0.0271	V	G. Lubcke	0.0010
V839 Oph	56169.6425	38438	0.2675	V	G. Samolyk	0.0001
EF Ori	56221.8826	2390.5	0.0016	V	K. Menzies	0.0009

Table continued on following pages

Table 1. Recent times of minima of stars in the AAVSO eclipsing binary program, cont.

Star	HJD 2400000+	Cycle	O–C (day)	F	Observer	Standard Error (day)
EQ Ori	55937.6270	14031	–0.0418	V	R. Poklar	0.0001
ER Ori	55931.6762	33786.5	0.1010	V	R. Poklar	0.0002
ET Ori	55962.6352	30789	–0.0040	V	G. Samolyk	0.0001
FH Ori	55936.6455	13963	–0.3886	V	R. Poklar	0.0004
FT Ori	56221.8092	4721	0.0167	V	B. Manske	0.0003
FZ Ori	55937.6057	29784	–0.0535	V	N. Simmons	0.0002
FZ Ori	55962.6068	29846.5	–0.0516	V	K. Menzies	0.0002
GU Ori	55964.6296	27396	–0.0501	V	G. Samolyk	0.0003
GU Ori	55981.3356	27431.5	–0.0532	R	L. Corp	0.0004
GU Ori	56217.8540	27934	–0.0521	V	K. Menzies	0.0001
GU Ori	56221.8536	27942.5	–0.0533	V	K. Menzies	0.0005
GU Ori	56256.9207	28017	–0.0519	V	K. Menzies	0.0003
U Peg	56163.7494	52436.5	–0.1458	V	G. Samolyk	0.0003
U Peg	56169.7446	52452.5	–0.1470	V	B. Manske	0.0003
U Peg	56185.6718	52495	–0.1481	V	B. Manske	0.0002
U Peg	56185.8609	52495.5	–0.1464	V	B. Manske	0.0002
U Peg	56206.4734	52550.5	–0.1469	R	L. Corp	0.0003
U Peg	56247.3248	52659.5	–0.1466	R	L. Corp	0.0003
BB Peg	56167.8237	34311	–0.0082	V	B. Manske	0.0003
BB Peg	56169.8127	34316.5	–0.0075	V	G. Samolyk	0.0003
BB Peg	56180.6581	34346.5	–0.0072	V	B. Manske	0.0002
BB Peg	56180.8387	34347	–0.0074	V	B. Manske	0.0002
BB Peg	56251.5117	34542.5	–0.0080	V	K. Menzies	0.0001
BG Peg	56170.8282	5449	–2.0611	V	G. Samolyk	0.0003
BN Peg	52437.8354	25994	0.0012	V	S. Dvorak	0.0001
BO Peg	52503.7466	11873	–0.0230	V	S. Dvorak	0.0003
BX Peg	56196.7191	42798	–0.1074	V	B. Manske	0.0002
CC Peg	52965.5990	46520	0.0114	V	S. Dvorak	0.0005
DI Peg	54016.5930	12391	–0.0170	R	G. Lubcke	0.0001
DI Peg	56189.7822	15444	–0.0044	V	R. Sabo	0.0001
DI Peg	56224.3030	15492.5	–0.0068	R	L. Corp	0.0008
DK Peg	52989.5442	4571	0.0669	V	S. Dvorak	0.0001
GP Peg	56181.8182	15317	–0.0492	V	G. Samolyk	0.0001
GP Peg	56182.7945	15318	–0.0484	V	R. Sabo	0.0001
Z Per	56181.8520	3443	–0.2566	V	G. Samolyk	0.0003
RT Per	55962.5380	26591	0.0758	V	K. Menzies	0.0001
RT Per	56180.8368	26848	0.0787	V	G. Samolyk	0.0002
RT Per	56226.7054	26902	0.0797	V	R. Poklar	0.0001

Table continued on following pages

Table 1. Recent times of minima of stars in the AAVSO eclipsing binary program, cont.

Star	*HJD 2400000+*	*Cycle*	*O–C (day)*	*F*	*Observer*	*Standard Error (day)*
RV Per	56194.8802	7169	–0.0021	V	G. Samolyk	0.0001
RY Per	50365.661 :	3394	0.009	—	S. Cook	—
ST Per	56186.8635	5192	0.3040	V	G. Samolyk	0.0001
XZ Per	56186.9049	11010	–0.0642	V	G. Samolyk	0.0001
XZ Per	56230.6663	11048	–0.0649	V	R. Poklar	0.0003
XZ Per	56238.7280	11055	–0.0646	V	R. Poklar	0.0001
DM Per	50414.637	3114	–0.008	—	S. Cook	—
HW Per	53027.5203	39387	0.0229	V	S. Dvorak	0.0003
IK Per	52325.5920	36874	–0.1067	V	S. Dvorak	0.005
IQ Per	54099.6762	5626	0.0047	V	V. Petriew	0.0001
IT Per	56187.8469	17477	–0.0244	V	G. Samolyk	0.0004
IU Per	56182.8483	12335	0.0076	V	G. Samolyk	0.0003
IU Per	56212.8431	12370	0.0066	V	K. Menzies	0.0001
IU Per	56255.6945	12420	0.0068	V	R. Poklar	0.0002
KL Per	52284.5757	7397	0.1159	V	S. Dvorak	0.0002
KW Per	56189.7719	14803	0.0153	V	G. Samolyk	0.0004
V432 Per	56228.6775	63307	0.0248	V	R. Poklar	0.0002
Beta Per	56181.8416	3676	0.1175	V	G. Samolyk	0.0003
RV Psc	56257.5396	57539	–0.0544	V	K. Menzies	0.0001
SX Psc	52669.5337	8085	–0.0016	V	S. Dvorak	0.0003
RW PsA	52221.5811	49641	–0.0209	V	S. Dvorak	0.0001
RW PsA	52597.5282	50684	–0.0242	V	S. Dvorak	0.0001
UZ Pup	55975.6922	14294.5	–0.0066	V	R. Poklar	0.0003
VY Pup	52608.9009	31366	0.0041	V	S. Dvorak	0.0005
DS Pup	51247.281	59593.5	0.072	—	H. Lund	—
MO Pup	52314.5220	15208.5	–0.0510	V	S. Dvorak	0.0010
U Sge	56186.7033	11553	–0.0032	V	G. Samolyk	0.0001
CU Sge	52486.6742	12446	0.0154	V	S. Dvorak	0.0001
V1968 Sgr	56073.8938	32407	–0.0147	V	G. Samolyk	0.0003
AO Ser	56068.7714	24945	–0.0148	V	G. Samolyk	0.0001
RW Tau	56188.9138	3794	–0.2525	V	R. Sabo	0.0001
RZ Tau	55935.5596	43926	0.0657	V	G. Samolyk	0.0001
TY Tau	55967.5338	32278	0.2580	V	G. Samolyk	0.0002
WY Tau	55967.5498	26799	0.0594	V	G. Samolyk	0.0002
WY Tau	56189.9247	27120	0.0589	V	R. Sabo	0.0002
AM Tau	55963.5297	5240	–0.0595	V	G. Samolyk	0.0002
AQ Tau	55956.5428	21631	0.5494	V	G. Samolyk	0.0003
CF Tau	54070.7043	8498	–0.0789	V	J. Bialozynski	0.0003

Table continued on following pages

Table 1. Recent times of minima of stars in the AAVSO eclipsing binary program, cont.

Star	HJD 2400000+	Cycle	O–C (day)	F	Observer	Standard Error (day)
CT Tau	55963.5592	15835	–0.0576	V	N. Simmons	0.0002
EQ Tau	55937.5166	46065	–0.0261	V	G. Samolyk	0.0001
EQ Tau	55962.7768	46139	–0.0258	V	N. Simmons	0.0004
EQ Tau	55963.6289	46141.5	–0.0270	V	R. Sabo	0.0002
EQ Tau	56182.7747	46783.5	–0.0269	V	K. Menzies	0.0001
EQ Tau	56243.7054	46962	–0.0269	V	K. Menzies	0.0001
EQ Tau	56247.8012	46974	–0.0273	V	B. Manske	0.0001
HU Tau	56193.8053	7255	0.0291	V	G. Samolyk	0.0002
V781 Tau	52597.6896	25290	–0.0383	V	S. Dvorak	0.0001
V1123 Tau	54089.6576	3974.5	–0.0004	V	V. Petriew	0.0003
V Tri	56258.5768	54313	–0.0054	V	K. Menzies	0.0001
X Tri	56180.8822	14079	–0.0829	V	G. Samolyk	0.0001
X Tri	56221.6864	14121	–0.0832	V	R. Poklar	0.0001
RS Tri	55962.5942	9441	–0.0416	V	N. Simmons	0.0007
RS Tri	56187.8441	9559	–0.0447	V	G. Samolyk	0.0002
RV Tri	56173.8542	13455	–0.0363	V	G. Samolyk	0.0001
W UMa	56009.6750	30704	–0.0690	V	R. Poklar	0.0005
TY UMa	55966.9130	46353.5	0.3115	V	G. Samolyk	0.0001
TY UMa	55998.6450	46443	0.3123	V	R. Poklar	0.0003
TY UMa	56004.8498	46460.5	0.3127	V	K. Menzies	0.0001
UX UMa	55942.9325	94117	0.0012	V	K. Menzies	0.0001
UX UMa	55978.9224	94300	0.0003	V	K. Menzies	0.0002
UY UMa	52415.6308	66032	0.0763	V	S. Dvorak	0.0004
VV UMa	55994.6960	14809	–0.0509	V	R. Poklar	0.0001
XY UMa	50582.655	32080	0.008	—	S. Cook	—
XY UMa	52608.8173	36310	0.0227	V	S. Dvorak	0.0003
ZZ UMa	55936.6487	8692	–0.0032	V	G. Samolyk	0.0001
HX UMa	53839.6526	3533	0.0000	V	V. Petriew	0.0002
AK Vir	56074.7780	11309	–0.0309	V	G. Samolyk	0.0004
AW Vir	56007.7266	31031.5	0.0253	V	K. Menzies	0.0001
AW Vir	56038.7012	31119	0.0251	V	R. Poklar	0.0001
AX Vir	56034.7093	40517	0.0112	V	R. Poklar	0.0001
AZ Vir	56044.6840	34513.5	–0.0228	V	R. Poklar	0.0002
BH Vir	56045.6829	15688	–0.0079	V	R. Poklar	0.0003
DL Vir	50192.641	8663	0.113	—	S. Cook	—
FO Vir	50573.645 :	6617	0.007	—	S. Cook	—
MS Vir	56048.6896	11358	0.0005	V	R. Poklar	0.0002
NY Vir	55979.5542	56983	–0.0013	R	L. Corp	0.0001

Table continued on next page

Table 1. Recent times of minima of stars in the AAVSO eclipsing binary program, cont.

Star	*HJD 2400000+*	*Cycle*	*O–C (day)*	*F*	*Observer*	*Standard Error (day)*
NY Vir	55979.6047	56983.5	–0.0012	R	L. Corp	0.0001
NY Vir	55979.6552	56984	–0.0012	R	L. Corp	0.0001
Z Vul	56125.5550	5368	–0.0084	R	L. Corp	0.0004
AW Vul	55838.6724	11846	–0.0160	V	J. A. Howell	0.0001
AW Vul	55851.5758	11862	–0.0158	V	J. A. Howell	0.0001
AW Vul	56184.6387	12275	–0.0173	V	K. Menzies	0.0001
BS Vul	56173.7084	27107	–0.0282	V	K. Menzies	0.0001
BU Vul	55849.6072	39220	0.0187	V	J. A. Howell	0.0001
CD Vul	56180.6713	14453	–0.0002	V	G. Samolyk	0.0002

BVRI Observations of SZ Lyncis at the EKU Observatory

Marco Ciocca
Department of Physics and Astronomy, Eastern Kentucky University, Richmond, KY; marco.ciocca@eku.edu

Received January 31, 2013; revised February 28, 2013; accepted April 3, 2013

Abstract Eastern Kentucky University (EKU) is a regional University serving the Kentucky part of Appalachia. In 2008 a small observatory was built and this work will describe the instrumentation and the site characterization. We have in fact measured the transformation parameters of the the telescope and camera combination and the first order extinction coefficients for our site. As an example of the capabilities of the observatory we have determined the pulsation period of the δ Scuti star SZ Lyncis and measured the standard magnitudes via BVRI and two color terms B–V and V–R.

1. Facilities

Eastern Kentucky University (EKU) is a regional comprehensive University located in the center of the Blue Grass region, in Richmond, Kentucky. Its service area includes much of the eastern part of Kentucky, commonly referred to as Appalachia. As such, Eastern has truly been a "school of opportunities" for the region.

In 2008 we had the opportunity to build a small observatory, for outreach and research. The facility, located at Lat. 37° 43' 35.92" N and Long. 84° 18' 0.67" W, consists of a 14-inch telescope (C-14 from Celestron), with a research grade tracking mount (Paramount ME), housed permanently in a two-room building. The observatory has a retractable roof, with the control room insulated against the elements, and is conveniently located near campus, but also away from city lights and vehicular traffic.

The instrument package consists of a SBIG STL-6303E CCD camera with filter wheel and full complement of photographic (Luminance, RGB), narrow-band, and photometric filters (H-alpha and Johnson-Cousins UBVRI). The camera's main CCD detector has an array of 3072×2048 pixels, with 9μm pixels, and is non anti-blooming (NABG). Binned 1×1, the combination of the telescope (an $f/11$ design) and camera results in a nominal image scale of 0.48 arcsec/pixel. This scale is rarely warranted by the prevalent seeing conditions, which range from 2 to 5 arcsec, and would produce unnecessary oversampling. This is solved by binning the CCD camera, with the twofold improvements of increased sensitivity and reduction of oversampling. While binned 3×3, the STL-6303 has been measured to produce an image scale of 1.23 arcsec/pixel, which is excellent for the local seeing conditions (approx. a

2 to 1 oversampling). A quick characterization of the CCD, using the routine in AIP4WIN (Berry and Burnell 2011), shows the camera, binned 3 × 3, to have a gain of 2.3 electrons/ADU, a readout noise of 28 electrons RMS, and a Mean Dark Current of 0.05 electrons/pixel/sec at –14.8°C. Camera and mount are controlled by the integrated package CCDSOFT-SKY X PRO from Software Bisque (2011).

2. Capabilities of the observatory and local conditions

The first step in precision photometry is the measurement of the CCD transformation coefficients, to be able to convert the raw instrumental magnitudes generated by the camera-telescope combination to standard magnitudes and to make comparison with other measurements possible. It also gives a means to assess the capabilities of the telescope-camera combination and its response through the photometric filters.

On four nights during March 2012 we imaged, through BVRI filters, Landolt standard fields centered at R.A. $07^h\ 24^m\ 15^s$, Dec. –00° 32' 00"; R.A. $07^h\ 30^m\ 00^s$, Dec. –02° 06' 00"; and R.A. $09^h\ 21^m\ 32^s$, Dec. +02° 47' 00". These fields were identified by Smith (2002) as fields # 55, 56, and 61, respectively. Data were obtained with time integration between 60 and 240 seconds, binned 3 × 3. After standard data reduction (with dark, bias, and flat frames) and following the procedures recommended by Sarty (2008) and Gary (2006), we obtained the transformation parameters shown in Table 1. The quoted values are the results of a weighted average of the parameters obtained during the four nights and three fields.

An ideal system would have the first three parameters equal to 1 and the last two to zero. Our results indicate a certain lack of sensitivity of the system in the range identified by the band pass of the Johnson B filter (centered around 440 nm), which is not surprising as CCD cameras, unless expressly designed, are not very sensitive in this range.

Our second set of measurements was made to ascertain the kind of atmospheric conditions that could be expected at our location and to see if they were conducive to photometry. In Richmond, Kentucky, prevalent weather patterns seem to indicate that the best photometric nights would occur during mid-spring (April–May) and mid-fall (September–October) due to a higher percentage of clear nights with lower humidity. Summers are quite humid and hot, not very favorable conditions, while winters are wet with many cloudy nights.

We measured the first order extinction coefficients for the filters BVRI at our location using the comp star method as explained by Warner (2006). The final goal of this observing campaign was the study of the δ Scuti Star SZ Lyn (a target of choice of the American Association of Variable Star Observers, AAVSO). For that purpose, we used the AAVSO Variable Star Plotter (VSP,

http://www.aavso.org/vsp) to plot a finder chart (Chart # 10399bsa) containing photometric star sequences for SZ Lyn. We identified three stars in this chart (AUID 000-BJR-415, 000-BJR-416, and 000-BJR-417) and their properties are presented in Table 2. These stars were present in all the images taken and were used for the comp star method.

Using the AIP4WIN magnitude measurement tool or MMT (Berry and Burnell 2011), we measured the instrumental magnitudes of the three stars through four standard photometric filters (BVRI), averaged their values, and plotted the resulting values as a function of the air mass. Given that in these measurements the air mass range covered was limited (1.1 to 1.5), and the three stars were of similar color, we assumed the second order extinction coefficient to be negligible. We fitted a straight line through the data, the slope of which will be the first order extinction coefficient for the particular photometric filter used. We performed these measurements during two nights (2012 April 6 and April 8).

The data are presented in Figures 1 through 4. Those two nights, while both clear and with good seeing, represent the range of variability in the local conditions. April 6 was clearly the better of the two nights, with smaller extinction coefficients across the board, while on April 8 the coefficients were all higher, probably due to high-lying cirrus clouds. Regardless, during the entire time of observation, the coefficients remained constant, thus making both nights "photometric nights."

The values obtained during the two nights are clearly different, but they are self-consistent: the difference in B and V values, k'_{bv} (Warner 2006), between the two nights is of the order of 0.15 (0.11 and 0.14, respectively, in our case, while the difference between V and R, k'_{vr}, is small and positive as expected, equaling 0.06 and 0.07, respectively. If these measurements were done on a single star, the regression lines zero point intercepts (that is, the intercepts at zero airmass) would give the instrumental magnitude above the atmosphere, and therefore they should be the same for any filter, regardless of the slope. In our case they are very close, averaging to a difference of 0.05 magnitude. Based on this measurement, we therefore claim that our reported magnitudes will have an overall uncertainty of 0.050 mag.

3. SZ Lyn measurements

The variability of the extinction coefficients highlighted clearly indicates why absolute photometry is not for the faint of heart. It is much easier to perform differential photometry, in which the photometry of the star of interest is obtained by comparing it with stars within the same field.

We report below the measurements on SZ Lyn (R.A. $08^h\ 09^m\ 35.8^s$, Dec. +48° 28' 18"), a variable star (Schneller 1961) belonging to the δ Scuti family and member of a binary system (Bardin and Imbert 1984; Gazeas *et al.* 2004). δ Scuti stars are short-period pulsating variables of A-F spectral types,

located at the intersection of the main sequence and the instability strip in the HR diagram. Typical periods are of the order of a few hours with amplitudes less than 1 mag. In particular, SZ Lyn belongs to the high-amplitude δ Scuti (HADS) stars, which have V-band amplitude changes larger than 0.3 mag. (for a review of δ Scuti stars see Rodríguez and Breger 2001). SZ Lyn has received in-depth coverage because of its rapid pulsation rate and because is known to be a member of a binary system.

Over several nights from March to May 2012 we conducted measurements on SZ Lyn, using the AAVSO comparison star sequence. Measurements were performed using BVRI filters. The star field, reproduced in Figure 5, was imaged through our 14-inch telescope with integration times of 30 to 45 seconds, in a rapid sequence, B-V-R-I-B-V-R-I, etc., so as to follow the star pulsation as closely as possible.

Each CCD frame obtained was reduced via CCDSOFT (Software Bisque 2011). The reduced files were then uploaded to the AAVSO and the light curves were generated via the software package VPHOT (AAVSO 2012), an online tool for photometric analysis provided by the AAVSO. As a sequence, we used AUID 000-BJR-415 and AUID 000-BJR-417 as comparison stars and AUID 000-BJR-416 as check star (see Table 2). The magnitudes obtained were then transformed using our measured transformation parameters according to the method outlined by Sarty (2008).

In Figures 6, 7, and 8 we present the transformed magnitudes and the color terms as a function of phase. These phase plots were generated using the software package PERANSO (Vanmuster 2011), which was also used to determine the period of pulsation of SZ Lyn from our data. As summarized in Table 3, we obtained P = 0.1205353(81) d. This value is in excellent agreement with values from Gazeas *et al.* (2004) of P = 0.1205349 (41) d, and with Paparó *et al.* (1988) of P = 0.120534910 (13) d.

We compared these results with the period obtained by analyzing, again using PERANSO, the AAVSO database of SZ Lyn observations. So as to compare similar techniques, we arbitrarily selected all the CCD observations through the V-filter reported since January 2005. We obtained, with this much larger data set, a period P = 0.1205350(1) d.

The uncertainty we reported in our data is simply due to the spread of the values of the period obtained by using all the routines available in PERANSO, and it is approximately 0.7 second. This value seems much better to us than the typical accuracy of the computer clocks present in typical desktop PCs, especially considering that the measurements were done over the course of a few weeks. While we routinely, at the beginning of each observation run, synchronized the computer clock with internet time servers connected with NIST sites, we did so without really relying on any further refinements of our time base. The uncertainty quoted by Gazeas *et al.* (2004) is comparable to ours (0.35 s), and just as in our case, there is no mention of a particular effort

to quantify the knowledge of the time base. Further, the uncertainties quoted by Paparó *et al.* (1988) and Gazeas and Niarchos (2005) appear to be approximately two orders of magnitude smaller (approx. 0.001 s).

The latter two results were obtained by fitting the times of all the light maxima observed over a span of 26 years and 34 years, respectively, all by different observers. It seems that all the quoted uncertainties, our case included, are simply an indication in the uncertainty of the computations to obtain the period (by Fourier transform techniques) of the time-series measurements. Unless a concerted effort is made, it is doubtful that the period of pulsation reported by Paparó *et al.*, this work, and Gazeas truly have the quoted uncertainty. We would categorize all these as lower limits of the uncertainty, probably superseded by larger uncertainties in the time base.

Given a large enough dataset, as in the case when we analyzed the AAVSO database, Fourier transform techniques pose a very small lower limit. The analysis of the AAVSO database, in fact, resulted in an uncertainty of approximately 0.09 second, but that should not be taken as the ultimate uncertainty, as the data were reported by a large number of individual observers over the course of many years. It is highly doubtful that all their clocks were all synchronized to within 0.09 second.

4. Conclusion

We performed measurements designed to characterize the instrumentation (telescope, camera, and filters) and the location. The former was achieved by determining the transformation coefficients of our telescope-camera combination, the latter by determining the extinction coefficients at our location. As an application, we determined the pulsation period of the δ scuti star SZ Lyn and its transformed standard magnitudes through the Johnson-Cousins BVRI filters. We found good agreement with values existing in the literature.

5. Acknowledgements

This work was supported in part by a grant from EKU's University Research Committee URC and a grant from the AAS Small Research Grant (SmRG) Program. We acknowledge with thanks the variable star observations from the AAVSO International Database contributed by observers worldwide and used in this research. We also wish to thank Dr. M. Pitts for a careful reading of the manuscript.

References

AAVSO. 2012, VPHOT AAVSO photometric software (http://www.aavso.org/vphot).

Bardin, C., and Imbert, M. 1984, *Astron. Astrophys., Suppl. Ser.*, **57**, 249.

Berry, R., and Burnell, J. 2011, "Astronomical Image Processing for Windows," version 2.4.0, provided with *The Handbook of Astronomical Image Processing*, Willmann-Bell, Richmond, VA.

Gary, B. L. 2006, "CCD Transformation Equations for use with Single-Image Photometry" (http://reductionism.net.seanic.net/CCD_TE/cte.html).

Gazeas, K. D., and Niarchos, P. G. 2005, in *The Light-Time Effect in Astrophysics*, ed. C. Sterken, ASP Conf. Ser. 335, Astron. Soc. Pacific, San Francisco, 297.

Gazeas, K. D., Niarchos, P. G., and Boutsia, K. A. 2004, *Commun. Asteroseismology*, **144**, 26.

Paparó, M., Szeidl, B., and Mahdy, H. A. 1988, *Astrophys. Space Sci.*, **149**, 73.

Rodríguez, E., and Breger, M. 2001, *Astron. Astrophys., Suppl. Ser.*, **366**, 178.

Sarty, G. E. 2008, "Photometry Transformation Coefficients," AAVSO internal document.

Schneller, H. 1961, *Astron. Nachr.*, **286**, 102.

Smith, P. S. 2002, *Standard Star Fields for UBVRI Photometric Calibration*, Univ. Arizona, Tuscon, AZ.

Software Bisque. 2011, CCD Soft v. 5.00.210, The Sky X Pro, v. 10.1.11 (http://www.bisque.com/sc/).

Vanmunster, T. 2011, PERANSO period analysis software (http://www.peranso.com).

Warner, B. D. 2006, in *A Practical Guide to Lightcurve Photometry and Analysis*, ed. Warner, B. D., and Harris, A. W., New York, Springer, 30.

Table 1. Transformation parameters for the EKU observatory (March 2012).

Transformation Parameters	*Value and Uncertainties*
T_{bv}	1.445 ± 0.003
T_{vr}	1.006 ± 0.002
T_{ri}	0.945 ± 0.002
T_{v}	-0.054 ± 0.002
T_{r}	0.061 ± 0.003

Table 2. Sequence stars used (AAVSO Chart 10399bsa) to observe SZ Lyn.

AUID	*R.A.* *h m s*	*Dec.* ° ′ ″		
B	*V*	*Rc*	*Ic*	*Comments*
000-BJR-415	08 09 55.81	+44 25 48.6		
11.701(0.024)	10.924(0.016)	10.481(0.037)	10.105(0.041)	Comp. Star
000-BJR-416	08 09 29.82	+44 24 28.6		
11.845(0.033)	11.456(0.012)	11.222(0.024)	11.002(0.031)	Comp. Star
000-BJR-417	08 09 39.83	+44 22 21.5		
12.689(0.031)	12.087(0.024)	11.743(0.048)	11.442(0.060)	Check Star

Table 3. SZ Lyn pulsation period.

Observer	*Pulsation Period (d)*
Paparó *et al.* (1988)	0.120534910(13)
Gazeas *et al.* (2004)	0.1205349(41)
Gazeas and Niarchos (2005)	0.120535068(13)
AAVSO Database	0.1205350(1)
This work	0.1205353 (81)

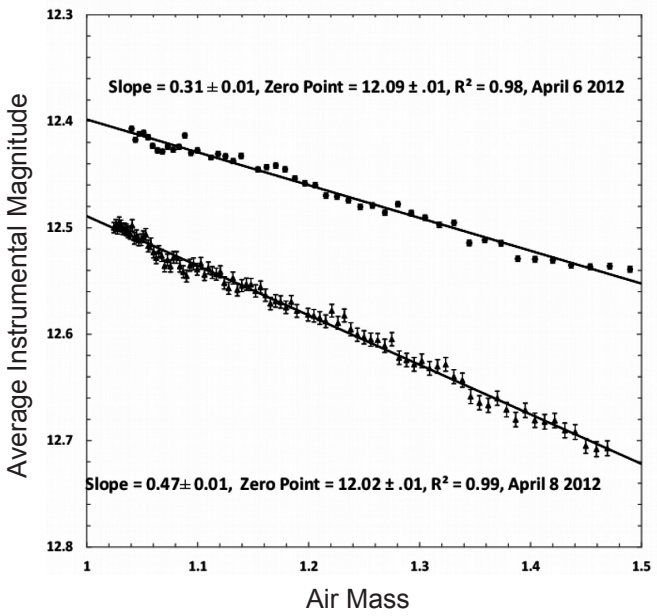

Figure 1. Extinction coefficient at EKU observatory through B filter.

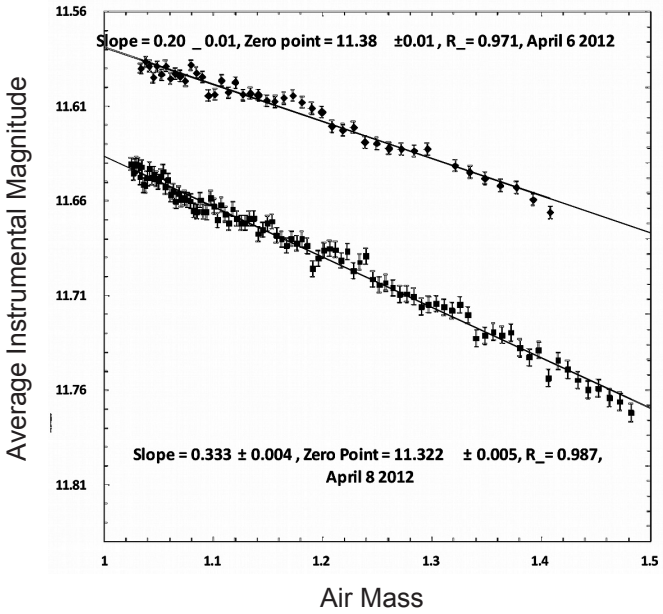

Figure 2. Extinction coefficient at EKU Observatory through V filter.

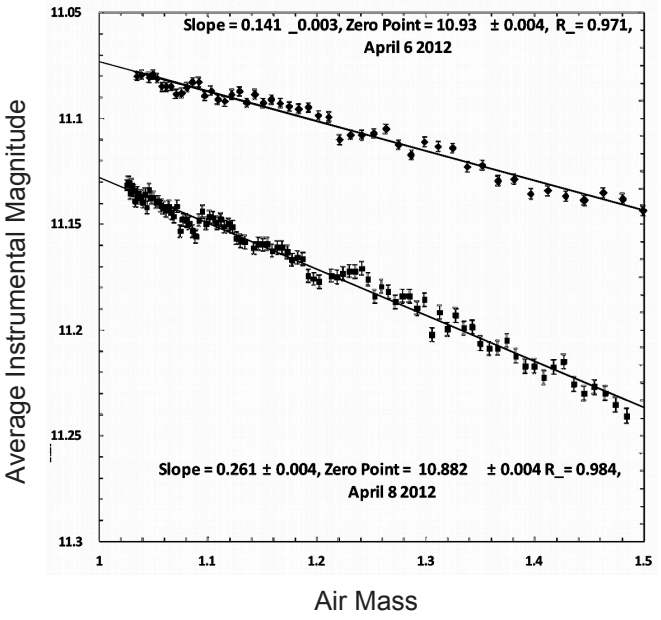

Figure 3. Extinction coefficient at EKU Observatory through Rc filter.

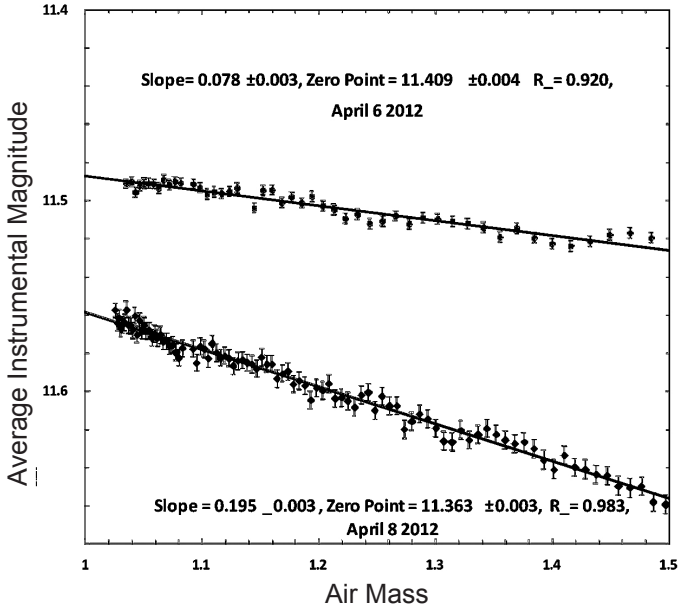

Figure 4. Extinction coefficient at EKU Observatory through Ic filter.

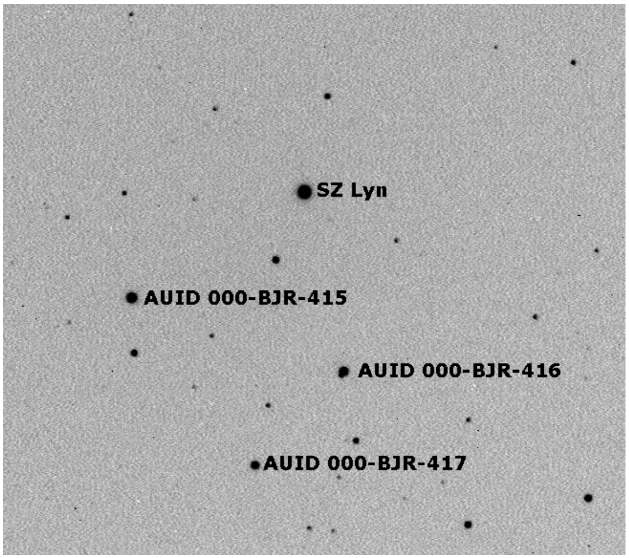

Figure 5. SZ Lyn and the sequence stars, as identified on AAVSO finder chart #10399bsa. This CCD image was obtained at the EKU Observatory on April 6, 2012. Image center is at R.A. 8^h 09^m 36.7^s, Dec. +44° 26' 48.0". Up, in this image, is 3° 12' West of true North. East is to the left. Scale size is 1.24 arcsec/pixel.

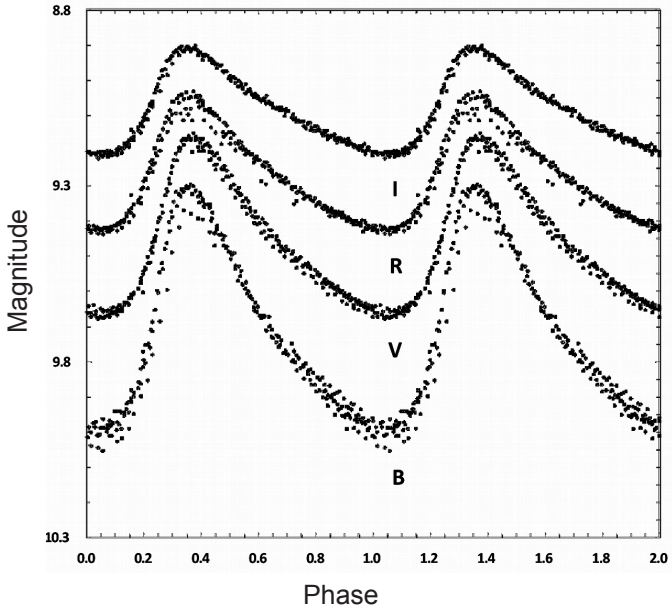

Figure 6. SZ Lyn phase plot.

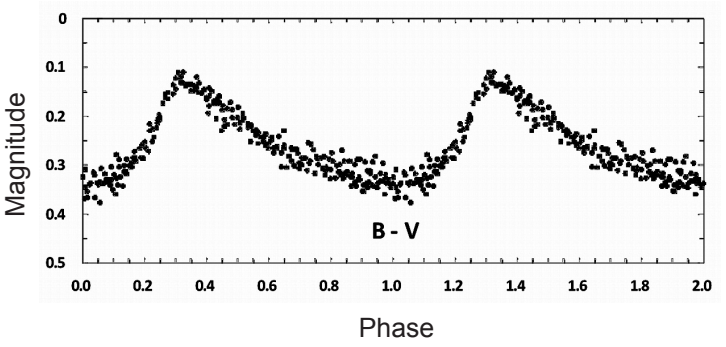

Figure 7. SZ Lyn B–V term.

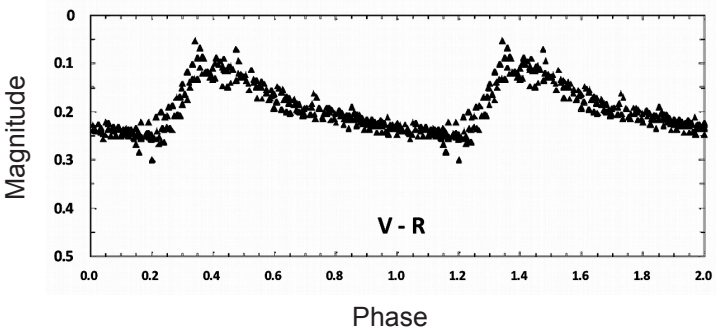

Figure 8. SZ Lyn V–R term.

Book Review

Received March 23, 2013

Scientific Writing for Young Astronomers

Christiaan Sterken, ed., 2011.

Part 1, 165 pp., hardcover, EAS Publication Series Volume 49, ISBN 978-2-7598-0506-8. Price 36 Euro, including VAT (http://www.edition-sciences.com/scientific-writing-for-young-astronomers-part-1.htm).

Part 2, 298 pp., hardcover, EAS Publication Series Volume 50, ISBN 987-2-7598-0639-3. Price 61 Euro, including VAT (http://www.edition-sciences.com/scientific-writing-for-young-astronomers-part-2.htm).

Both parts include subject and name index and list of acronyms. Published by EAS, EDP Sciences, Les Ulis, France.

In 2007, the Board of Directors of the renowned journal *Astronomy and Astrophysics* (*A&A*), and EDP Sciences, the publisher of *A&A*, decided to organize a School on the various aspects of scientific writing and publishing. In 2008 and 2009 these Scientific Writing for Young Astronomers (SWYA) Schools were organized in Blankenberge, Belgium, under the direction of Christiaan Sterken.

Both volumes are based on these Schools. Part one contains eight papers which deal with all aspects of scientific publication, from the peer-review process to the role of the publisher and beyond. Two of the papers provide insight in the services provided by astronomical libraries in a broad sense, and discuss how information on papers, and information provided in papers, are integrated in databases and repositories such as the NASA Abstract Data Server (ADS), the arXiv.org e-print repository, SIMBAD, and VizieR. Two contributions discuss language editing. One of these papers provides the guidelines to the English editing currently in use at *A&A*. Another paper, written by S. R. Pottasch, who was, together with J. L. Steinberg, the first Editor-in-Chief of *A&A*, provides an interesting overview on the creation of *A&A* and the obstacles encountered in merging several national and observatory publications into an international journal. Although most contributions are written from an *A&A* perspective, the discussed topics apply also to other major astronomical journals, probably with some nuances.

Part two, which is completely written by Christiaan Sterken, consists of three very extensive papers. The first paper deals with all aspects of writing a scholarly paper, from the initial drafting up to and including the deep

proofreading of the manuscript. One section amplifies on what to avoid at all price. Another section provides detailed answers on twenty-six frequently asked questions, such as "May I reproduce complete sentences?" and "How do I communicate with the referee?". The second paper discusses communication by graphics, images, diagrams, and tables. Not only the types of graphs and the graph components are discussed, but also an in-depth look at technical aspects of file formats, image quality, and colors is included. While discussing colors, the author also takes color blindness into account. Many of the gray-scale graphs included in this paper are reprinted in color at the end of the paper. The paper also contains a section on what to avoid at all costs. The third paper, devoted to ethical aspects, elaborates on the truthful communication of scientific results and concepts of truth, error, quality, and value. Different kinds of misconduct together with a number of causes and cures are addressed. One section deals with bibliometry and bibliometrics, and another section assesses the biases of bibliometric indices and questions the value of these indices.

Both volumes cover, from an astronomical perspective, all aspects of scientific writing and publishing very extensively. Many of the discussed topics are accompanied by historical examples or examples from the personal experience of the editor. Numerous footnotes provide additional information and references to websites, or clarify terms used in the papers. Some overlap exists between both volumes, and even between papers in the same volume. The editor explicitly mentions that this overlap is built in intentionally, in order to allow the readers to consult the sections of their interest, instead of having to read the book and papers from start to finish. Both parts contain an expanded table of contents, an extensive subject and name index, and a list of acronyms. The books are well-produced and well-typeset, with keywords, key-sentences, important concepts, and important literary quotations clearly emphasized in Part 2. Although the title of these books indicates that they are written specifically for young astronomers, these books are undoubtedly also useful for astronomers in general, including amateur astronomers who want to publish their results in an astronomical journal.

Eric Broens
Vereniging Voor Sterrenkunde, Belgium
Wateringstraat 143, B-2400
Mol, Belgium; eric.broens@skynet.be

Abstracts of Papers and Posters Presented at the 101st Annual Meeting of the American Association of Variable Star Observers, Held in Woburn, Massachusetts, November 1–3, 2012

Variability of Young Stars: the Importance of Keeping an Eye on Children

William Herbst
Astronomy Department, Wesleyan University, Middletown, CT 06459; wherbst@wesleyan.edu

Abstract I will review the state of our understanding of young stars with an emphasis on how and why they vary in brightness. The main causes of the variations will be reviewed, including the rotation of spotted weak-lined T Tauri stars, accretion onto classical T Tauri stars, the eruptive behavior of FUors, and the enigmatic variations of the UXors. The important role that amateurs have and will continue to play in these studies is highlighted. I will also discuss the latest results on two unusual young binaries, BM Orionis in the Trapezium asterism and KH 15D in NGC 2264.

Variable Stars in the Trapezium Region: the View From Ground and Space

Matthew R. Templeton
AAVSO, 49 Bay State Road, Cambridge, MA 02138; matthewt@aavso.org

Abstract We present the results of our project to study variability among stars of the Trapezium Region of the Orion Nebula using both ground- and space-based observations. Continuous, broad-band optical photometry were collected over twenty-seven days using the orbiting MOST satellite in late 2010 and early 2011, while ground-based data were collected by AAVSO observers and the AAVSO's Bright Star Monitor telescope. Fifteen of thirty-seven stars showed clear evidence of variability of various types. The sample includes a dozen stars showing variability typical of YSOs, including T Tauri type and rotational variability; additionally, we found evidence of β Cephei pulsation in two stars, and we also obtained four full cycles of the primary target—the 6.5-day eclipsing binary BM Orionis. We show examples of the MOST and AAVSO light curves for these stars, what the results tell us about these stars, and what remains to be learned from these stars.

YSOs as Photometric Targets

Arne A. Henden
AAVSO, 49 Bay State Road, Cambridge, MA 02138; arne@aavso.org

Abstract Young stellar object research is an active and growing field within astronomy, and YSOs are targets for both optical photometry and multiwavelength studies from ground and space. They vary due to a number of different physical processes; they are also often red objects in dust-rich environments, making their spectra complex. Understanding of their optical variations requires calibrated photometry in standardized filters. In this short talk, we cover the most straightforward ways to perform observations of these objects that yield scientifically useful data.

Working Together to Understand Novae

Jeno Sokoloski
Columbia Astrophysics Lab, 1027 Pupin Hall, Mail Code 5247, 550 West 120th Street, New York, NY 10027; jeno@astro.columbia.edu

Abstract In ancient times, people occasionally looked up to find a "nova," or new star, in the sky. With at least thirty-five per year in our galaxy, novae are the most common major stellar explosions. Although researchers now understand what causes a white dwarf to suddenly brighten into a nova, many puzzles remain, such as why novae appear to eject orders of magnitude more material than predicted by theory, and how a uniform eruption on a spherical white dwarf can expel matter in the form of jets, clumps, and rings. Coordinated observations at radio, optical, and X-ray wavelengths can answer these questions. I will describe how the AAVSO's new nova forum (http://www.aavso.org/forums/variable-stars/nova-project) is designed to enhance communication between amateur astronomers and professional astronomers who are using X-ray and newly upgraded radio telescopes to observe novae. Participants in the nova forum will have the opportunity to learn about novae, share their own expertise, and be a part of the process of scientific discovery.

Campaign of AAVSO Monitoring of the CH Cyg Symbiotic System in Support of Chandra and HST Observations

Margarita Karovska
Harvard-Smithsonian Center for Astrophysics, 60 Garden Street, Cambridge, MA 02138; mkarovska@cfa.harvard.edu

Abstract CH Cyg is one of the most interesting interacting binaries in which

a compact object, a white dwarf or a neutron star, accretes from the wind of an evolved giant or supergiant. CH Cyg is a member of the symbiotic systems group, and at about 250pc it is one of the closest systems. Symbiotic systems are accreting binaries, which are likely progenitors of a fraction of Pre-Planetary and Planetary Nebulae, and of a fraction of SN type Ia (the cosmic distance scale indicators). We carried out Chandra and HST observations of CH Cyg in March 2012 as part of a follow-up investigation of the central region of CH Cyg and its precessing jet, including the multi-structures that were discovered in 2008. I will describe here the campaign of multi-wavelength observations, including photometry and spectroscopy, that were carried out by AAVSO members in support of the space-based observations.

2012: a Goldmine of Novae

Arne A. Henden
AAVSO, 49 Bay State Road, Cambridge, MA 02138; arne@aavso.org

Abstract So far in 2012, sixteen objects have been at least initially classified as galactic novae. This total includes five confirmed novae in Sagittarius alone! This paper will discuss the observations for these objects that have been submitted to the AAVSO, with some thoughts about the future of nova discoveries and the role of amateurs.

Introducing Solar Observation to Elementary Students

Gerald P. Dyck
29 Pleasant Street, Assonet, MA 02702; geraldpdyck@yahoo.com

Abstract I will demonstrate the presentation I have developed for introducing solar observation to elementary students in Dartmouth, Massachusetts, and surrounding public schools. Copies of my program will be available for AAVSO members who would like to use it.

AAVSO Solar Observers Worldwide

Rodney Howe
3343 Riva Ridge Drive, Fort Collins, CO 80526; ahowe@frii.com

Abstract For visual solar observers there has been no biological change in the "detector" (human eye)—at century scales (eye + visual cortex) does not change much over time. Our capacity to "integrate" seeing distortions is not just simple averaging! The visual cortex plays an essential role, and until recently only the SDO-HMI (Solar Dynamics Observatory, Helioseismic and Magnetic

Imager) has had the capacity to detect the smallest sunspots, called pores. Prior to this the eye was superior to photography and CCD. Imaged data are not directly comparable or substitutable to counts by eye, as the effects of sensor/optical resolution and seeing will have a different influence on the resulting sunspot counts for images when compared to the human eye.

Also contributing to the complex task of counting sunspots is differentiating between a sunspot (which is usually defined as having a darker center (umbra) and lighter outer ring (penumbra)) and a pore, made even more complex by the conflicting definitions of the word "pore" in the solar context: "pore" can mean a small spot without penumbra or "pore" can mean a random intergranular blemish that is not a true sunspot. The overall agreement is that the smallest spot size is near 2,000 km or ~3 arc sec, (Loughhead, R. E. and Bray, R. J. 1961, *Australian J. Phys.*, **14**, 347). Sunspot size is dictated by granulation dynamics rather than spot size (cancellation of convective motion), and by the lifetime of the pore, which averages from 10 to 30 minutes.

There is no specific aperture required for AAVSO observers contributing sunspot observations. However, the detection of the smallest spots is influenced by the resolution of the telescope. Two factors to consider are the theoretical optical resolution (unobstructed aperture), Rayleigh criterion: theta = 138 / D(mm), and Dawes criterion: theta = 116 / D(mm) (http://www.telescope-optics.net/telescope_resolution.htm). However, seeing is variable with time; daytime range will be similar for all low-altitude sites, within the range of 1.5 to 3 arc sec, (typically = 2 arc sec equivalent diameter D = 45–90 mm, the typical solar scope = 70 mm aperture). Where large apertures are more affected by size of turbulent eddies ~8–12 cm, small-aperture telescopes reduce these differences, i.e. large aperture is not always beneficial.

Statistical Evidence for a Mid-Period Change in Daily Sunspot Group Counts from August 2011 through August 2012, and the Effect on Daily Relative Sunspot Numbers

Rodney Howe
3343 Riva Ridge Drive, Fort Collins, CO 80526; ahowe@frii.com

Abstract A combination of statistical counts modeling methods, time series analysis, and t-tests were applied to daily sunspot group counts data obtained from the American Association of Variable Star Observers (AAVSO) Solar Section. The data span the period from August 2011 through August 2012. The analysis investigates whether a statistically significant difference in daily sunspot group counts occurs between the first and second halves of this period. We show that a significant statistical difference exists between the two halves, and this difference also exists in the sunspot number. Also, the rate of change between daily sunspot group counts is shown to be stable between the two

periods. These results indicate that between the two periods, the sunspot group count averages and the corresponding sunspot numbers differ, and suggests the sunspot group counts submitted by AAVSO contributors are consistent between the two periods. The change between these time periods may give insight into an apparent bi-modal clustering of sunspots and sunspot groups during this twenty-forth cycle maximum.

Mentoring, a Shared Responsibility

Timothy R. Crawford
79916 W. Beach Road, Arch Cape, OR 97102; tcarchcape@yahoo.com

Abstract While the AAVSO has a variety of mentoring resources, including the Mentoring team supervised by Mike Simonsen, there is an enormous need for AAVSO participants to individually and actively mentor observers who have missed some of the basics of observing (visual or CCD), whether they are new or have been observing for a long time. Without this shared responsibility, by our silence we risk either losing new observers or enabling observers not following good procedures to contribute erroneous data. We will discuss some of the common mistakes that both visual and CCD observers make, how they can be detected, and how AAVSO members and observers can and should help those in need of mentoring.

66 Oph Decides to "Be"

John Martin
University of Illinois at Springfield Observatory, One University Plaza, MS HSB 314, Springfield, IL 62704; jmart5@uis.edu

Abstract 66 Oph was first identified as a Be star by Merrill and Burwell (1933, *Contrib. Mt. Wilson Obs.*, No. 471, 1). Normally its spectrum exhibits pronounced Balmer line emission with some short-term variability. In the 1950s the emission disappeared and returned within a few years. When the emission started decreasing in 1993 and disappeared in 2009, Miroshnichenko *et al.* (2011, *Be Star Newsl.*, No. 40, 42.) predicted a similar recovery. Here we present the results to date of spectroscopic monitoring of 66 Oph through its "low" state and report that it appears to be on the verge of resuming an active Be status.

V439 Cygni: Insights into the Nature of an Exotic Variable Star

David G. Turner
Saint Mary's University, Halifax, NS B3H 3C3, Canada; turner@ap.smu.ca

Abstract V439 Cyg is a 12th magnitude irregular variable in the core of the very young cluster Berkeley 87 that has defied straightforward characterization in previous years. Prior to the last thirty years it was an irregular variable that displayed occasional erratic 0.5-magnitude flareups lasting several days. In 1959 it was classified as a late-type carbon star from an objective-prism survey, but a photometric study of the cluster in 1982 and an image-tube spectrum in 1983 revealed it to be a highly-reddened early-type star. Attempts to study the star spectroscopically have been hampered by its peculiar nature. The star always exhibits emission in the lower Balmer series hydrogen lines superposed on an almost featureless continuum. But the spectral veiling of V439 Cyg sometimes lifts, revealing characteristics of a very rapidly-rotating star that recently displays features of a nitrogen-enriched B0 dwarf. The star's light variability apparently ceased thirty years ago, yet it remains an exotic example of slightly evolved massive stars that display the effects of CNO-processed elements in stellar cores mixed into their surface layers. Is V439 Cyg an example of a merged binary?

Elizabeth Brown and Citizen Science in the Late 1800s (poster)

Kristine Larsen
Physics and Earth Sciences, Central Connecticut State University, 1615 Stanley Street, New Britain, CT 06053; larsen@ccsu.edu

Abstract While "Citizen Science" projects are sometimes thought of as a recent permutation of the professional-amateur relationship in science, the AAVSO is an example of an organization that has been encouraging such participation for over a century. Although the AAVSO's Solar Observing Program dates back only to 1944, AAVSO members had been submitting sunspot counts to other agencies long before this time. Other countries also have a long history of collecting valuable sunspot observations. For example, prior to the AAVSO's founding in 1911, British amateurs had been collecting solar data in organizations such as the British Astronomical Association (BAA) and Liverpool Astronomical Society (LAS) since the 1880s. British amateur astronomer Elizabeth Brown served as Solar Section Director of both the BAA and the LAS, and played an important role in promoting participation in citizen science projects, not only in solar observing, but in other astronomical and meteorological projects as well. This poster will summarize this work and

argue that Brown's contributions should be more widely known and studied in modern citizen science project circles.

APASS Data Product Developments

Douglas L. Welch
McMaster University, Department of Physics and Astronomy, Hamilton, ON L8S 4M1, Canada; welch@physics.mcmaster.ca

Abstract Data Release 6 (DR6) of the AAVSO Photometric All-Sky Survey (APASS) was a significant milestone in the ambitious project to provide calibrated photometry for 10 < V < 17 over the entire sky in Johnson B and V and Sloan g',r',I', bandpasses. DR6 itself was a list of mean magnitudes and colors for about 42 million objects and sky coverage was approximately 95% complete. The photometric means database has now been supplemented by additional data products: an epoch photometry database and a publicly-accessible store of the dark-subtracted, flat-fielded images at the Canadian Astronomy Data Centre. In this talk, I will describe the processes and challenges of producing these new, useful resources and the contributions of numerous people to the success of this effort. As new data releases occur, the epoch photometry database—which contains data for all measured stars, not just variables—will be updated to include all newly available measurements. As of October 2012, 861,322,813 individual photometric measurements exist in the epoch photometry database. The breakdown of measurements per filter is: B 167,682,680; V 170,005,969; u 25,457; g 181,303,298; r 181,266,321; i 160,374,091; z 664,997. A VStar plug-in to access and analyse the APASS epoch photometry database will be demonstrated and future developments discussed.

The Case of the Tail Wagging the Dog: HD 189733—Evidence of Hot Jupiter Exoplanets Spinning-up Their Host Stars

Edward F. Guinan
Department of Astronomy and Astrophysics, Villanova University, Villanova, PA 19085; edward.guinan@villanova.edu

Abstract HD 189733A is an eighth mag K1.5V star that has attracted much attention because it hosts a short period, transiting, hot-Jupiter planet. This planet, HD 189733b, has one of the shortest known orbital periods (P = 2.22 days) and is only 0.031 AU from its host star. Because the system undergoes eclipses and is bright, HD 189733 has been extensively studied. The planet's atmosphere has been found to contain water vapor, methane, CO2, and sodium and possible haze. Spitzer IR observations indicate planet temperature, varying ~970 K to ~1,200 K over its surface (Tinetti (2007). Based on measurements

of the K-star's P(rot) from starspot modulations of ~11.95 d, strong coronal X-ray emission and chromospheric Ca II-HK emission indicate a young age of ~0.7 Gyr. But this apparent young age is discrepant with a much older age (> 4 Gyr) inferred from the star's very low Lithium abundance. However, the age of the HD 189733 system can be independently determined by the presence of a faint dM4 companion (HD 189733B) some 12" away. Our Age-Activity relations for this star (no detectable coronal X-ray emission and no H-alpha emission) indicate an age > 4 Gyr (and < 8 Gyr from kinematics and metallicity). This age should apply to its K star companion and its planet. The fast rotation and resultant high activity levels of the K star can best be explained from the increase in its (rotation) angular momentum (AM) from the orbital AM of the planet. This AM transfer occurs from tidal and magnetic interactions of the K star with its planet. Determining the possible decrease in the planet's orbital period is possible from studying the planet eclipse times (which can be done by AAVSO members with CCD photometry). We also discuss the properties of other related short-period exoplanet systems found by the Kepler Mission that show similar behavior—in that close-in hot Jupiter size planets appear to be physically interacting with their host stars. This work is supported by NSF/RUI grant AST-1009903.

An Overview of the Swinburne Online Astronomy Courses

Frank Dempsey
RR 1, 3285 Sideline 20, Locust Hill, ON L0H 1J0, Canada;
dempseyfrank@gmail.com

Abstract An overview of the online astronomy courses at Swinburne University of Technology is presented for the benefit of AAVSO members who might be interested in the courses or programs. The decision to take the online Master's degree in astronomy at Swinburne was a natural evolution from being interested in astronomy at an early age, being an amateur astronomer all my life, and being a variable star observer and member of the AAVSO for the past several decades. This presentation provides an overview of the program and examples of the course materials, assignments, and projects that may provide some idea of the commitment and expectations for AAVSO members considering the program.

The AAVSO CENTENNIAL HISTORY

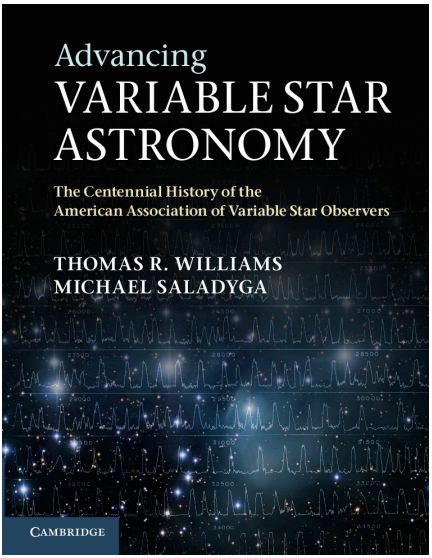

Advancing Variable Star Astronomy: The Centennial History of The American Association of Variable Star Observers

by Thomas R. Williams and Michael Saladyga,
published by Cambridge University Press,
is available through the AAVSO at a special reduced price of $80

Thanks to the generosity of a donor, the purchase price of each book sold through the AAVSO online store will go to benefit the AAVSO

To order, visit the AAVSO online store:

http://www.aavso.org/aavso-online-store

or contact the AAVSO,
49 Bay State Road, Cambridge, MA 02138, USA
phone: 617-354-0484 email: aavso@aavso.org

Now also available as a Kindle e-book through Amazon.com

NOTES